WATERSHED-SCALE CONTROLS ON SNOW DISTRIBUTION IN A MONTANE WATERSHED

JAMES DAVID NEIL DIXON

B.Sc. Geography (Hons), Trent University, Peterborough, Ontario, Canada 2006
B.Ed., Queen's University, Kingston, Ontario, Canada, 2007

A Thesis
Submitted to the School of Graduate Studies
of the University of Lethbridge
in Partial Fulfilment of the
Requirements for the Degree

MASTER OF SCIENCE

Department of Geography
University of Lethbridge
LETHBRIDGE, ALBERTA, CANADA

Abstract

Snow accumulation in mountain headwater basins is vitally important to southern Alberta, where snowmelt supplies more than 80% of annual downstream runoff. This study evaluated two snow measurement techniques, and snow accumulation in southwestern Alberta. The SnowHydro sampler was compared with existing designs and observed to perform better under the forest canopy. A total station was evaluated for remotely measuring snow depth in avalanche terrain, but found to have accuracy limitations in low snow accumulation conditions. Field data were combined with indices of snow accumulation drivers to run classification and regression tree analysis (C&RT). Results quantified controls on accumulation over two years, and created spatial distributions of snow water equivalent across the watershed. Elevation was the dominant control between years, while canopy closure, slope angle, and aspect varied in importance between years and within seasons. Accurate representations of SWE suggest that C&RT could improve annual provincial water supply forecasts.

Acknowledgements

I am indebted to all who have contributed to this project over the past two years. First and foremost, I wish to extend my sincere thanks to my supervisor, Dr. Sarah Boon, for her guidance, patience, support, encouragement, and for giving "some guy from Ontario" the opportunity to work in her research group. I greatly appreciate her enthusiasm for this project, and allowing me to expand the project into the two sub-studies that evolved into the two techniques chapters in this thesis. I am extremely grateful to her for allowing me to attend a variety of international conferences, and for forcing me to improve my speaking skills by signing me up for as many talks as possible.

Financial support for this project was received from the University of Lethbridge, Alberta Sustainable Resource Development (ASRD) Forest Management Branch, and the Geological Society of America. I wish to also acknowledge the in-kind support received from the Southern Rockies Watershed Project, University of Alberta Forest Hydrology Lab, and the University of Lethbridge Mountain Hydrology Lab.

I wish to thank my thesis committee members: Dr. Hester Jiskoot and Dr. Stewart Rood. Their participation in our committee meetings provided invaluable insight, direction, and encouragement that helped me accomplish this project.

The field program was fundamental to this research, and this aspect could not have been completed without a group of hard working individuals who took time away from their own projects to help out. I wish to thank Chris Williams, Jolene Lust, and Jeremy Fitzpatrick of the Southern Rockies Core Crew for their assistance throughout the project, and for going out of their way to help me accomplish my fieldwork despite the fact that I ruined their dinner on my first shift with them.

I thank my colleagues from the Mountain Hydrology Lab: Katie Burles, Ryan MacDonald, Reed Davis, and Dave Lewis for field assistance, technical support, hydrology talk, coffee runs, and for generally tolerating my constant questions and complaining. I especially thank Reed Davis, my office mate and field assistant. His tireless efforts in the field were essential to the successful completion of my field program, even if he couldn't walk in snowshoes. His attitude, sense of humour, and ability to "do it live" has kept me laughing throughout my time in Lethbridge, which has made the work go that much easier.

Finally, I greatly appreciate my friends and family for their interest and encouragement along the way, and for tolerating my prolonged absences from home. Special thanks go to my loving partner and best friend Angela Adkinson, who has been extremely supportive, understanding, and always willing to explain various aspects of trigonometry and statistics to me, and then re-explaining them when I didn't get it the first time. Thanks for a great couple of years in Lethbridge.

Table of Contents

List of Figures

List of Tables

1.0: Introduction

In many watersheds worldwide, snowmelt is the dominant hydrologic event of the annual hydrograph, accounting for up to 80% of annual runoff (Elder *et al.*, 1998; Jost *et al.*, 2007). This event replenishes soil moisture and groundwater reserves that have been depleted throughout the year, and replenishes reservoirs used for irrigation, urban water supplies, and recreation (Pomeroy and Gray, 1995; López-Moreno and Nogués-Bravo, 2005). It is estimated that up to one-sixth of the global population depends on melting snow and ice for their water needs (Barnett *et al.*, 2005; Stern, 2007).

In Alberta, approximately 97% of water allocations are derived from surface water resources, which are largely fed by melting glaciers and snowpacks in the Rocky Mountains. The Oldman River watershed, the largest in southern Alberta (Rock and Mayer, 2007), provides nearly 25% of all water allocations in the province despite containing only 5% of the province's population (AMEC, 2007). Surface water resources are stressed in southern Alberta due to the semi-arid climate, declining summer stream discharge and high consumption by municipal, industrial, and agricultural users (Byrne *et al.*, 2006; Rock and Mayer, 2007; Rood *et al.*, 2008).

Climate change will likely contribute to increased water stress in this area through significant effects on snow processes, including shifts in the amount and extent of accumulation, the type of winter precipitation received, and the timing of melt. In the northern hemisphere, spring snowcover extent has decreased by approximately 2% per decade since 1966 (Groisman *et al.*, 2004). This is apparent in western North America, where the observed decline in snowpack extent has been greatest during spring months throughout the last half of the 20th century (Groisman *et al.*, 2004). A decrease in April

1st snow water equivalent (SWE) has been observed at 75% of instrumented mountain locations (Mote *et al.*, 2005). The onset of spring, and the corresponding date of maximum SWE, now occur 2 – 3 weeks earlier than the long-term average over the same period (Stewart *et al.*, 2005). Increasingly, winter precipitation has been in the form of rain rather than snow, which contributes to mid-winter and early spring melting and a corresponding decline in spring snowpack (Cayan *et al.*, 2001; Easterling, 2002; McCabe *et al.*, 2007; Trenberth *et al.*, 2007). Despite increased snow accumulation in the early portion of the snow season, higher air temperatures later in the snow season are leading to earlier melt periods (Mote *et al.*, 2005; Lemke *et al.*, 2007).

This is a global pattern, with similar snowpack decline observed in the Spanish Pyrenees (López-Moreno, 2005), the Swiss and Italian Alps (Scherrer *et al.*, 2004; Valt and Cianfarra, 2010), the Tibetan Plateau (Zhang *et al.*, 2004), and the Snowy Mountains of south-east Australia (Hennessy *et al.*, 2003). This trend is economically important for agricultural activity on the Canadian prairies and western United States, where snowmelt is predicted to occur earlier in spring, and summer flows are likely to be reduced from their current levels (Stern, 2007).

Climate change will result in forest change due to vegetation migration and forest disturbance, particularly in montane areas (Graumlich, 1993; Parmesan *et al.*, 2000; Flannigan *et al.*, 2005; Soja *et al.*, 2007). Forests are an important component of the hydrologic cycle, affecting both water quality and quantity through their role in interception, infiltration, evapotranspiration, and soil moisture retention (Chang, 2003). As the climate warms, montane forests are expected to migrate to higher elevations and latitudes as their ideal climate zones shift in these directions. This could result in the

complete removal of some tree species from large portions of their current ranges, and invasion of other, non-native, species to replace them (Field *et al.*, 2007; Coops and Waring, 2011). This may also result in large areas of alpine tundra being colonized by migrating tree and shrub species, with a corresponding reduction in snow accumulation due to increased vegetation interception (Soja *et al.*, 2007).

It is also predicted that forest disturbance due to destructive insect infestations and wildfire will increase. A reduction in the number of days with air temperatures < -30° C during winter means that insects (i.e., mountain pine beetle) are no longer being eliminated during winter months (Hélie *et al.*, 2005; Stahl *et al.*, 2006; Fischlin *et al.*, 2007; Aukema *et al.*, 2008). Warmer and drier conditions overall will increase the probability, frequency, and severity of wildfire (Field *et al.*, 2007; Littell *et al.*, 2009). Forest disturbance can result in a more extreme, event-based hydrologic response from a basin due to a greater proportion of precipitation inputs being routed directly to the ground, rather than being intercepted by vegetation (Jones, 2000; Winkler *et al.*, 2005). These changes may be large in snowmelt-dominated watersheds where removal of the canopy reduces interception, resulting in deeper snowpacks and thus greater water storage, but also increases the exposure of the pack to solar radiation resulting in faster and earlier snowmelt (Winkler *et al.*, 2005; Boon, 2007). Given the key role of forests and snow in the hydrologic cycle, it is important to understand the interactions between them so that the impacts of future alterations to existing conditions can be better understood and addressed.

This study investigates topographic and vegetation controls on snow accumulation and distribution within a small montane watershed. The following objectives have been identified:

1) Establish a comprehensive snow survey network that incorporates terrain and vegetation variability within the watershed.

    a. Perform an error analysis of the snow samplers used in the snow surveys.

    b. Develop and validate a new method to remotely measure snow depth at high elevations and in hazardous terrain.

2) Quantify peak SWE across the watershed from the snow survey data and a range of interpolation methods.

3) Quantify the primary controls on snow accumulation across the watershed using statistical approaches.

The thesis is structured to first provide foundational information required to understand the experimental design of the thesis, followed by a discussion of controls on snow accumulation at the study site. Chapter 2: Background introduces the thesis topic and places the research in the context of previous work. Chapter 3: Study Area provides a description of the study watershed, as well as a discussion of the regional research context. Chapters 4: Snow Sampler Error Analysis and 5: Remote Snow Depth Measurements with a Robotic Total Station outline the experimental design, results, and discussion for Objectives 1a and b, respectively, which are required to understand the data collected for Chapter 6. Chapter 6: Controls on Snow Accumulation and Distribution in the Star Creek Basin deals with Objectives 2 and 3, and Chapter 7: Conclusion provides research conclusions and future outlook.

2.0: Background

2.1 Snowfall Formation

Precipitation is primarily formed as a result of the vertical motion of air in the atmosphere. In mountainous terrain, this motion is caused mainly by either convective activity or orographic lifting. Rising air cools adiabatically, thus the lack of heat exchange between the air parcel and the surrounding atmosphere results in condensation of water vapour (Schemenauer *et al.*, 1981; Robinson and Henderson-Sellers, 1999). The rate of adiabatic cooling, referred to as the lapse rate, varies between 5 and 10°C km^{-1} depending on the moisture content of the air parcel. Formation of snow commences once the air parcel has cooled to 0°C. The process of snowfall formation is similar to that of other types of precipitation, with the exception that atmospheric temperature must be below 0°C (Schemenauer *et al.*, 1981). At atmospheric temperatures ≤ -5ºC, some atmospheric aerosols provide ideal sites for ice nucleation, where water vapour condenses and freezes on the surface of particles to create snow crystals (Schemenauer *et al.*, 1981). Snow crystals grow rapidly as increasing amounts of water vapour sublimate from the atmosphere to the crystal surface. Additionally, droplets of water may freeze on contact with the ice crystal in a process called riming. In extreme cases, riming may form dense graupel particles, which deposit much higher density layers than snow crystals (Magono, 1953; Magono and Lee, 1966; Schemenauer *et al.*, 1981; Robinson and Henderson-Sellers, 1999).

Between -5ºC and 0ºC, precipitation particles are partially melted with a moist surface, and form mainly by aggregation: accumulation through impact with other particles (Robinson and Henderson-Sellers, 1999). Eventually, the particle will gain

enough mass that it can no longer be held aloft by air currents within the cloud, and the particle falls as snow (Robinson and Henderson-Sellers, 1999).

2.2 Properties of Snow and Snowcover

As snow falls to the ground, it is deposited in layers that can accumulate to a considerable depth over the course of the winter season, resulting in large-scale effects on climate at local and global scales. The albedo of a fresh snow surface is very high, but declines as the snowpack ages and impurities accumulate on the surface (e.g. through deposition of atmospheric contaminants, forest litter, etc., Table 2.1) (Berry, 1981). This high albedo allows snow surfaces to reflect a large proportion of incoming shortwave radiation, thus extensive snowcover may cause cooling in the lower troposphere if the snow persists for a sufficiently long period, resulting in a positive feedback between snowcover and air temperature (Kukla and Kukla, 1974). Conversely, in the longwave portion of the spectrum, snow emits substantial longwave energy while it is melting, warming the adjacent atmosphere and promoting further melting (Oke, 1987).

Table 2.1. Comparison of albedo values for common surfaces (from Berry, 1981; Oke, 1987)

Surface	***Albedo (%)***
Fresh snow	75-95
Old snow	40-70
Water	Low zenith angle - 3-10 High zenith angle - 10-100
Crops	3-25
Forest	3-20

For hydrologic investigations, depth, density, and SWE are the most important physical properties of a snowpack (Pomeroy and Gray, 1995). Snow depth is highly variable, and is largely a function of a series of interrelated topographic, vegetation, and

redistribution processes that control how much snowfall is generated, and where it accumulates. These processes are described in detail in sections 2.2, 2.3, and 2.5.

Density is controlled by a range of complex interactions between the snowpack and the environment, and is largely independent of terrain. The density of freshly fallen snow is generally assumed 100 kg m^{-3}, which is a convenient assumption resulting in a 10:1 ratio of snow depth to SWE (Goodison *et al.*, 1981). However, measured snowpack densities rarely match this ideal value, thus large over- and underestimations in the calculation of SWE are possible if an assumed density is used (United States Army Corps of Engineers, 1956; Seligman, 1980; Langham, 1981; Pomeroy and Gray, 1995).

Several studies have shown that for snowstorms of 12 to 24 hour duration, density increases rapidly as snow accumulates, and the snow settles under the increased weight (Gray *et al.*, 1970). However, these studies were conducted under non-drifting conditions, where the effects of wind were minimized (Gray *et al.*, 1970; Goodison *et al.*, 1981). Under blizzard conditions, where the effects of wind may be large, the density of fresh snow may increase considerably throughout the storm as wind slab, a hard crust caused by the erosion and compaction of snow, is formed (Gray *et al.*, 1970; Langham, 1981).

Once snow has accumulated on the ground, density increases as the snowpack undergoes metamorphism due to temperature and vapour pressure gradients, compaction under the weight of overlying snow, wind effects, and melt water percolation through the snowpack (Gray *et al.*, 1970; Pomeroy and Gray, 1995). Snowpack metamorphism occurs when a strong temperature gradient exists in the pack (~10°C m^{-1}), which also causes a gradient in vapour pressure (Pfeffer and Mrugala, 2002). These gradients cause

water vapour sublimation from crystal surfaces, which then move between crystals from higher to lower temperatures and vapour pressures. This process results in the formation of depth hoar near the base of a snowpack, which lacks cohesion and contributes to avalanche formation (Langham, 1981).

Mean snowpack density increases throughout the season with continued metamorphism and additional snow accumulation. As the snowpack ages, ice layers with densities of ~800 kg m^{-3} may form (Pomeroy and Brun, 2001) from percolating melt water that originates at the snow surface due to incoming solar radiation or rain-on-snow (ROS) events. Alternatively, melt water may accumulate at the snow surface, freeze, and subsequently be covered with fresh snow, creating an ice layer. The presence of such layers can significantly increase mean snowpack density (Langham, 1981; Male and Gray, 1981).

Finally, during the melt period snowpack density may vary diurnally as melt water accumulates within, and is lost from, the snowpack. Density may change from 350 kg m^{-3} in the morning when the pack is relatively dry, to 500 kg m^{-3} in the afternoon as the snowpack ripens and free water is present (Male and Gray, 1981; Pomeroy and Gray, 1995). Table 2.2 presents the range of densities found in different snow types under dry conditions. Despite the wide range in values, density is less spatially variable than depth in montane watersheds. This reduces the sampling intensity required to capture density versus depth variability (Logan, 1973; Goodison *et al.*, 1981; Elder *et al.*, 1991; Elder *et al.*, 1998; Judson and Doesken, 2000)

Table 2.2. Typical range of snowpack densities for a variety of snow types (from Seligman, 1980)

Snow Type	***Density kg m^{-3}***
Cold, dry snow	10-30
New snow, immediately after falling	50-65
Settling snow	70-190
Settled snow	200-300
Slightly wind toughened snow, immediately after falling	63-80
Average wind toughened snow	280
Wind slab	350

SWE represents the depth of liquid water that would be produced if a snowpack were melted instantaneously (Brooks *et al.*, 1991). It provides a measure of the volume of water stored in a snowpack, thus allowing hydrologists to estimate of the amount of water potentially stored in a watershed and available for downstream users such as irrigators and municipalities. SWE is calculated as:

$$SWE = d_S \frac{\rho_s}{\rho_w} \quad 2.1$$

where *SWE* is the depth of water (cm), d_s is the depth of snow (cm), and ρ_s and ρ_w are the density of snow and water, respectively (g cm^{-3}) (Pomeroy and Gray, 1995; Dingman, 2002).

2.3 Topographic Controls on Snow Distribution

2.3.1 Elevation

Elevation is generally assumed to be the strongest determinant of snow distribution within a watershed, particularly in montane catchments. Generally, snowcover increases in depth and extent with increasing elevation, eventually creating conditions where perennial snowpacks can persist (McKay and Gray, 1981). This is

largely due to decreasing air temperatures with increasing elevation, which suppress ablation and increase potential for snowfall events (McKay and Gray, 1981; Anderton *et al.*, 2004; Barry, 2008).

However, the trend of increasing snow depth with elevation may be reversed or confounded by climatic factors (Barry, 2008). High wind speeds are more common at high elevations where slopes are more exposed. This may result in higher rates of snow transport, redistribution, and densification than at lower elevations, resulting in a thinner but more dense snowpack (see Section 2.5.1) (McKay and Gray, 1981; Pomeroy and Gray, 1995). Where atmospheric inversions are common, air temperature *increases* with elevation, driven by weather fronts or radiation imbalances (i.e., more radiation is emitted by the surface than is received, often at night or during winter when the sun angle is low) (Oke, 1987). Inversions typically start in valley bottoms and extend upslope, resulting in decreasing snow accumulation with elevation. If the slope extends above the inversion extent, snow accumulation may begin to increase again with increasing elevation (Barry, 2008). Thus, while a strong linear relationship between SWE and elevation may occur within selected elevation bands at specific locations, elevation alone is an imperfect indicator of snow distribution.

2.3.2 Slope

Snow accumulation is typically lowest on steep slopes (>37°), where the high gradient produces unstable snowpacks and results in a greater incidence of avalanching (Elder *et al.*, 1998; Anderton *et al.*, 2004). On slopes < 37° accumulation increases due to increased snowpack stability, and through avalanche deposition from higher elevations. Redistribution due to avalanching may reverse the trend of increasing

accumulation with elevation, by moving large volumes of snow from high to low elevations (Zalikhanov, 1971) while having no effect on the total snow storage within a basin (Section 2.4.2) (Elder *et al.*, 1991).

In general, snow accumulation is greatest on windward slopes (McKay and Gray, 1981; Pomeroy and Brun, 2001). When combined with wind speed, slope is a stronger driving factor in snow accumulation than elevation alone. If a parcel of air is saturated when it meets a topographic barrier, the rate of precipitation generation is then proportional to wind speed multiplied by slope angle, potentially leading to deep snowpacks (Rhea and Grant, 1974; McKay and Gray, 1981). Slopes that are sheltered from prevailing winds generally accumulate less snow, particularly if they are exposed to solar radiation inputs or are at lower elevations where orographic effects are less pronounced (McKay and Gray, 1981).

2.3.3 Aspect

Aspect controls snow cover through exposure to prevailing winds and solar radiation (Meiman, 1970; McKay and Gray, 1981). In the Rocky Mountains, snow depth increases rapidly with elevation on west-facing slopes as prevailing westerly winds bring moisture from the Pacific Ocean. On east-facing slopes, however, snow depth increases more slowly with elevation because the majority of moisture has already been lost by deposition on western slopes. Easterly winds are less common; those that do occur contain much less moisture resulting in less snow accumulation (Claus *et al.*, 1984; Slaymaker, 1993).

Aspect also controls accumulation through exposure to solar radiation and subsequent ablation. In the northern hemisphere, the sun is predominantly in the

southern portion of the sky, thus north facing slopes typically receive less than half the incoming shortwave radiation of south facing slopes (Barry, 2008). The latter accumulate less snow throughout the winter, with complete snowcover ablation well before north facing slopes (Pomeroy and Gray, 1995; Elder *et al.*, 1998).

Diurnal variation in radiation received at the surface has been observed on east and west facing slopes (Matzinger *et al.*, 2003; Oliphant *et al.*, 2003). This variability exerts a smaller control on snow accumulation than north vs. south aspects although the processes are the same (Barry, 2008). During winter months, when the sun is at its lowest zenith angle, steeper south-facing slopes tend to capture more incoming radiation than gentle slopes; this situation reverses in summer when the sun achieves its highest zenith angle (Barry, 2008). These patterns may also reverse in areas where cloud cover commonly occurs in winter. Because clouds tend to diffuse solar radiation, the flux of shortwave energy is more evenly distributed across the range of aspects (Matzinger *et al.*, 2003).

2.4 Vegetative Controls on Snow Accumulation – Interception

The above discussion is primarily concerned with basin-scale effects, where topographic controls operate most effectively. At smaller scales (10 – 100's of metres), microtopography exerts a small effect on snow accumulation. At these scales accumulation is primarily controlled by snowfall interactions with vegetation and wind (McKay and Gray, 1981).

Vegetation influences snow accumulation and distribution through two main processes. First, the roughness of a vegetated surface causes turbulent airflow both above

and within the forest canopy. Wind velocities at the forest edge are considerably lower than in open areas and large clearings, due to a rapid increase in friction generated by the vegetation. A reduction in wind velocity to below the threshold value for snow transport causes entrained snow to be deposited, thus maximum snow depths are often recorded at the forest edge. Subsequently, less snow is available to be transported into the stand, thus snow depth declines with distance into the forest (Steppuhn, 1981; Troendle *et al.*, 1988). This process is dependent on wind redistribution processes (see Section 2.4.1). Second, snow is intercepted by and retained within the vegetated canopy, from which it may either sublimate back to the atmosphere or fall to the ground (Meiman, 1970; Schmidt and Gluns, 1991; Hedstrom and Pomeroy, 1998).

A combination of wind processes and their interaction with forest canopy can lead to recurring patterns of interception and accumulation that are related to vegetation type and density (i.e., canopy area, trunk and stem density) and the presence of nearby clearings (Pomeroy and Gray, 1995). For example, snow depth is generally greater within a deciduous forest than a coniferous forest due to a more open canopy that lacks winter foliage. Coniferous forests, which are the dominant forest type in the southern Canadian Rockies, retain their foliage throughout the year, thus canopy density is much higher resulting in greater interception rates (McKay and Gray, 1981). A clearing typically accumulates more snow than a forest due to both the lack of interception and the wind transport and deposition of snow from the surrounding canopy. However, as clearing size increases snow accumulation decreases, because snow is transported out of the clearing by wind (Swanson, 1988).

Interception results from snow accumulation on tree branches, from both snowfall and unloading from higher branches (Fig. 2.1). A portion of intercepted snow will eventually reach the ground surface as either solid, liquid, or through deposition of vapour onto the snow surface. Snow that does not reach the ground will be lost directly to the atmosphere through sublimation (Pomeroy and Brun, 2001; Essery *et al.*, 2003; Varhola *et al.*, 2010).

Figure 2.1. Illustration of snow intercepted on a conifer branch. Bridges between individual needles are visible. As the bridges grow the surface area of the branches increases, thus increasing its ability to intercept falling snow.

It is estimated that up to 45% of annual snowfall is lost to the atmosphere through sublimation of intercepted snow in the Canadian Rockies (Schmidt *et al.*, 1988; Pomeroy and Gray, 1995). Conversely, in areas where the surface area to mass ratio of the snow is smaller, such as at the snow surface, sublimation rates are typically much lower (Pomeroy and Gray, 1995).

It is widely acknowledged that snow accumulation increases as canopy density decreases, and that more rapid snowmelt can be expected due to lack of shading

(Pomeroy *et al.*, 2002; Murray and Buttle, 2003; Winkler *et al.*, 2005; Burles and Boon, 2011). Snow depth increases in clearcuts, as well as in natural clearings, for a number of reasons. Interception processes are eliminated, sublimation of snow is greatly reduced, and snow is redistributed into the clearing from other areas of the basin (Schmidt and Gluns, 1991; Stegman, 1996; Storck *et al.*, 1999; Montesi *et al.*, 2004; Buttle *et al.*, 2005; Molotch *et al.*, 2007). The difference in accumulation can range from 5-70% higher in clearings than under the canopy (Winkler *et al.*, 2005). Multiple studies have shown that the optimal size for accumulating snow in clearings is a diameter of approximately five times the average tree height of the surrounding forest (5*H*) (Golding and Swanson, 1986; Toews and Gluns, 1986; Troendle *et al.*, 1988; Pomeroy *et al.*, 2002). Beyond diameters of 12*H*, increased wind speed in the clearings tends to erode snowpack rather than depositing new snow, resulting in shallower snowpacks in these large clearings (Pomeroy and Gray, 1995; Pomeroy and Brun, 2001). In the foothills of the Rocky Mountains, Swanson (1988) found that clearings with diameters of 2-3*H* accumulated the most snow, and accumulation quickly decreased as clearing diameter increased.

Loss of foliage from a coniferous forest due to forest disturbance (i.e., beetle infestation, wildfire, and forestry) dramatically reduces interception efficiency to values closer to that of a deciduous forest in winter. A greater proportion of total snowfall accumulates on the ground surface (Murray and Buttle, 2003), resulting in increased water storage and higher runoff during the melt season (Buttle and Metcalfe, 2000; Murray and Buttle, 2003; Redding *et al.*, 2008). Canopy removal also results in greater incident solar radiation at the snow surface, driving higher melt rates and an earlier onset of the melt season than observed in undisturbed forest stands (Murray and Buttle, 2003;

Burles, 2010; Burles and Boon, 2011). An open forest structure in general may also expose the snowpack to greater wind effects, resulting in enhanced snow transport into and out of the stand.

2.5 Redistribution Processes

2.5.1 Wind

The mechanism of aeolian snow transport is very similar to sediment transport mechanisms in both air and water, thus the principles of particle entrainment derived by Hjulstrøm (1935) , Bagnold (1941), and others can be easily applied. However, unlike a grain of sand, a transported snow crystal may undergo major changes in size, shape, and mass due to sublimation and erosion. Despite these similarities, aeolian redistribution of snow creates unique depositional formations due to the cohesiveness of snow (Fig. 2.2).

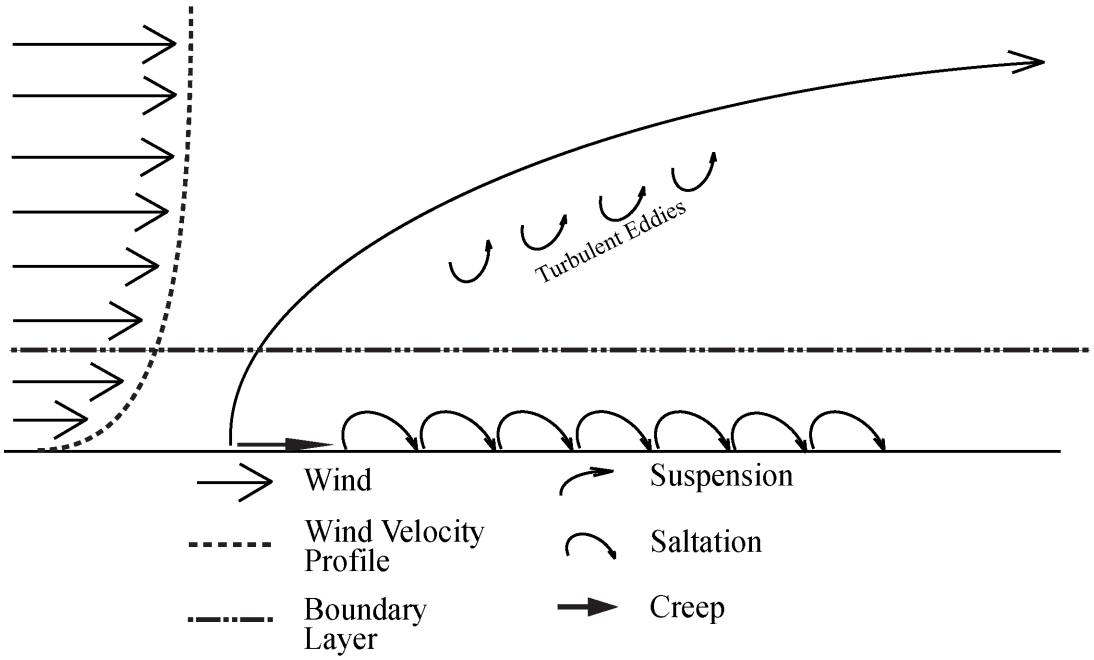

Figure 2.2. A schematic of wind transport of snow over a simple surface. Wind velocity is proportional to the length of the arrows, being lower in the boundary layer than in the free stream. Suspension involves very small grains of snow, which are carried into the atmosphere by turbulent eddies, some of which may hold very small grains in suspension for great distances. Saltation involves particles that are too heavy to be held in suspension, and so skip along the surface. Creep involves particles that are too heavy to skip, and so slide across the surface (Modified from Oke, 1987; Ritter *et al.*, 2002).

Wind is an important factor in snow redistribution within a catchment. Snowcover is eroded from exposed areas such as large clearings, clearcuts, and alpine slopes, and deposited in more sheltered areas such as lee slopes or the edge of forest stands (Hiemstra *et al.*, 2002; Hiemstra *et al.*, 2006). In montane and alpine areas, snow often forms cornices on the lee side of ridges where flow is separated from the ground and velocity is reduced due to increased turbulence. Similarly, small hollows and valleys may also completely fill with wind-deposited snow (Elder *et al.*, 1991; Anderton *et al.*, 2004; Barry, 2008), resulting in a highly heterogeneous snowcover with recurring interannual accumulation patterns (Fig. 2.3) (Winstral and Marks, 2002; Hiemstra *et al.*, 2006; Bernhardt *et al.*, 2009).

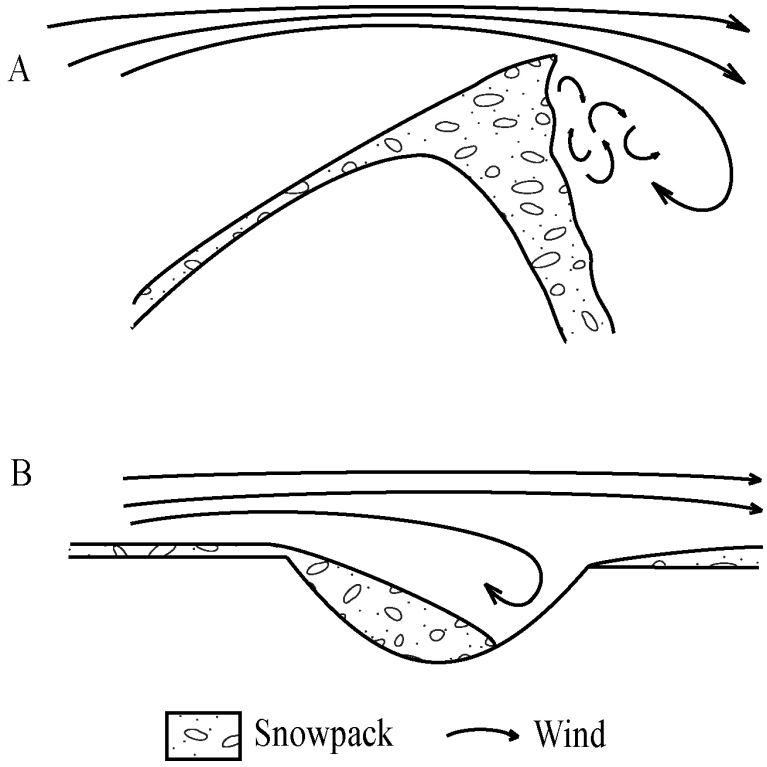

Figure 2.3. As wind flows over ridges and depressions, part of the stream becomes detached from the surface, causing turbulence on the lee side and resulting in deposition of snow entrained in the stream. When this flow occurs over a ridge (A) a cornice is often formed as snow is deposited and scoured away by the turbulent eddies on the lee side, gaining its characteristic shape. Over a depression (B), snow is deposited on the upwind edge of the depression, and scoured away on the downwind side (Modified from Kind, 1981; Oke, 1987; Ritter *et al.*, 2002)

2.5.2 Avalanche Processes

Avalanches are important modes of snow redistribution in mountainous watersheds, moving large quantities of snow from high to low elevations and creating deposits of considerably higher density than the surrounding snowpack (Zalikhanov, 1971). Although avalanches generally do not add or remove snow from a basin, they are nonetheless hydrologically important due to the quantities of water that are being moved, and the reduced melt rates found in dense avalanche deposits (Zalikhanov, 1971; Elder *et al.*, 1991). As mentioned in Section 2.2.2, these events occur primarily on steep slopes (30° – 45°) and in locations where deep snowpacks develop highly stratified layers due to metamorphism (Schaerer, 1981; Elder *et al.*, 1998). Snowpacks that have undergone sintering, a metamorphosis process where inter-crystal bonds are strengthened, have a lower likelihood of failure (Langham, 1981; Schaerer, 1981) (Fig. 2.4). As weak layers consisting of hoar crystals form on the snow surface and are subsequently buried by fresh snow, they provide a point of failure that increases the avalanche potential (Schaerer, 1981; McClung and Schaerer, 1993; Pigeon and Jiskoot, 2008).

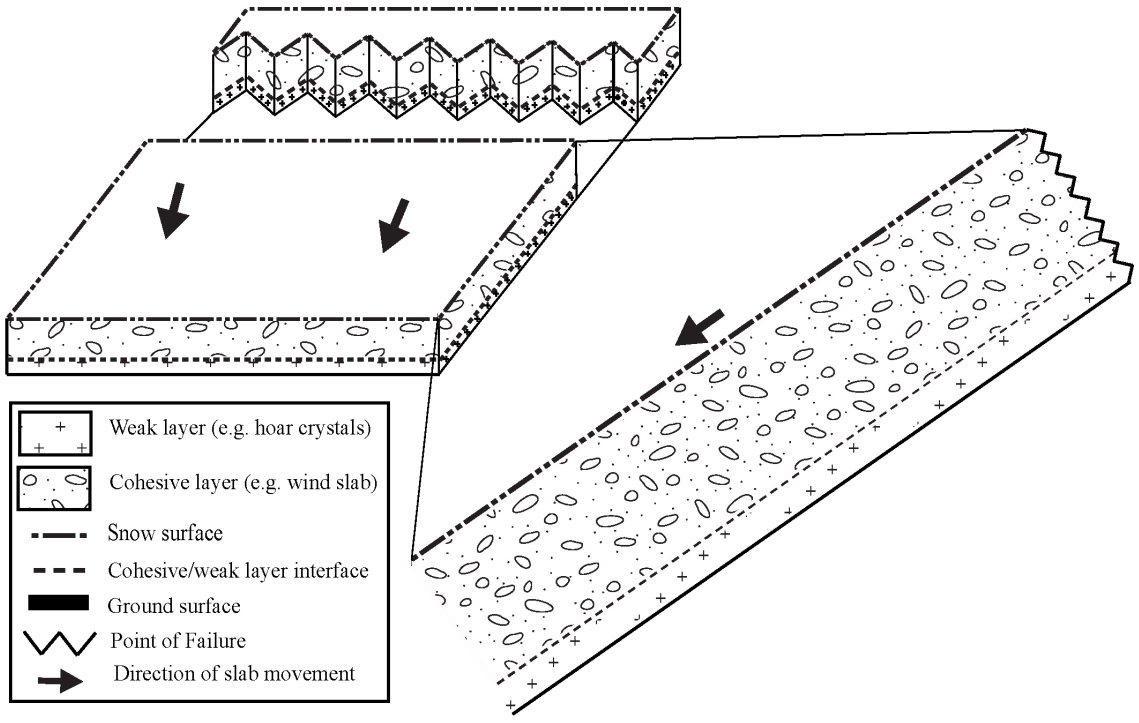

Figure 2.4. A schematic of a slab avalanche. A weak layer of depth hoar crystals is overlain with a consolidated layer of metamorphosed snow. Given enough accumulation, the stress on the depth hoar layer exceeds its capacity, and the slab breaks free. Note that a natural snowpack may contain many layers of differing strengths resulting from weather conditions at deposition. The schematic is simplified for clarity (Modified from Schaerer, 1981).

Avalanches are virtually non-existent on slopes ≤ 25°, unless the snowpack is highly unstable or an avalanche propagates from a steeper slope above (Schaerer, 1971; Schaerer, 1981; Elder *et al.*, 1998). Cornices may also be a driving factor in the generation of avalanches as they grow, become unstable, and break off (Butler, 1979; Dyunin and Kotlyakov, 1980; McClung and Schaerer, 1993). In the eastern Rockies, frequent chinook events may create conditions ideally suited to the formation of weak snow layers that lead to snowpack instability (Johnson, 1987).

Forest disturbance may also create conditions that promote avalanche activity. Dense forests typically add structure to a snowpack allowing deep snowpacks to occur on slopes that are considerably steeper than the 30° threshold. Areas of the northern Gaspé

Peninsula in eastern Canada that have been subjected to extensive logging and wildfire now show evidence of avalanche activity where there was previously none (Germain *et al.*, 2005).

2.6 Local Climatic Controls – Chinook Events

The southeastern Canadian Rocky Mountains are subject to frequent chinook events. Chinooks are characterized by warm and dry westerly winds that flow down the eastern slopes of the Rockies and onto the plains. Similar events are observed in the Alps and Andes (Barry, 2008) These events dramatically increase air temperatures over a short time period and, because the air mass is often very dry, high rates of ablation due to melt and sublimation may be observed throughout the duration of the event (Nkemdirim, 1996; Barry, 2008). The highest frequency of these events, up to 53 days per winter on average, occurs in the Crowsnest Pass region of southwestern Alberta (Nkemdirim, 1996). Melting induced by frequent chinook events may produce multiple ice layers within the snowpack, significantly increasing the average density of the snowpack (McClung and Schaerer, 1993). Additionally, these mid-winter melt events may contribute to high variability in the spatial distribution of snow depth and density, potentially masking the role of topographic and vegetation controls.

2.6 Summary

At large-scales (i.e. watershed, regional) topography exerts considerable control on the distribution of snow, with its main components (elevation, slope, aspect) producing complex and interdependent effects (Schemenauer *et al.*, 1981). However, at

smaller scales (10's to 100's of m) snow accumulation is primarily controlled by interception and redistribution processes. Climate contributes to snow distribution at both scales through a number of interactions that promote snowfall and melting. Because snow depth, density, and SWE are controlled by interactions between elevation, slope, aspect, and climate, these variables must be considered collectively when quantifying snow distribution (McKay and Gray, 1981; Elder *et al.*, 1991; Pomeroy and Gray, 1995; Pomeroy and Brun, 2001; Barry, 2008). However, due to the high small-scale variability in depth, density, and SWE that is characteristic of a snowcover, large-scale relationships between snowcover and terrain features can be hidden, or attributed to random variation (Elder *et al.*, 1991; Jost *et al.*, 2007) rather than interpreted as an actual control signal. Thus, sampling at both small and large scales is essential to determine which set of controls is operating on a particular snowpack.

3.0: Study Area

3.1 Regional Context

Research for this thesis was conducted in the Star Creek watershed, located in the Crowsnest Pass, Alberta, Canada. The Crowsnest Pass encompasses approximately 25% of the headwaters of the Oldman River basin (ORB), which is the largest basin in southern Alberta (Rock and Mayer, 2007) (Fig. 3.1). Star Creek represents ~0.25% of the total headwaters area.

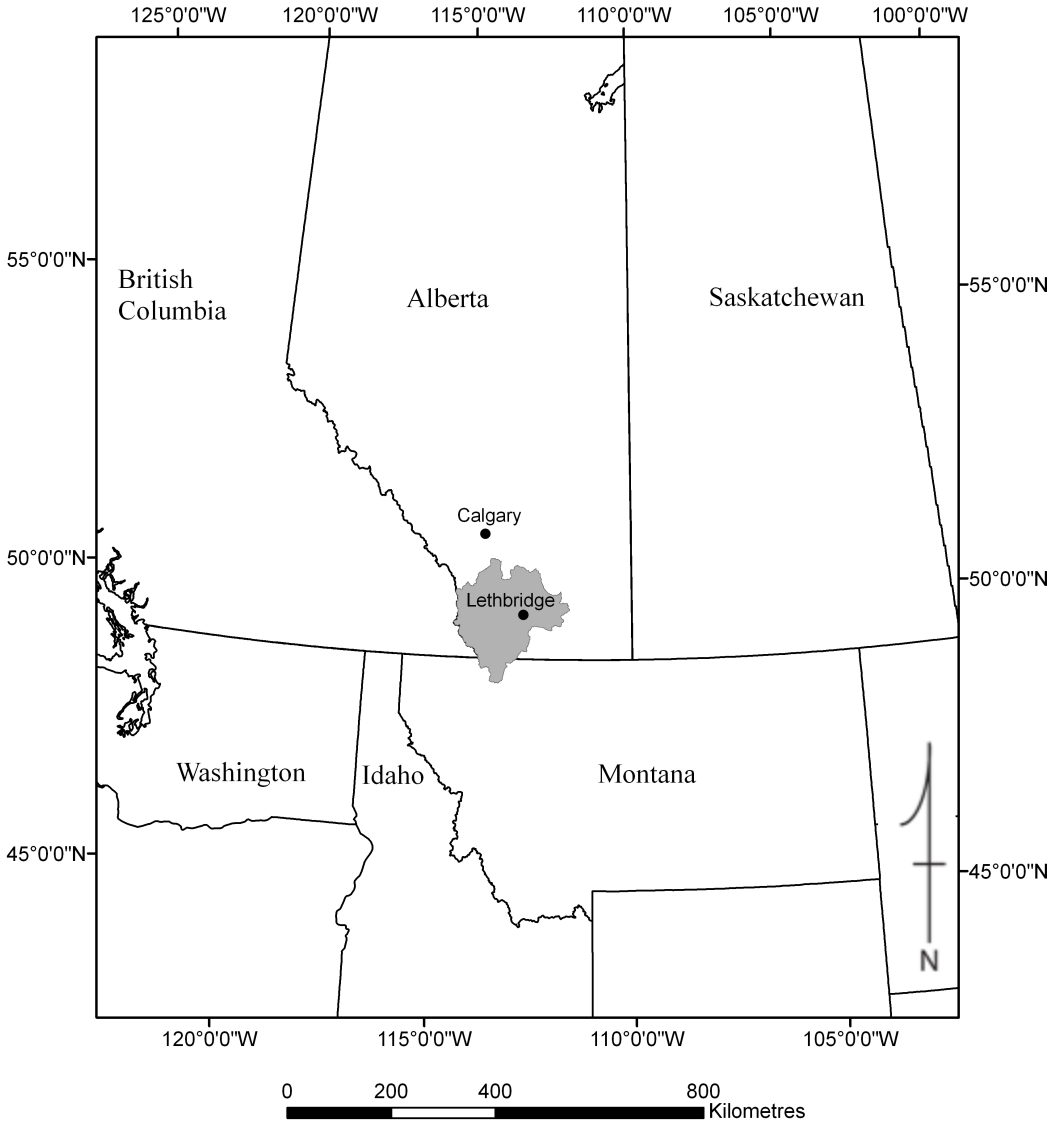

Figure 3.1. Location of the Oldman River basin (ORB, shaded region) in the context of western North America.

Climate and geology vary considerably within the ORB, producing an east-west gradient in vegetation and hydrology. The ORB is sub-divided into four primary sub-regions based on climate and geology: Prairie, Southern Tributaries, Foothills, and Mountain (Fig. 3.2).

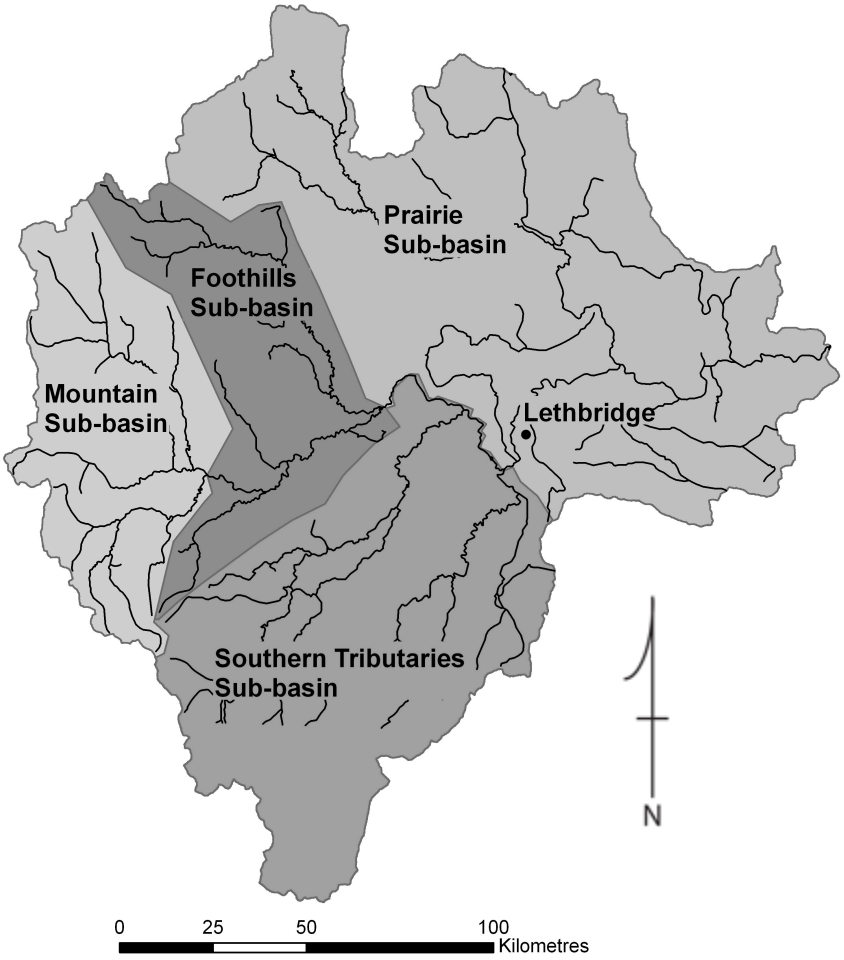

Figure 3.2. Sub-basins of the Oldman River, with primary stream channels.

The Prairie and Southern Tributaries regions cover the southern and eastern portions of the watershed, which have similar climatic and geologic features. This region is primarily underlain by sandstones and shales of Cretaceous age (Russell and Landes, 1940; Oldman Watershed Council, 2010), and overlain with glacial and glaciolacustrine deposits up to 100 m thick. These two sub-regions contain the St. Mary, Belly, and

Waterton Rivers, all of which originate in northern Montana and flow north into Canada. Native grasslands, consisting of mixed short and medium height prairie grasses, have been reduced by as much as 80% in these sub-basins. Stands of plains cottonwood (*Populus deltoides* subsp. *monilifera*) are common along watercourses (Oldman Watershed Council, 2010). The climate in these sub-basins is semi-arid, receiving 300 – 450 mm of precipitation annually.

The Foothills region lies between the prairies to the east and the Rocky Mountains to the west. This area is characterized by rolling hills, fescue grasslands, and forests consisting of Douglas fir (*Pseudotsuga menziesii* subsp. *glauca*), lodgepole pine (*Pinus contorta*), trembling aspen (*Populus tremuloides*), and cottonwood (*Populus trichocarpa* and *Populus angustifolia*). Bedrock in this area is steeply sloping shale and sandstone, overlain by glacial and glacio-fluvial deposits of sands and gravels; bedrock outcrops are common (Russell and Landes, 1940; Oldman Watershed Council, 2010). The Oldman Reservoir is also located in this region, near the confluence of the Crowsnest, Castle, and Oldman Rivers. It captures spring streamflow originating from melting snowpack in the headwaters, thus ensuring a late-summer water supply for irrigation diversions and other downstream users (i.e., municipalities) (Oldman Watershed Council, 2010).

The headwaters of the ORB are located in the Rocky Mountains in the western-most portion of the basin, between the Foothills Region and the Continental Divide. Three sub-basins drain this region: the Castle, Crowsnest, and Oldman Rivers, which join the main stem of the Oldman River at the Oldman Reservoir. This region is underlain by carbonate and quartzite bedrock of Palaeozoic and Mesozoic age, as well as Devonian limestones. Surface cover is primarily composed of glacial deposits of late Wisconsinan

age (Workum and Hedinger, 1992; Bayrock and Reimchen, 2007). Valley bottoms throughout the Rocky Mountain region of the ORB, and specifically the Crowsnest Pass, are characterized by coarse, non-glacial alluvium on stream banks, surrounded by glacial outwash plains and kames. Vegetation in this region is dominated by montane forests consisting of lodgepole pine (*Pinus contorta*), whitebark pine (*Pinus albicaulis*), white spruce (*Picea glauca*), Engelmann spruce (*Picea engelmannii*), Douglas fir (*Pseudotsuga menziesii* var. *glauca*), subalpine fir (*Abies lasiocarpa*), alpine larch (*Larix lyallii*), and trembling aspen (*Populus tremuloides*). At high elevations, alpine meadows consist of low shrubs and grasses. Vegetation in this region is described in more detail in section 3.2, as the study watershed is characteristic of the larger headwaters region.

As mentioned, the climate of the ORB varies along an east-west gradient. The foothills represent a transition zone: east of the foothills the region is semi-arid, receiving 300 – 450 mm of precipitation annually; west of the foothills, 500 - 600 mm of precipitation is received. In the semi-arid portion of the basin, potential evapotranspiration exceeds precipitation due to low precipitation and hot, dry, windy summers. This causes very dry soil conditions, thus irrigation is essential to maintain agricultural productivity. The main tributaries of the Oldman River are therefore highly controlled with reservoirs, water diversions, and irrigation canals to divert water from the Oldman River to agricultural users. The water used throughout the summer is captured during the spring freshet, when melting snowpack in the headwaters produces high river discharges. Population growth, combined with water withdrawals by irrigators and decreasing river discharge has placed considerable stress on water resources in the ORB (Rood *et al.*, 2008).

3.2 Detailed Site Description

The watershed under investigation is located in the Crowsnest Pass region of southwestern Alberta, Canada. Star Creek is a small montane headwater basin of ~1059 ha that feeds the Crowsnest River. The watershed is located at 5496117 m N, 674968 m E (UTM Zone 11N), 7.5 km southwest of the town of Coleman, Alberta (Fig. 3.3).

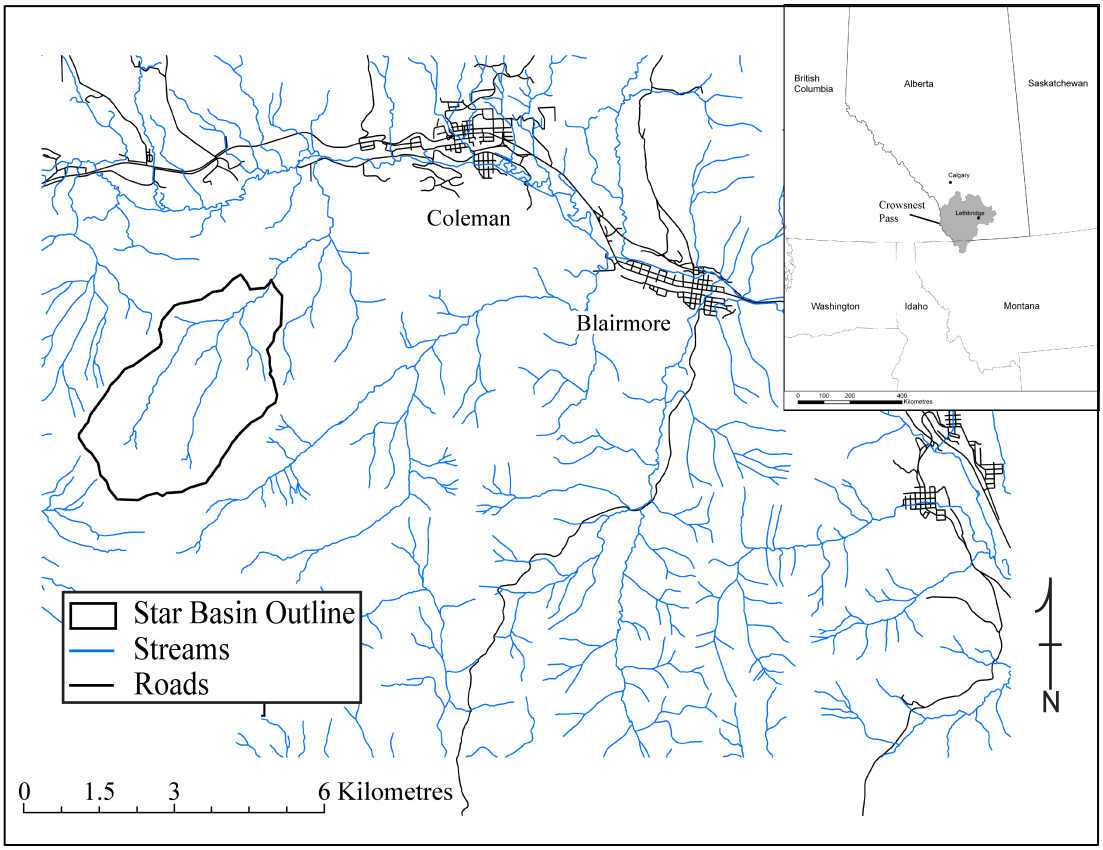

Figure 3.3. Location of Star Creek watershed, in relation to the communities of Coleman, Blairmore, and Bellevue-Hillcrest, Alberta Canada.

This watershed is part of the Southern Rockies Watershed Project (SRWP), which was initiated after the 2003 Lost Creek Fire to investigate the effects of wildfire on water quality and quantity. The SRWP includes seven instrumented watersheds that sustained a range of disturbance severities due to the fire and post-fire salvage logging. Star Creek is a 'control watershed', as it has not been subjected to disturbance, and has been

instrumented with meteorological and hydrometric stations since 2004. Four meteorological stations in the Star Creek basin record precipitation, air temperature, and relative humidity, and are equipped with telemetry systems for remote data collection. Three hydrometric stations continuously record stream stage and water quality using a variety of methods (Bladon *et al.*, 2008) (Fig. 3.4).

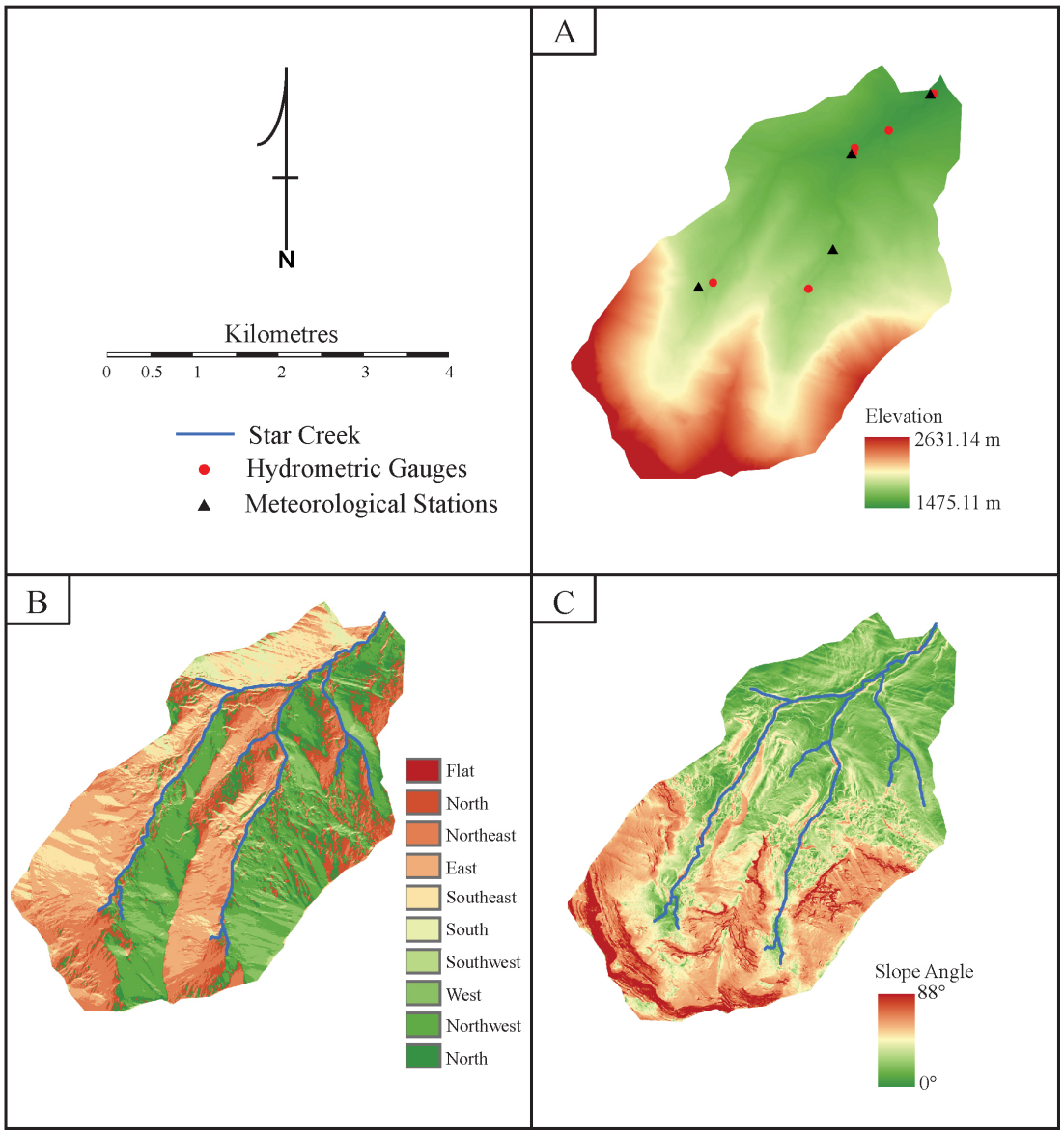

Figure 3.4. Topography within the Star Creek watershed derived from a 1 m resolution Light Detection and Ranging (LiDAR) digital elevation model (DEM) (data provided by Alberta Sustainable Resource Development, Forest Management Branch): (a) elevation, (b) slope aspect, (c) slope angle.

Three tributaries feed the main stream of Star Creek: West Fork, East Fork, and McLaren Creek. These tributaries are largely groundwater fed and originate at high elevations in the southwest portion of the watershed. These tributaries form a confluence just upstream of a SRWP hydrometric gauge at the northeast tip of the watershed, which represents the basin outlet (Silins and Wagner, 2007; Bladon *et al.*, 2008; Silins *et al.*, 2009). For the purposes of the project, the gauge location was used to define the watershed outlet (Wagner, pers. comm.).

Elevations in the watershed range from 1475 m to 2631 m.a.s.l. (Fig. 3.5), aspects are primarily east and west facing, and slopes are moderate (flat - 20°) across much of the watershed. Steep slopes (> 30°) occur in the high alpine zone, and along the banks of several stream reaches (Silins and Wagner, 2007) (Fig. 3.4).

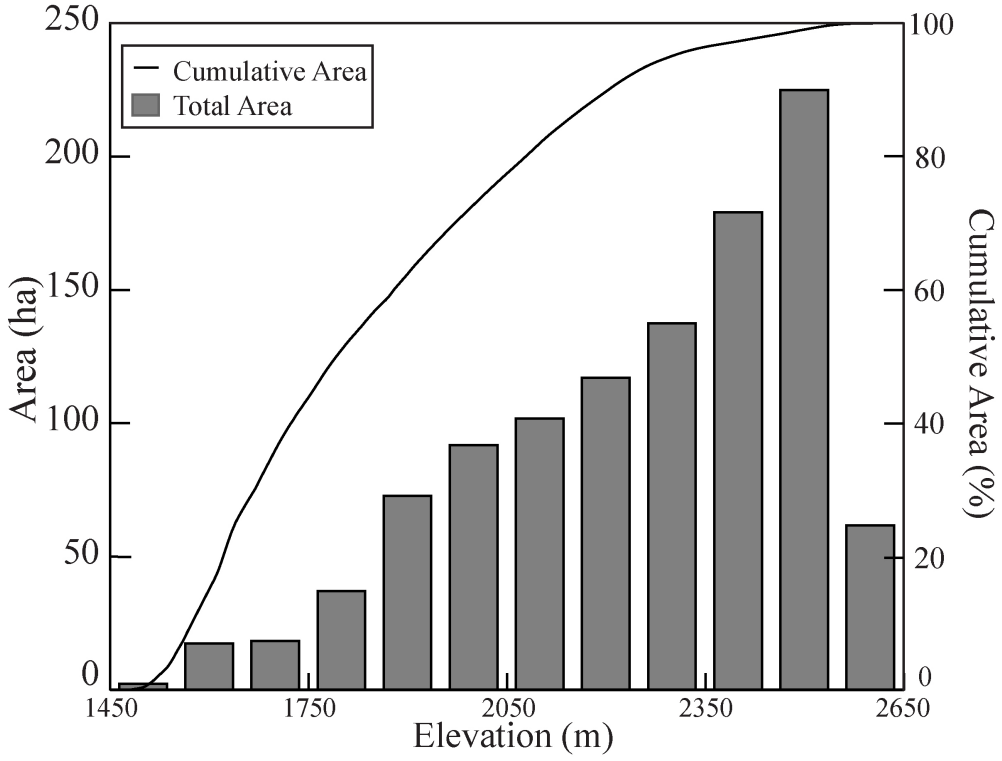

Figure 3.5. Hypsometry of Star Creek: cumulative and absolute area (100 m elevation bands).

Geologically, this region encompasses the northern tip of the Flathead Range, and portions of the Blairmore Ranges of the southern Canadian Rockies (Silins *et al.*, 2009). In Star Creek, surficial geology ranges from leached glacial till and colluvium at low elevations to talus, cirque tills, and exposed bedrock at higher elevations, which is characteristic of other catchments in this region (Bayrock and Reimchen, 2007).

Vegetation cover in the watershed consists of montane forest below elevations of 1900 m. At lower elevations (< 1700 m), the forest is dominated by lodgepole pine and Engelmann spruce with interspersed clonal stands of trembling aspen. At mid-elevations (1700 – 1900 m), subalpine forest dominates with a combination of subalpine fir and Engelmann and white spruce. Above 1900 m elevation, alpine meadows consisting of low grasses and coniferous shrubs, talus slopes, and bare rock are characteristic (Silins *et al.*, 2009) (Fig. 3.6).

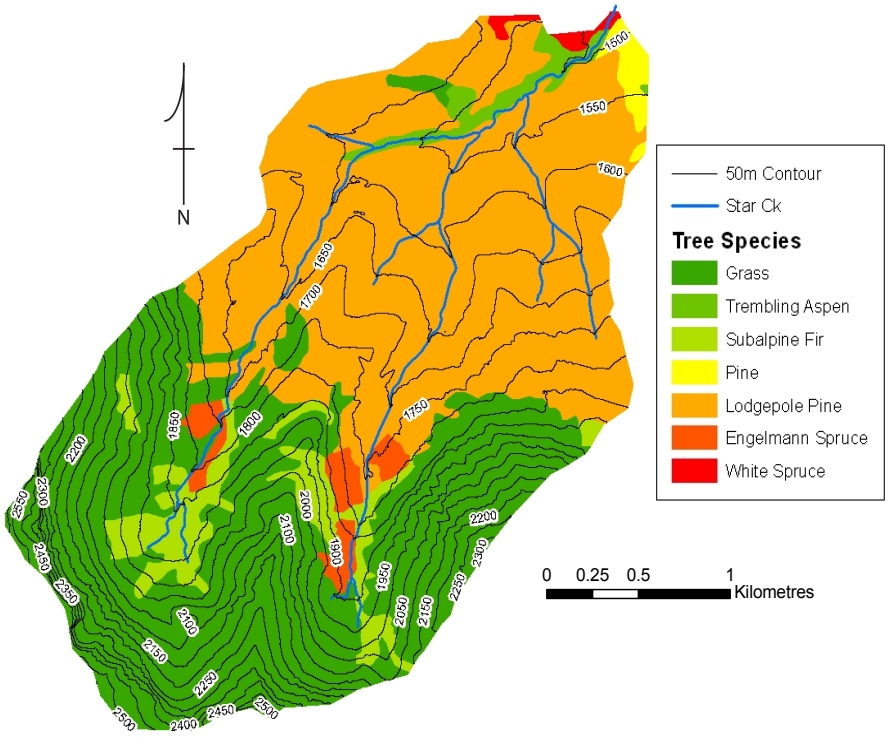

Figure 3.6. Distribution of vegetation species within Star Creek (Alberta Vegetation Index data provided by Alberta Sustainable Resource Development, Forest Management Branch).

The study basin is characterized by a cold, temperate continental climate (Nkemdirim, 1996). Precipitation in Star Creek shows high interannual variability and strong topographic gradients. Average annual precipitation is 882 mm, ~50% of which falls as rain (2004 – 2008 average from SRWP Star Creek meteorological station, Silins *et al.* (2009)) (Fig. 3.7) (Environment Canada, 2011). Unlike other Rocky Mountain basins with similar topography and located along the Continental Divide, substantial rain events are common during the winter and spring months (December to May) (Silins *et al.*, 2009).

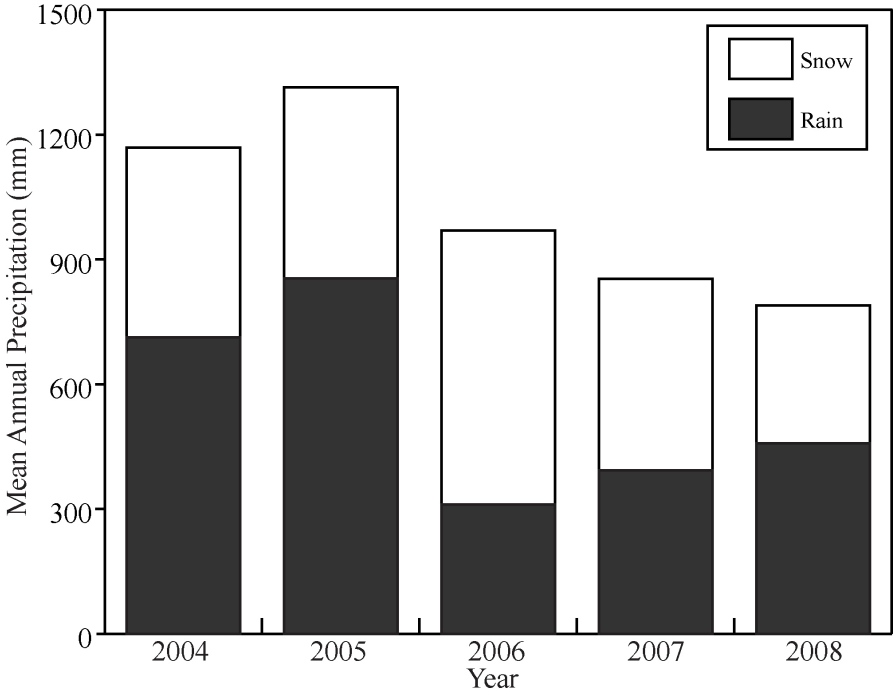

Figure 3.7. Proportion of mean annual precipitation falling as rain or snow for the period 2004 – 2008 measured by SRWP (modified from Silins *et al*. (2009)).

The 30-year average annual precipitation and air temperature record from Environment Canada's weather station in Coleman (Environment Canada, 2011) (Fig. 3.8) indicates that rain may account for 20 – 45% of mean monthly precipitation during winter. Air temperatures can be well above 0°C during winter months, which results in

average winter air temperatures > -7°C. This region of Alberta experiences frequent chinook activity during winter, with an average of 48 – 50 chinook days per winter, potentially resulting in high rates of mid-winter melt (Nkemdirim, 1996). While Environment Canada's weather station is at an elevation of 1341 m.a.s.l., ~100 m lower than the minimum elevation in Star Creek, it provides key information on long-term climate patterns.

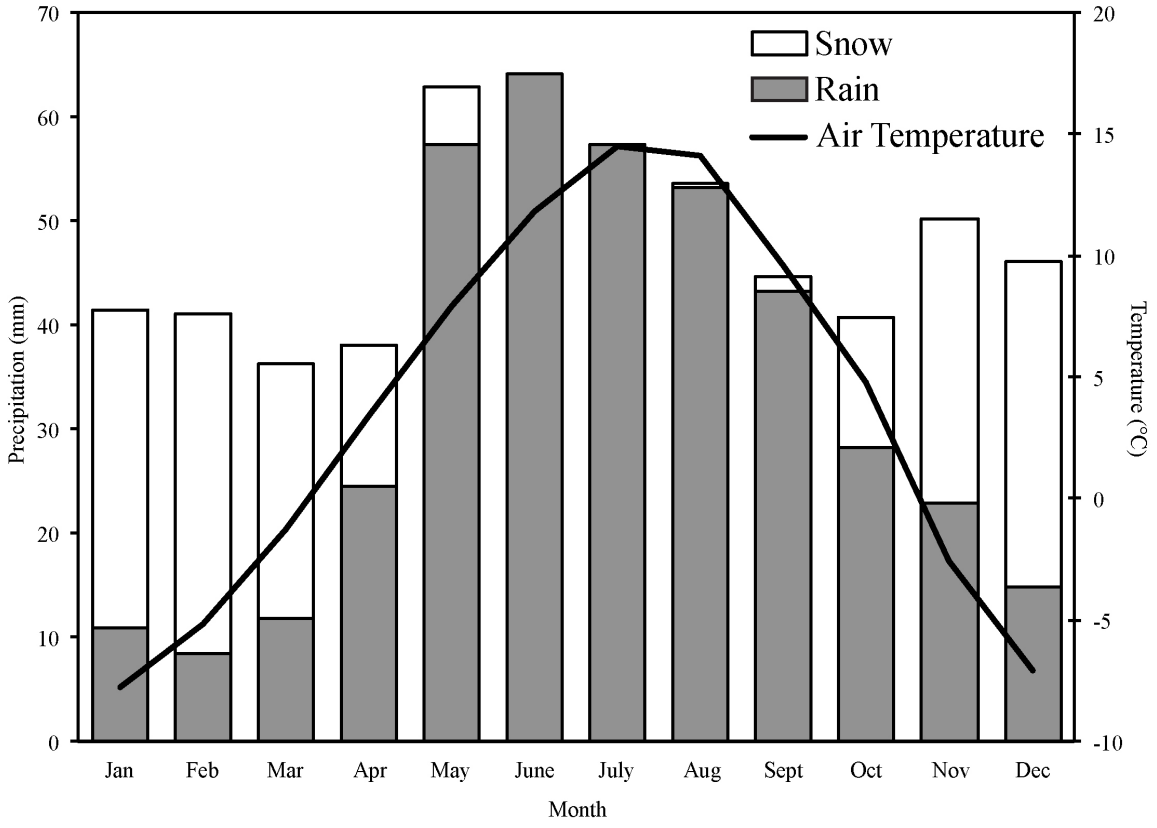

Figure 3.8. 30-year (1971 – 2000) monthly average precipitation and air temperature from Environment Canada's station at Coleman, Alberta. The station is located approximately 7 km NE of Star Creek, and 100 m below its minimum elevation (modified from Silins *et al.*, 2009 with additional data from Environment Canada, 2010).

4.0: Snow Sampler Error Analysis

4.1 Introduction

Snow water equivalent (SWE) is the most important property when measuring snow in the field, and is calculated from measurements of snow depth and density collected via snow surveys (Adams and Barr, 1974a; Pomeroy and Gray, 1995). Snow depth is generally recorded using a graduated probe inserted into the snowpack until the ground surface is reached. Typically, more snow depth than density measurements are collected (Dickinson and Whiteley, 1972; Goodison *et al.*, 1981), as depth is more spatiotemporally variable given its dependence on accumulation and redistribution processes rather than meteorological and metamorphic processes. A 3:1 ratio of depth to density measurements usually provides sufficient statistical power to detect moderate differences in SWE (~ 4 cm) (Spittlehouse and Winkler, 1996). Due to high small-scale variability in snow depth, multiple measurements are made at each sampling station and averaged to account for this variability (Goodison *et al.*, 1981).

Snow density is measured using snow pits or snow surveys. Snow pits are dug to the base of the snowpack, and samples are collected at regular vertical intervals along the snow profile using a cutter of known volume, then bagged and weighed on a balance (Adams and Barr, 1974b). This method provides the greatest vertical resolution within the snowpack and consequently is the most accurate measure of snow density (Woo, 1997). However, it is very time consuming and destructive, particularly in deep snowpacks (Pomeroy and Gray, 1995). For large-scale measurements of snow density, snow surveys are conducted along a series of snow courses using a snow tube (Church, 1933; Adams and Barr, 1974b; Goodison *et al.*, 1987; Woo, 1997). Snow courses are

transects that have been designed to allow repeated measurements of snow properties to monitor temporal changes in snow accumulation. Permanently marked sampling points ensure that subsequent sampling occurs in a well-defined area to minimize the effects of confounding factors such as topography and vegetation cover (Goodison *et al.*, 1981; Woo, 1997).

A snow tube is a hollow tube with a toothed cutter on one end and a handle on the other to twist the tube through the snowpack. Tubes can be constructed of virtually any rigid material; aluminum, fibreglass, or Lexan are most common (Adams and Barr, 1974b). The purpose of the cutter is to allow penetration of any ice layers within the snowpack (including ground ice) with a minimum of effort and as little compression of the snow core as possible. The cutter is usually tapered such that the toothed end is of smaller diameter than the tubing, thus allowing the snow core to slide up the tube with a minimum of resistance (Bindon, 1964). The cutter also incorporates a narrow ledge just above the teeth to aid core retention (Clyde, 1932; Bindon, 1964). The cutter must also be able to cut a plug of soil from the ground to help ensure the snow core is retained as the tube is extracted from the snowpack (Pomeroy and Gray, 1995). The snow tube is less precise than a snowpit because it collects a snow core from the full depth of the snowpack, vertically integrating the densities of all snowpack layers into a single sample; however, workload and snowpack destruction are considerably reduced with this method (Adams and Barr, 1974a; BC Ministry of Environment, 1981; Goodison *et al.*, 1981; Pomeroy and Gray, 1995).

Snow tubes sample the snowpack by forcing the tube through the snowpack to ground. The presence of hard layers within the snowpack – particularly ice lenses – may

lead the surveyor to incorrectly assume that the complete snow depth has been sampled. Additionally, the increased downward force and sawing action required to cut through these layers may cause the underlying snow to collapse, thus shortening the apparent snow core. This is particularly problematic if layers of loose, granular snow or depth hoar crystals are present at the base of the snowpack or below hard layers or ice lenses. Thus, the surveyor is required to obtain a core length that is ≥ 80% of the measured snow depth (BC Ministry of Environment, 1981). This ensures that the snow core is minimally compressed, and that the full depth of the pack is sampled.

4.1.1 Description of Samplers

Three snow tubes were compared in this study (in order of age): Standard Federal, Meteorological Service of Canada (MSC), and SnowHydro (Fig. 4.1). The Adirondack design is another large diameter, fixed length tube that has been extensively tested. While it is also discussed here, it was not evaluated in this study because an example was not available.

The Standard Federal dates from the 1930's and is the oldest snow tube design, and the most widely used sampler in North America, primarily in the western mountain ranges (Clyde, 1932; Beaumont, 1967; Goodison *et al.*, 1981; Woo, 1997). The current Federal design is based on the Mt. Rose sampler, designed in 1908 by J.E. Church, which was modified in the 1930's by G.D. Clyde to reduce the diameter. Although the terms Mt. Rose and Standard Federal are often used interchangeably in the literature, they actually refer to the original and current designs, respectively (Clyde, 1932).

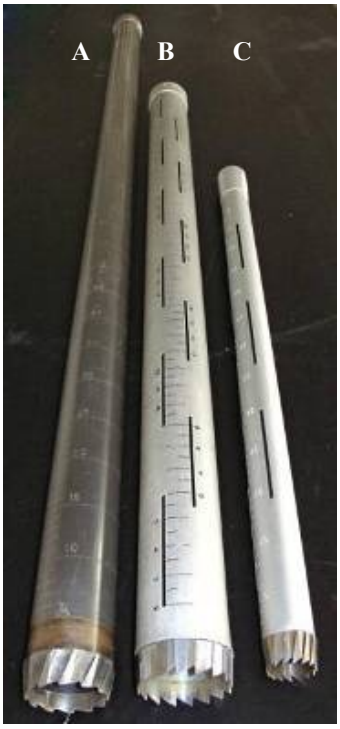

Figure 4.1. Snow tubes used in this study: A: SnowHydro, B: MSC, C: Standard Federal (one section)

The Federal snow tube is constructed of aluminum and has observation slots cut lengthwise to read the length of the core. It has a small diameter (3.772 cm, Fig. 4.2) to facilitate penetration to snow depths ≥ 5 m (Woo, 1997), and is constructed of several 0.78 m sections that can be added or removed depending on snow depth. Both an 8- and a 16-tooth steel cutter design are available, with the latter being the most common. This tube is used in conjunction with a specially calibrated spring scale that reads in units of SWE: given the cutter diameter, 2.54 cm (1 inch) of SWE will weigh ~28.4 g (1 ounce), allowing simple calibration of the scale (Clyde, 1931; Clyde, 1932; Bindon, 1964).

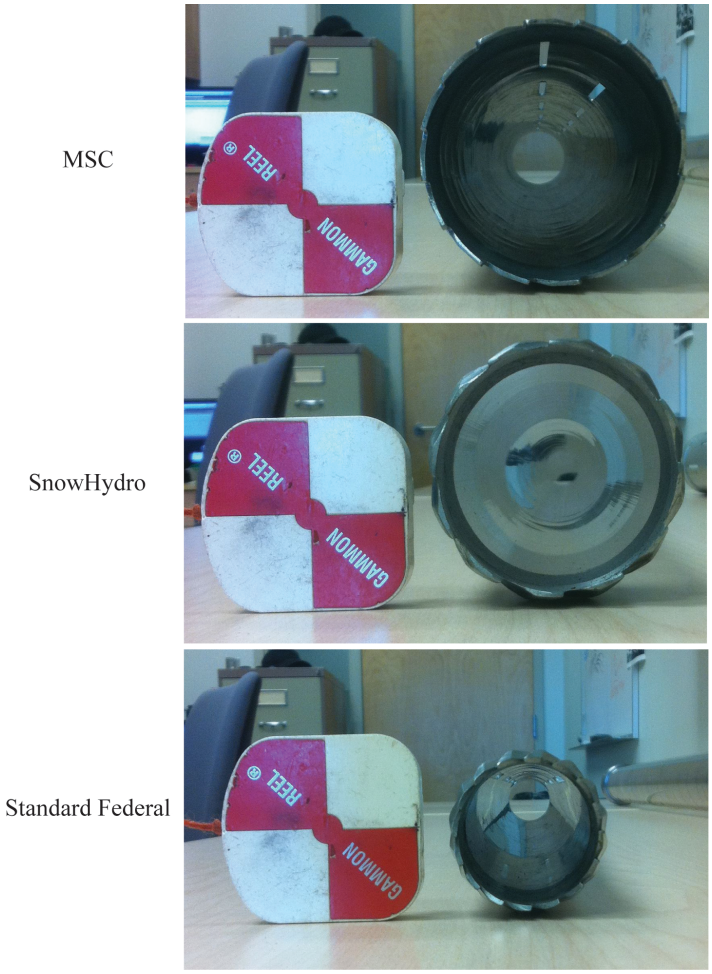

Figure 4.2. Comparison of inner diameter of snow tubes used in this study: A: MSC, B: SnowHydro, C: Standard Federal.

The Adirondack snow tube is a large diameter, fixed length design that is commonly used in the eastern United States. It is constructed of aluminum or fibreglass, the aluminum version having observation slots. The inner diameter of the Adirondack is 6.774 cm, allowing a larger sample to be collected, and thus increasing accuracy. At ~1.5 m in length, it was primarily designed for the ≤ 1.5 m snowpacks encountered in the Adirondack and Appalachian Mountains. As these snowpacks are deeper than those of the surrounding area (e.g., western New York, southeastern Ontario, Vermont), the Adirondack is seldom used outside this area. Two cutter designs are common: a steel cutter with 40 teeth or a simple toothless ring for sampling unstratified snowpacks

(Goodison *et al.*, 1981). No specially calibrated scale is provided with this tube, so samples are bagged for later weighing.

The MSC snow tube was designed by the Meteorological Service of Canada specifically for use in snowpacks on the prairies or in eastern Canada that are generally < 1.0 m deep (Bindon, 1964; Goodison, 1978; Goodison *et al.*, 1981). The MSC can be constructed of either aluminum or clear Lexan, with the aluminum version having either slots or holes to read core length. The inner diameter of 7.051 cm is nearly twice that of the Standard Federal (Fig. 4.2), and somewhat larger than the Adirondack. This allows the MSC to collect larger samples to provide increased accuracy in shallow snow. The MSC has a 16-tooth steel cutter similar to the Standard Federal, and a fixed length of ~1.1 m. A scale reading in units of SWE may be included with the tube, but samples are commonly bagged for later weighing on a balance.

The SnowHydro is a relatively new design fabricated by Matthew Sturm's SnowHydro company in Fairbanks, AK. It has a fixed length of 1.6 m and is constructed of clear Lexan, eliminating the need for observation slots and thus improving tube accuracy (SnowHydro, 2004). It is meant to merge the increased accuracy of the larger diameter Adirondack with the advantages of the proven Federal cutter design (SnowHydro, 2004): the 6.185 cm inner diameter of the SnowHydro is similar to the Adirondack, and its 12-tooth cutter is similar in design to the Standard Federal (Fig. 4.2). The tube length is appropriate for snow depths ≤ 1.6 m, slightly deeper than the Adirondack. A calibrated spring scale is not available for this tube, so samples are bagged in the field for later weighing. Detailed technical specifications for each sampler are summarized in Table 4.1.

Table 4.1. Technical specifications of snow tubes used in this study. Although not tested, specifications for the Adirondack are provided for comparison (after Goodison et al., 1981; SnowHydro, 2004).

	Standard Federal	**MSC**	**Adirondack**	**SnowHydro**
Material	Aluminum	Aluminum or Lexan	Aluminum or fibreglass	Lexan
Tube Length (m)	0.76 (each section)	1.1	1.5	1.6
I.D. of cutter (cm)	3.772	7.051	6.744	6.185
Cutter teeth (#)	16	16	0 or 40	12
Depth of snow that can be sampled (m)	≥ 5.0	1.0	1.5	1.6

4.1.2 Previous Work on Uncertainty in Snow Tube Measurements

Extensive studies were completed in the 1960's and 1970's to characterize the errors involved in sampling with snow tubes (Bindon, 1964; Freeman, 1965; Work *et al.*, 1965; Beaumont, 1967; Peterson and Brown, 1975; Goodison, 1978; Farnes *et al.*, 1982; see Table 4.2). This previous research focused primarily on the effect of snow tube and cutter design on the accuracy of tube measurements under a variety of snow conditions. The most significant sources of error were found to be the presence/absence of slots in the tube, and cutter design and maintenance.

Table 4.2. Average % error of common snow tube designs. See Farnes et al. (1982) for detailed testing results (data from Bindon, 1964; Freeman, 1965; Work et al., 1965; Beaumont, 1967; Peterson and Brown, 1975; Goodison, 1978; Farnes et al., 1982). Notes: NT

Study	**Location**	**Average % Error**			
		Standard Federal (slotted)	***Standard Federal (non-slotted)***	***Adirondack***	***MSC***
Bindon (1964)	Mount Forest, Ontario, Canada	6	NT	NT	NT
Freeman (1965)	Mt. Hood, Oregon, U.S.A.	9.8	11.3	1.7	NT
Work *et al.* (1965)	Mt. Hood, Oregon, U.S.A.	10.5	NT	1.5	NT
Work *et al*. (1965)	Alaska, U.S.A.	8.2	10	1.9	NT
Beaumont (1967)	Mt. Hood, Oregon, U.S.A.	11.2	10.8	-0.4	NT
Peterson and Brown (1975)	California, U.S.A.	9	NT	NT	NT
Goodison (1978)	southern Ontario, Canada	4.6	NT	0	6
Farnes *et al.* (1982)	Alaska, U.S.A.	10	NT	-0.2	7

In a comparison between a slotted and non-slotted Standard Federal in deep snow conditions (> 2 m), the slotted sampler measured 109 mm greater SWE than the non-slotted sampler (Beaumont and Work, 1963). Importantly, the measurement error of the Standard Federal increased as snow density approaches 250 kg m^{-3}; this is likely due to the twisting action required to penetrate a dense snowpack, which allows the slots to 'shave' snow into the tube (Beaumont and Work, 1963; Peterson and Brown, 1975; Goodison *et al.*, 1981). Non-slotted tubes (e.g. Lexan) do not have this problem.

The design and maintenance of the cutter may also influence the amount of snow collected in the tube (Bindon, 1964; Work *et al.*, 1965). A portion of the SWE overestimation observed with the Standard Federal can be attributed to the cutter design, which tends to force excess snow into the tube (Work *et al.*, 1965). A sharp, well

maintained cutter allows for cleaner separation of the core from the snowpack, thus reducing SWE overestimation by up to half (Bindon, 1964; Beaumont, 1967). The number of cutter teeth may also influence tube performance. Generally, cutters with fewer but larger teeth tend to break crust or ice layers into larger chunks, which may jam a small diameter tube and cause snow ploughing (i.e., pushing snow away from the tube opening before it can be collected) and snowpack under-sampling. A cutter with more, smaller teeth is less likely to experience this issue, although smaller teeth require greater effort to cut hard layers (Bindon, 1964).

A well-maintained cutter with sharp teeth will minimize the downward force required to cut through hard layers, and reduce the possibility of collapsing the underlying snow. Regardless, the 80% sampling rule ensures that the full snow depth is collected. Collection of a soil plug with the snow core provides further confidence that the entire snowpack has been sampled, and helps with core retention in the tube (BC Ministry of Environment, 1981).

4.1.3 Rationale and Objectives

Although the Standard Federal and MSC tubes used in this study have previously undergone error analyses, these studies have primarily been conducted at two locations: Mt. Hood, Oregon, a maritime climate with deep, rain-on-snow dominated snowpacks producing high SWE (Work *et al.*, 1965; Lillquist and Walker, 2006), and southern Ontario, a continental climate with shallow, highly stratified snowpacks typically < 1 m deep (Adams, 1976; Goodison, 1978). In this study, I re-assess the performance of each sampler given the snow conditions particular to our study site (Crowsnest Pass, AB),

where a dry continental climate results in a shallower snowpack, but mid-winter melt due to frequent chinook events creates a highly stratified snowpack.

In addition, the SnowHydro design is relatively new and has therefore not undergone a rigorous analysis of its sampling error. As we primarily use this sampler in our field campaign, error information is required to determine data quality for analysis related to basin-wide snow distribution calculations.

The relative performance of the SnowHydro, Standard Federal, and MSC snow tubes are compared under the snowpack conditions encountered in Star Creek. The Standard Federal and MSC results are compared with previous research to assess differing performance under these conditions; however, to our knowledge this is the first analysis of the SnowHydro design in comparison with the other snow tubes. To accomplish these goals, the following objectives were identified:

1) Collect collocated samples in the field with each sampler type, thus minimizing variability in snowpack properties between samplers

2) Statistically compare SWE measured with each sampler to determine relative performance under a mature forest canopy and clearcut conditions given the unique meteorological and snow accumulation conditions of the study area

3) Statistically compare the sampler SWE data to SWE data derived from high-resolution snow pit and snow depth measurements to quantify relative accuracy.

4.2 Study Area

Fieldwork was completed in the Star Creek watershed (Fig. 4.3), located in the Crowsnest Pass, Alberta, Canada (see Ch. 3.2 for a detailed description of the watershed).

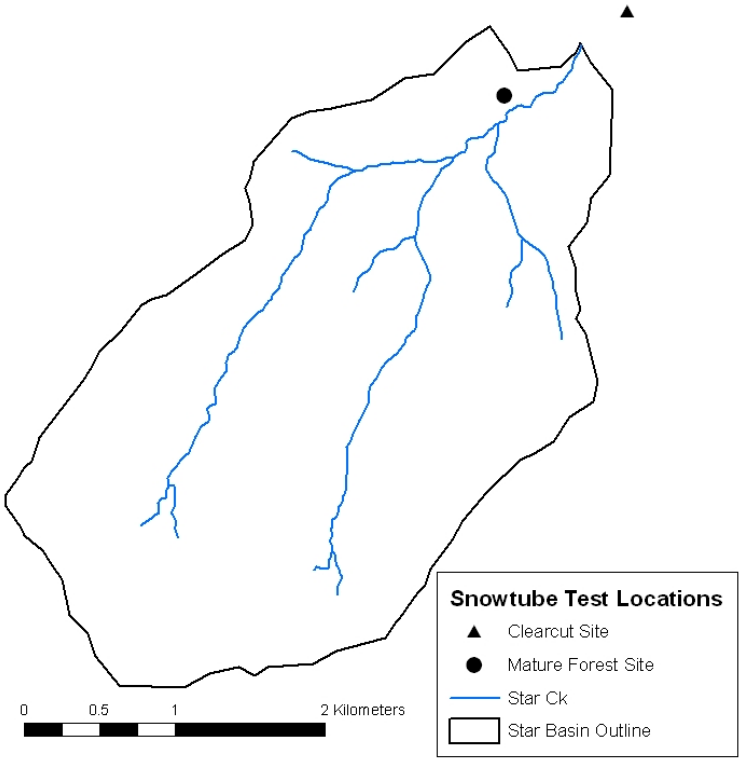

Figure 4.3. Location of sampling grids with respect to Star Creek watershed (see Fig. 3.3 for location of Star Creek in Alberta, Canada).

Two snow survey grids with 36 permanently marked sampling points spaced at 5 m intervals were established within the watershed to capture within- and between-stand variability in each of the two vegetation cover types that dominate the larger study watershed (Fig. 4.4). The first grid was located in a clearcut just north east of the Star Creek watershed boundary, and the second grid was established in a homogeneous mature lodgepole pine (*Pinus contorta* var. *latifolia*) stand (Fig. 4.5a, b). The sites were ~1 km apart, both are level, and have an elevation difference of 50 m.

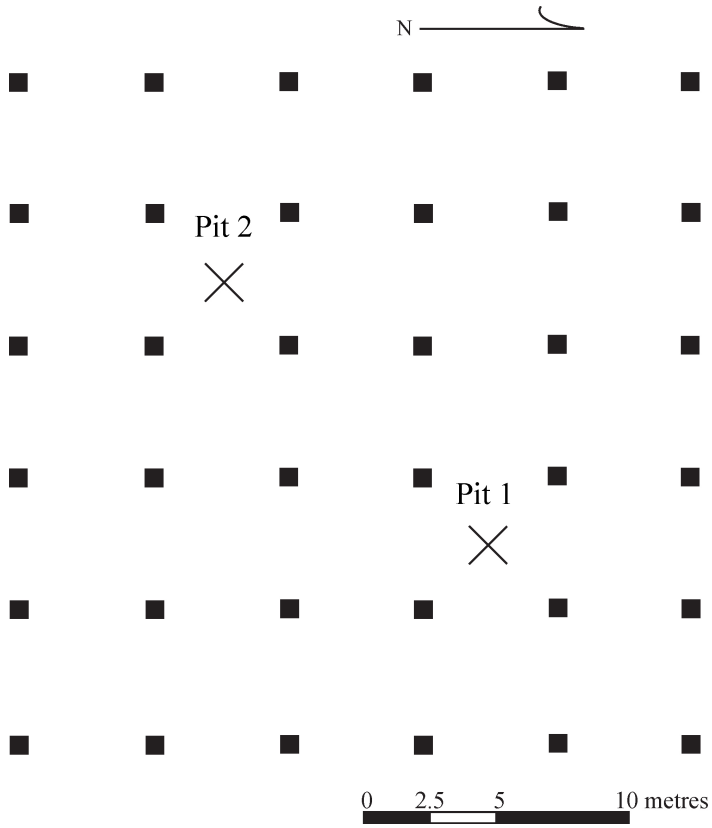

Figure 4.4. Schematic of the snow survey grids, both of which were oriented in approximately the same direction. Snow pits (noted by X) were located away from the edge of the grid to provide representative measurements of snow conditions encountered in the grid.

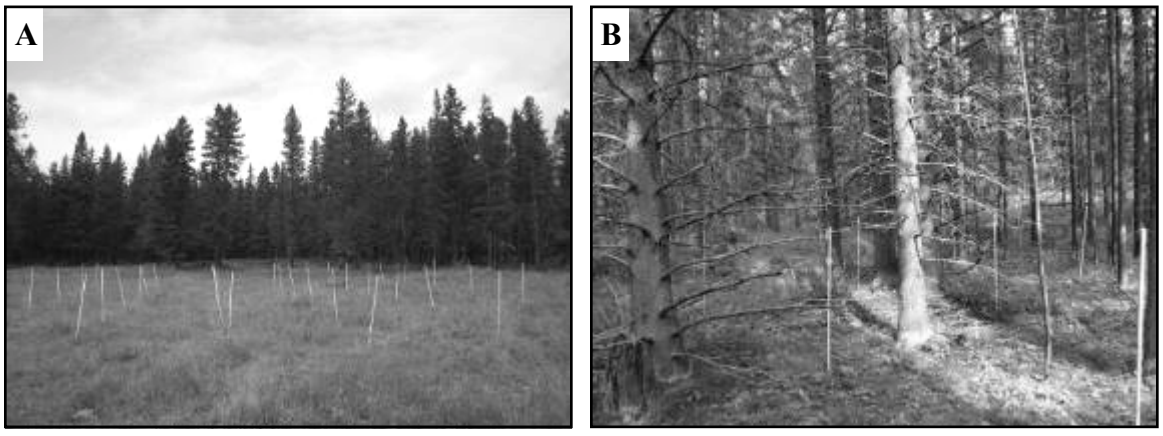

Figure 4.5. Sample grids: (A) clearcut site; and (B) mature forest site.

The clearcut site is highly wind-exposed and thus had potential for high rates of wind transport; however, the sampling grid was sheltered from the prevailing wind by a mature pine stand ~100 m west of the grid location. Wind conditions may, however,

contribute to snow compaction and wind slab development in this area. Additionally, the lack of forest canopy allows for maximum incoming solar radiation, which may form solar crusts and melt/freeze layers. These factors may result in considerable snowpack stratification, potentially creating challenging sampling conditions. Despite the potential for greater wind transport and higher melt rates, snow depths will be greater in this site than the forest, as there is no canopy to intercept incoming snow.

While the forest site is highly sheltered from wind and solar radiation, the forest canopy creates a mosaic of sun-lit and shaded areas that can potentially cause high variability in snowpack properties within the grid. Snow depth is likely to be shallower in sun-lit areas, and have higher density due to melting effects caused by exposure to direct solar radiation (Ellis *et al.*, 2011). This grid is exposed to high longwave fluxes from the surrounding tree stems, resulting in differential melt rates with proximity to tree trunks, and subsequent effects on snow depth, density, and SWE in these areas (Pomeroy *et al.*, 2009). This site is also subject to internal ice layer formation due to canopy drip of melting intercepted snow (Schmidt *et al.*, 1988; Schmidt and Gluns, 1991; Storck *et al.*, 2002). Interception is very important relative to the clearcut, thus lower snow depths are expected in this site.

4.3 Methods

4.3.1 Sampling Strategy

Snow tube measurements were collected on March 21 and 22, 2011. Snow cores were collected with each of the three samplers at each of the 36 sampling points at each study site, ensuring a snow core of at least 80% of the measured snow depth was

collected (BC Ministry of Environment, 1981). A soil plug was extracted with each snow core, and removed from the snow tube prior to bagging the sample using a knife so that no snow was lost. Snow depth was also measured at each sample point using a graduated probe (cm). Cores were placed in numbered, pre-weighed Ziploc bags, and then weighed on a calibrated Denver Instrument MXX-2001 balance with 2000 g capacity and 0.1 g resolution. Snow density was calculated from Eq. 4.1, with individual bag weights used to tare the total sample weights.

$$\rho_s = \frac{W_s}{(\pi \times (Radius_{Cutter})^2) \times d_s} \quad 4.1$$

where ρ_s is the density of the snow sample (g cm^{-3}), W_S is the weight of the snow sample, RadiusCutter is the inside radius of the cutter on the snow tube (cm), and d_s is snow depth measured from the snowtube (cm).

SWE was then calculated from Eq. 4.2:

$$SWE = d_S \frac{\rho_s}{\rho_w} \quad 4.2$$

where d_s is the measured snow depth (cm), ρ_s is the density of the snow sample (g cm^{-3}), and ρ_w is the density of water (1 g cm^{-3}).

As noted previously, the Standard Federal tube includes a spring balance that reads in units of SWE. This balance was also used to measure SWE (termed *Cradle SWE*) prior to bagging and weighing the tube sample. As the balance weighs the tube and snow sample together, the initial weight (in SWE) of the empty tube was recorded. Filled tubes were then weighed and the empty tube weight used to tare the scale to obtain the sample SWE. The weight of the empty tube was recorded repeatedly throughout the test to account for any snow or ice build-up inside the tube caused by thermal changes.

Two snow pits were dug at each site using standard techniques (cf. Adams and Barr, 1974b), at approximately the same time on each sampling day. The pits were located within the grid to characterize snowpack structure and collect high-resolution measurements of snow density (Fig. 4.4). These data allowed for identification of hard layers, ice lenses, depth hoar, and other features that may be associated with potential sampling issues, thus allowing for better explanation of sampler performance. Each was dug through the full snow profile to ground level, the full depth measured, and dial thermometers distributed at 0.1 m intervals through the vertical profile. Snowpack temperature was measured at 0.5° C resolution. Individual layers were identified and marked with wood markers; layer depth and thickness were measured for each. Crystal type and size within each layer was assessed using a crystal card and magnifying loupe. Density samples were then extracted from the pit face in a vertical profile using a 250 cm^3 cutter (Snowmetrics, Ft. Collins, CO). Samples were placed in numbered, pre-weighed Ziploc bags and weighed on a calibrated balance (Denver Instruments MXX-2001). Density was calculated as:

$$\rho_s = \frac{W_{Sample}}{V_{Sample}} \tag{4.3}$$

where ρ_s is snow density (g cm^{-3}), W_{Sample} is the weight of the snow sample corrected for sample bag weight (g), and V_{Sample} is the volume of the density cutter (cm^3). Within each stand, snowpack densities from both snowpits were averaged, and Eq. 4.2 was used, along with depth measurements from the graduated probe at each sampling stake, to calculate SWE (termed *Pit SWE*). As snow pits provide the most accurate measure of snowpack density, this value was used as a relative control against which snow tube results were compared (Woo, 1997).

4.3.2 Data Analysis

Data were plotted with notched box plots using SYSTAT 13 (Chambers Software, Chicago, IL). Notches that overlap between boxes indicate that median values are not statistically different at $p = 0.05$ (Chambers *et al.*, 1983). Data were then analyzed with Statistica DataMiner software (StatSoft, Tulsa, OK) to calculate descriptive statistics, test normality using a Shapiro-Wilks' W test (Shapiro *et al.*, 1968), and test for homogeneity of variances using Levene's test (Quinn and Keough, 2002). A one-way analysis of variance (ANOVA) was run to quantify differences between samplers and sampling locations (Quinn and Keough, 2002). If a statistically significant difference between samplers was detected a Tukey's Honestly Squared Difference (HSD) post-hoc test was performed to determine which sampling techniques were statistically different (all tests at $p < 0.05$) (Duncan, 1955; Quinn and Keough, 2002).

Anomalous results for *Cradle SWE* were observed between the mature forest and the clearcut. Thus, the spring scale calibration was tested in the lab using two techniques: (1) converting the SWE measurement from the scale to weight in grams, and comparing that value with the core weight measured with the electronic balance; and, (2) weighing known weights of water on the spring scale at different scale temperatures. These masses spanned the weight range of the spring scale, while the temperature of the scale started at room temperature, and was cooled in three stages to -25°C. Once the scale had equilibrated at each test temperature, the control weights were measured and recorded.

4.4 Results

4.4.1 Mature Forest Stand

Weather on the day of sampling was clear and sunny with an air temperature of 5° C. Mean snow depth at the site was 52.5 ± 6.4 cm, and the mean *Pit SWE* for this grid was 13.5 ± 1.7 cm. The snowpack was characterised by three main crystal types: (1) highly metamorphosed snow with large, rounded irregular crystals with no faceting (3 – 4 mm) (stage II-B-2, Sommerfeld and LaChapelle, 1970) below ~ 19 cm above ground level (AGL); (2) consolidated fined grained snow (1 – 2 mm, stage I-A) between 19 – 23 cm AGL; and, (3) highly consolidated fine-grained, stellar crystals (< 1 mm) (stage I-A) in the upper half (above ~ 35 cm AGL). A 3 cm thick ice layer located at ~30 cm AGL was observed in both pits, and is attributed to canopy drip from a previous melt episode. A melt/freeze crust was also present at ~43 cm AGL. These layers caused sampling problems only with the Standard Federal, consistently causing jamming and snow ploughing with this tube. Thus, resampling at most points to achieve a core ≥ 80% of measured snow depth was required. Free water was present at all depths, and mean snowpack temperature was -2°C (Fig. 4.6).

Snowpack structure was similar between pits below 45 cm AGL (Fig. 4.6). The base of both pits was characterized by coarse, granular snow (3 – 4 mm), which was ~10 cm thicker in Pit 1. At 18 – 22 cm AGL, snow crystals were smaller and more consolidated (1 – 2 mm), and crystals at 20 – 25 cm AGL were a highly consolidated wind slab. These consolidated layers were overlain by an ice layer at 30 – 33 cm AGL, above which there was a layer of highly consolidated snow (1 – 2 mm) at 33 – 43 cm AGL. A melt/freeze crust was located at 43 – 48 cm AGL, and formed the surface of Pit

2, which was located under dense forest canopy. At Pit 1, located in a small clearing (~ 20 m wide), there was an additional 22 cm of highly metamorphosed, coarse grained snow (3 – 4 mm) above this crust, caused by increased accumulation due to reduced canopy interception.

All layers discussed above were encountered at similar heights AGL across the stand when performing snow tube measurements. Thus, the pits were representative of the snow conditions across this plot. Sample data from this site were normally distributed with homogeneous variances, thus meeting the assumptions required to use parametric statistics.

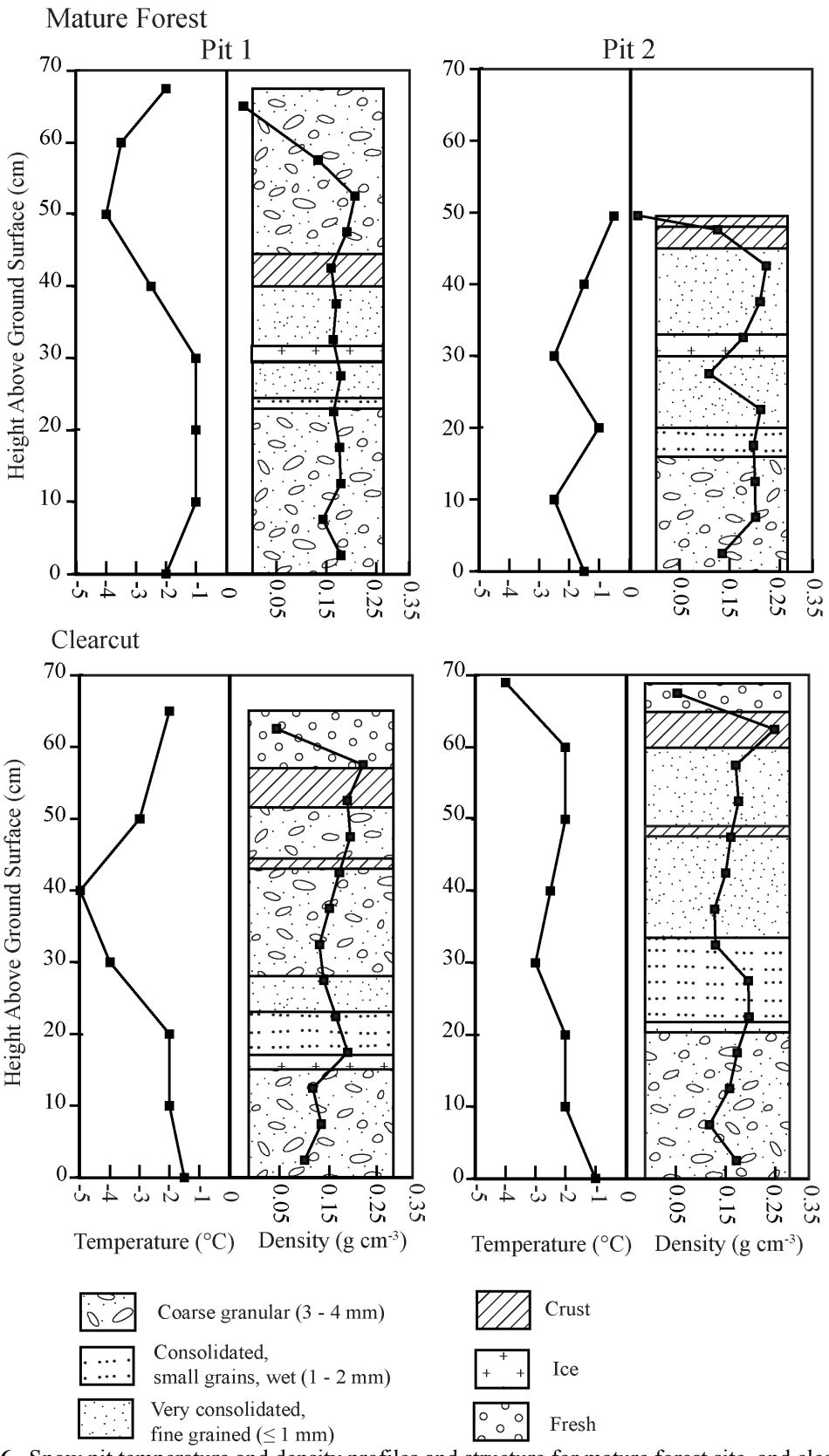

Figure 4.6. Snow pit temperature and density profiles and structure for mature forest site, and clearcut site.

In the mature forest, all snow tubes underestimated SWE, while *Cradle SWE* overestimated SWE (Table 4.3; Fig. 4.7). Relative to mean *Pit SWE*, the SnowHydro measured 12.7 ± 1.6 cm (93.5%), the Standard Federal 13.2 ± 1.8 cm (97.2%), *Cradle SWE* 15.8 ± 2.1 cm (116%), and the MSC 12.35 ± 2.1 cm (91.3%). The Cradle and MSC produced the most variable measurements of SWE across this stand, with the greatest range of values.

Table 4.3. Descriptive statistics for Pit SWE and all samplers in the mature forest site.

	Pit SWE	**SnowHydro**	**Standard Federal**	***Cradle SWE***	**MSC**
Mean SWE (cm)	13.5	12.7	13.2	15.8	12.4
Median SWE (cm)	13.6	12.5	13.1	16	12.4
Min SWE (cm)	10.8	10.0	10.36	12	4.7
Max SWE (cm)	17.1	15.8	17.5	20	15.6
Standard Deviation (cm)	1.7	1.6	1.8	2.1	2.1
Standard Error (cm)	0.3	0.3	0.3	0.3	0.4

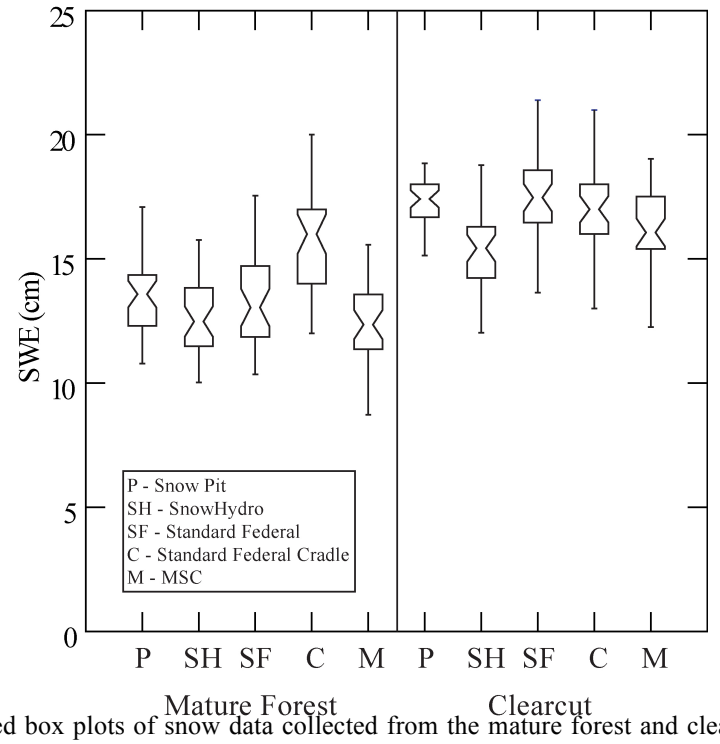

Figure 4.7. Notched box plots of snow data collected from the mature forest and clearcut stands. Boxes show 25th and 75th percentiles, the notch represents the median value, and bars represent non-outlier maximum and minimum values. Overlapping notches indicate that the median values are not statistically different. Sample size is $n = 36$ for each sampler.

The range of values from the MSC was approximately twice that of the SnowHydro and the Standard Federal. A one-way ANOVA indicated a significant difference between all samplers and *Pit SWE* ($p = 0.00$). The Tukey HSD post-hoc test indicated that none of the snow tubes were statistically different from *Pit SWE*, but *Cradle SWE* was statistically different from all other techniques (Table 4.4).

Table 4.4. Summary of results from a Tukey's HSD post-hoc test for the mature forest site. Bold cells are significantly different at $p < 0.05$.

Snow tube	SnowHydro	Standard Federal	*Cradle SWE*	MSC	*Pit SWE*
SnowHydro		0.78	**0.00**	0.96	0.25
Standard Federal	0.78		**0.00**	0.35	0.91
Cradle SWE	**0.00**	**0.00**		**0.00**	**0.00**
MSC	0.96	0.35	**0.00**		0.05
Pit	0.25	0.91	**0.00**	0.05	

4.4.2 Clearcut

Weather on the day of the clearcut survey was overcast with very light snow and an air temperature of -2° C. Mean snow depth in the clearcut site was 67.0 ± 3.5 cm and mean SWE for this grid was 17.3 ± 0.9 cm. The snowpack was characterised by highly metamorphosed, rounded, irregular crystals with no faceting (3 – 4 mm; stage II-B-2) in the lower 15 – 20 cm of the snowpack. This layer was separated from an overlying consolidated layer of small fine grained, stellar crystals (1 – 2 mm; stage I-A) by a 1 – 2 cm thick ice lens located at 25 cm depth. This lens created challenging sampling conditions, often resulting in collapsed snow cores that were less than 80% of the depth; thus multiple attempts were required to extract a valid core at each point. Another hard layer of wind slab consisting of small rounded crystals (1 – 2 mm), at ~50 cm AGL had less of an effect on sampling. The top 5 cm of the snowpack was fresh, low-density snow that accumulated overnight between surveys, but was of low density and so had little effect on total SWE. Free water was present at all levels of the snowpack, and mean pack temperature was -3°C. The ground surface was covered in logging slash, creating problems with core retention in snow tubes as it was difficult to obtain a soil core. Despite identical average snow densities, *Pit SWE* varied by 2.5 cm between Pits 1 and 2 due to a 5 cm difference in snow depth (Fig. 4.6).

Snowpack structure was very similar between pits, with the exception of a layer of coarse granular (3 – 4 mm) snow at 38 – 51 cm AGL in Pit 1. In Pit 2, this range of depths was composed of consolidated, fine-grained snow (stellar crystals, ~1 mm). A crust mid-way through these layers was encountered in both pits. The two primary hard layers identified in Fig. 4.6 (43 – 46 cm; 16 – 20 cm AGL), were consistently observed

across the plot within that depth range, thus the pits were representative of the snow conditions across this plot. Sample data from this site were normally distributed with homogeneous variances, thus the assumptions required to use parametric statistics were fulfilled.

At this site, both the Standard Federal and Cradle SWE values were virtually identical to *Pit SWE*, but the SnowHydro and MSC tubes underestimated SWE (Table 4.5; Fig. 4.7). Relative to mean *Pit SWE*, the SnowHydro measured 15.4 ± 1.6 cm (88.6%), the Standard Federal 17.5 ± 1.6 cm (101%), *Cradle SWE* 17.1 ± 1.6 cm (98.8%), and the MSC 16.1 ± 1.8 cm (93.2%). Ranges and standard deviations from all sampling methods were similar in this stand, in contrast to the mature forest. A one-way ANOVA showed a significant difference between sampling techniques (p = 0.00) (Fig. 4.7). Tukey's HSD post-hoc test showed that the Standard Federal and Cradle SWE were not significantly different from *Pit SWE*, while the MSC and SnowHydro were (Table 4.6).

Table 4.5. Descriptive statistics for Pit SWE and all samplers in the clearcut site.

	Pit SWE	**SnowHydro**	**Standard Federal**	***Cradle SWE***	**MSC**
Mean SWE (cm)	17.3	15.4	17.5	17.1	16.1
Median SWE (cm)	17.4	15.4	17.5	17	16.1
Min SWE (cm)	15.1	12.0	13.4	13	11.8
Max SWE (cm)	18.9	19.5	21.4	21	19.0
Standard Deviation (cm)	0.9	1.6	1.6	1.6	1.8
Standard Error (cm)	0.2	0.3	0.3	0.3	0.3

Table 4.6. Summary of results from a Tukey's HSD post-hoc test for the clearcut site. Bold cells are significantly different at $p < 0.05$.

Snow tube	SnowHydro	Standard Federal	*Cradle SWE*	MSC	*Pit SWE*
SnowHydro		**0.00**	**0.00**	0.19	**0.00**
Standard Federal	**0.00**		0.84	**0.00**	0.99
Cradle SWE	**0.00**	0.84		0.06	0.98
MSC	0.19	**0.00**	0.06		**0.01**
Pit	**0.00**	0.99	0.98	**0.01**	

4.4.3 Calibration of Standard Federal Spring Scale

We expected that *Cradle SWE* measurements would produce similar errors between sites, as the response of the spring scale should be independent of site and snow conditions. However, in the mature forest, the cradle weight (in grams) was consistently higher than the core weight, while in the clearcut the two were comparable (Fig. 4.8). While the spring scale is independent of site and snow conditions, it may be sensitive to air temperature. Air temperatures differed by only ~7°C between surveys, but the plots in Fig. 4.8 suggest considerable thermal drift in the scale over this small temperature range. Testing control weights at various scale temperatures confirmed this thermal drift (Table 4.7; Fig. 4.9).

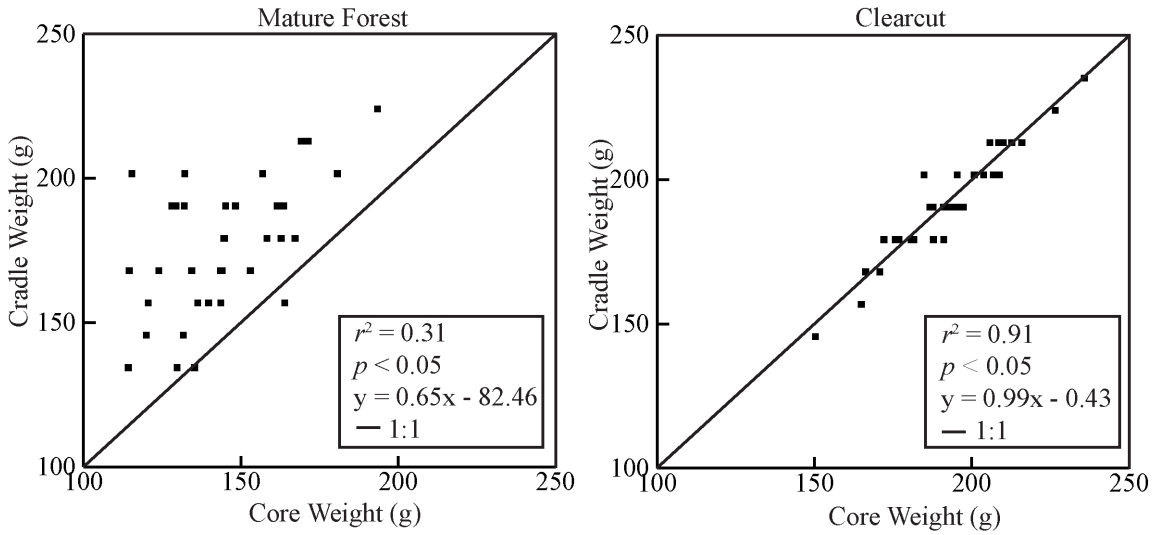

Figure 4.8. Comparison of core weights measured on an electronic balance with tube weights produced by the Standard Federal spring scale. Solid line represents 1:1 relationship; equation is for linear regression line, which is statistically significant at both sites.

Table 4.7. Summary of temperature-based Standard Federal spring scale calibration.

Control Weight (g)	Scale Temperature			
	20 °C	***0 °C***	***-18 °C***	***-25 °C***
1104	1075	1053	1053	1053
1257	1221	1210	1210	1210
1767	1702	1714	1702	1702
3024	2934	2979	2957	2657
3161	3136	3124	3114	3114

The temperature response of the scale varies depending on scale temperature and weight being measured. Overall, the scale consistently underweighs by up to 5%, with the greatest error observed at the low range of the scale and increasing accuracy with increasing weight. At the low range of the scale, the differences in weight accuracy are greatest between 20°C and 0°C, with a ~1.5% reduction in accuracy between the two. However, below 0°C scale accuracy remains consistent.

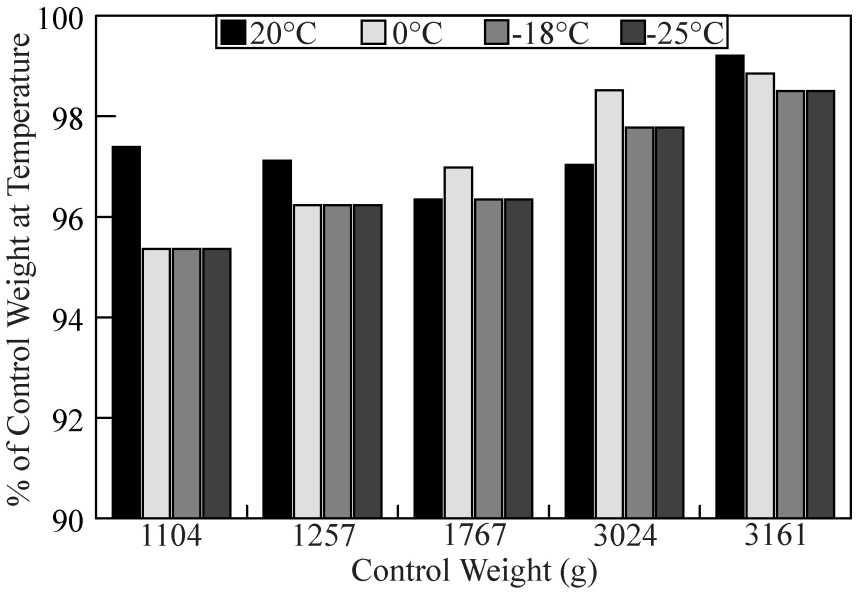

Figure 4.9. Plot of temperature response of Standard Federal spring scale over a 40°C temperature range.

At the mid-range, there is a ~0.75% increase in accuracy between 20°C and 0°C, but accuracy declines by this same amount at temperatures below 0°C. For the lower high range weight (3024 g), accuracy improved by ~1.5% between 20°C and 0°C, and then stabilized at ~ 98% below 0°C. At the highest range (3161 g) the scale produces the greatest accuracy at 20°C, and then drops as scale temperature decreases. The accuracy then stabilizes ~ 0.5% lower at a temperature of -18°C.

4.5 Discussion

Qualitatively, the performance of the three tubes was quite different. In both sites, the MSC and SnowHydro retained snow cores more consistently than the Standard Federal. The MSC and SnowHydro tubes generally did not collapse the snow profile when encountering hard layers, because their larger diameter better resisted blockage. This resulted in the MSC and SnowHydro regularly extracting cores that were ≥ 90% and ≥ 88% of snow depth, respectively. This, combined with the ability to retain cores,

meant that both tubes collected a useable sample on the first attempt without requiring resampling, thus increasing sampling speed. By contrast, the Standard Federal could only extract cores of ~80% of snow depth, due largely to the snow profile collapsing when hard layers were encountered. Multiple attempts were required to collect these cores, considerably increasing the time required to sample the grid. This is attributed to the small inner diameter of the tube, which tended to jam easily. These conditions were observed at both study sites, although all samplers had slightly more difficulty in the clearcut. The latter is due to the logging slash that was integrated into the base of the snowpack, which often prevented cutting a soil plug, or produced areas of weak snow structure that disintegrated as the tube was extracted.

The conditions encountered in this study are likely not ideal conditions for the Federal. This snow tube is specifically designed to sample deep, wind hardened snowpacks in contrast to the shallow, highly metamorphosed snow conditions encountered here. These conditions are characteristic of an early-spring snowpack, but are commonly encountered in the Crowsnest Pass throughout the winter due to frequent chinook events and resultant mid-winter melting. However, in unrelated sampling performed earlier in 2011 for data related to Ch. 6, when the snowpack was highly consolidated with little internal stratification, the Federal tube worked very well, regularly collecting valid snow cores on the first attempt and resisting jamming. Snowpack metamorphism following this sampling date resulted in a number of hard layers underlain by soft, granular layers. These metamorphic processes created challenging sampling conditions for the Standard Federal during this study, as jamming was highly likely.

SWE values measured with the Federal tube were more consistent across stands than the MSC, with lower standard deviations. The MSC was only slightly more variable because it had the most difficultly retaining cores and required resampling. However, in both stands the SnowHydro produced the lowest standard deviations in SWE that were closest to *Pit SWE*, suggesting that its design produces more consistent measurements than the other designs under these snow conditions.

Overall, greater standard deviations in the mature forest stand were likely due to the greater variability in snow depth and density produced by the mosaic of sun-lit and shaded areas across the plot. Measurement variability is reduced between samplers in the clearcut because snow depth and density were more homogeneous across the plot. There was little shelter in the clearcut plot, thus ensuring that the snowpack was uniformly exposed to meteorological processes. In this plot, the large-diameter tubes had slightly more trouble retaining cores due to the depth hoar layer at the base of the pack, which fell out as the tube was extracted or collapsed when the tube encountered an overlying hard layer. This problem was common to all samplers. Frozen ground contributed to difficulty retaining soil plugs, in addition to issues due to the presence of logging slash. However, there is no statistical reason why the two large-diameter snow tubes should be different from *Pit SWE* and the Standard Federal in this plot.

The lab test showed that the spring scale consistently under-weighs samples by ~50 g. Although this may be insignificant when sampling deep, dense snowpacks, this under-measurement becomes increasingly important when shallow or low-density snowpacks are measured. We hypothesize that the variability in the forest measurements is caused by a shift to a lower spring rate (i.e., less force required to activate the spring)

caused by higher air temperatures. With the lower spring rate, the scale is more sensitive to vibrations and thus the surveyor is more likely to read the scale incorrectly as it oscillates between values. Despite the scale weighing more accurately at higher temperatures, this oscillation may cause reading errors of ±4 cm SWE; even greater if samples are collected in windy conditions. At lower air temperatures the scale is much more resistant to this oscillation, allowing the scale to quickly settle on a value, though this value is likely not as accurate as would be expected at higher temperatures (up to –5% depending on weight). Thus, it appears that the scale worked better on the colder sampling day simply because the increased spring rate reduced human error in reading the scale. The large variability seen on the warmer day can, therefore, probably be attributed to the oscillation in the scale and associated reading errors. Although these errors may cancel out over the course of a field season, this testing highlights the potential for significant measurement error when using the spring scale. Thus, we recommend that samples always be bagged for later weighing. The errors observed in the scale match well with those reported by Howe (2006), where higher accuracy was observed at higher temperatures.

A portion of the error observed in *Cradle SWE* can also be attributed to interpolation of measurements from the scale. The scale is etched in 2 cm SWE intervals, with 2 mm between tic marks (Fig 4.10). This low resolution introduces user bias into the SWE measurement, resulting in a potential error of ±1 cm SWE, as the surveyor is required to estimate the position of the scale, potentially incorrectly rounding the value up or down. This error may represent a large proportion of shallow or low-density snowpacks.

Bray (1973) notes that scale calibration drifts through time and thus should be checked frequently; however, there is inherently error involved in using a spring scale to measure SWE (Sturm *et al.*, 2010). Over-measurement errors of SWE, similar to those found in this study were reported by Bray (1973) under similar weather conditions to those encountered on the forest survey day. Bray (1973) was able to correct his measurements by calibrating the spring scale, after which it produced similar results to weighing bagged samples. Calibration of the scale may also drift through time due to rough handling or fatigue in the spring. We found that under the colder conditions encountered in the clearcut, spring scale vs. bag weights were very comparable.

Figure 4.10. Detail of Standard Federal spring scale. Units are in 2 cm intervals of SWE, while the interval between tic marks is 2 mm.

The SnowHydro performed very well under the sampling conditions encountered for this test, and for all conditions encountered throughout data collection for Ch. 6. The large diameter resisted plugging with hard layers, and prevented cores from collapsing. The tube is constructed of Lexan, which better resists snow and ice build-up inside the

tube due to heat transfer from handling. While the SnowHydro is slightly more cumbersome to use than the modular design of the Standard Federal, its performance makes up for that limitation.

The MSC was the most resistant to collapsing snow cores, and was very difficult to jam because this tube had the largest diameter in the test. However, although it retained cores better than the Standard Federal when being extracted, it could not retain cores as well as the SnowHydro. The large diameter required much more snowpack cohesion in the lower layers to support the overlying snow. If a layer of depth hoar exists at the base of the pack, the surveyor must ensure a soil plug is collected or the sample will be lost when the tube is extracted. This was problematic in the clearcut, where logging slash often resulted in lost cores.

In contrast to previous work, overestimation of SWE with the Standard Federal and MSC samplers was not observed in this test (See Table 4.2). Rather, the MSC underestimated by approximately the same magnitude as the overestimates reported by Goodison (1978) and Farnes *et al.* (1982). Standard Federal measurements were virtually identical to *Pit SWE*, rather than the ~10% overestimate usually reported (Table 4.2). Statistical results show that the SnowHydro is not significantly different than *Pit SWE* under the mature forest canopy, the primary forest condition for sampling points used in Ch. 6. However, individual SWE measurements at each stake were underestimated by 6 – 12%, a similar magnitude of measurement error reported in other studies.

Sturm *et al.* (2010) report consistent under-measurement of SWE for surveys across the region from Manitoba to Alaska. They highlight a number of potential sources of under measurement, particularly the type of snow being sampled. Snow jamming the

tube due to internal stratification may cause snow to be pushed away from – rather than entering – the tube. Thus, the stratification observed in this study may have contributed to the observed under-measurement.

The snowpack in this study was most similar to the snowpacks reported for studies completed in southern Ontario. We measured SWE ranging from 13-17 cm SWE, while SWE measured in southern Ontario commonly ranged between 5-18 cm (Bindon, 1964; Goodison, 1978; Farnes *et al.*, 1982). Snowpack stratification was similar to that reported in the literature regarding testing in southern Ontario. In contrast, studies performed at Mt. Hood recorded 20 – 120 cm SWE, and had less stratification than we observed (Work *et al.*, 1965; Beaumont, 1967).

Thus, we do not recommended that the Standard Federal be used under the conditions observed in this study (i.e. snowpacks with internal layering) due to issues with jamming and snow ploughing. Having the spring scale to directly measure SWE in the field is very useful, especially if long transects, deep snowpacks, or large numbers of sampling points are measured at once. However, caution must be exercised when using this scale to ensure that it is not affected by wind, and calibration curves based on temperature should be used. It should be noted that a similar scale is commonly used with the MSC, and any spring scale with sufficient capacity and resolution could be adapted for use with the SnowHydro, though they were not used in this study or for data collection related to Ch. 6. In practice, samples from the SnowHydro are bagged for later weighing on a balance.

4.6 Conclusions

This study re-evaluated the performance of two existing snow tube designs, and compared them to a new design that had not yet been tested. While the magnitude of the error for the existing designs was in the same range as previous work, they were in the opposite direction: measurements tended to under- rather than over-estimate SWE. In the mature forest plot, the three samplers collected statistically identical measurements to the snow pits, which are considered the most accurate method of determining SWE. In the clearcut, only the Standard Federal measurements were statistically similar to pit measurements, but SWE underestimates were < 10% for all samplers. The Standard Federal also consistently produced the lowest error relative to *Pit SWE*, in contrast to the literature.

Qualitatively, the larger diameter tubes allowed for faster sampling because valid cores were typically extracted on the first try, whereas the small diameter Standard Federal typically required multiple attempts. Comparing the two large-diameter tubes, the SnowHydro and MSC, we recommend the SnowHydro due to its ability to sample greater snow depths, its Lexan construction that allows examination of the core, and lower heat transmission from handling. Snow surveys for Ch. 6 are predominantly under a mature forest canopy where the SnowHydro performs better than the MSC, and is faster to use than the Standard Federal.

5.0: Remote Snow Depth Measurements using a Robotic Total Station

5.1 Introduction

Quantifying snow accumulation volumes in high elevation mountainous regions is essential for water supply forecasting given its major contribution to downstream water supplies in western North America (Gillan *et al.*, 2010). Snowpacks in these montane or alpine watersheds can be highly unstable and spatiotemporally variable, and are often located in areas of steep slope that are typically also key snow accumulation zones (Deems, 2007; Hood and Hayashi, 2010; MacDonald *et al.*, 2010). Such conditions often result in avalanche hazard and dangerous travel conditions, thus restricting access to these remote areas and making it difficult to quantify annual snow accumulation using conventional snow survey techniques. However, failing to account for accumulation in these areas biases water storage and yield predictions towards data collected at lower elevations, and likely under forest cover, potentially resulting in underestimation of water resources from snow.

Given the difficulty in manually measuring snow accumulation in these high-elevation regions, methods to remotely monitor snow accumulation conditions in near-real time have been developed. The primary method for obtaining large-scale snow accumulation data in the western United States is the snowpack telemetry (SNOTEL) network (Serreze *et al.*, 1999). This network consists of a series of remotely operated stations that measure meteorological conditions, snow depth, and snow water equivalent, and relay those data to a controlling station via meteor burst radio link (Goodison *et al.*, 1981). A remote snow pillow network also exists in Alberta; however, it is much less capable than the SNOTEL network due to the lack of meteorological instrumentation.

Snow pillows in these networks are widely spaced and primarily located in forested areas, while high elevations are underrepresented (Alberta Environment, 2011a). Given this sparse network of point data, the high spatiotemporal variability of depth, density, and SWE of mountain snowpacks is not adequately captured (Goodison *et al.*, 1981).

More recently, researchers have applied remote sensing techniques utilizing modern technologies to sample snow depth remotely in inaccessible terrain. However, these technologies have inherent limitations that reduce their applicability and/or widespread adoption in snow science. This study presents and tests a new remote measurement method based on the robotic total station, which aims to reduce these limitations.

5.2 Background

There are three primary remote measurement techniques currently described in the literature: (1) airborne light detection and ranging (LiDAR); (2) terrestrial laser scanning (TLS) systems; and, (3) hand-held distance meters. All techniques use electronic distance meter (EDM) technology, an active electro-optical system that utilizes laser energy emitted by the instrument to estimate the distance between the instrument and a target ("range"). Typically, a target such as a retroreflector or prism is employed for measurement, as it directs the energy back towards the instrument. However, newer instruments are capable of determining range to any surface without a retroreflector ("reflectorless mode", RL).

There are two methods to determine range with an EDM: (1) time of flight (TOF) or pulsed laser; and, (2) phase shift or continuous wave (CW). The TOF method is a

direct measurement technique in which a laser pulse emitted from the instrument reflects off the target and returns to the instrument, where the returning energy is directed to a photo detector that registers the pulse return (Höglund and Large, 2005; Bayoud, 2006). The time differential between pulse emission and return is measured with a highly accurate clock; range to target is then calculated from the speed of light (~ 300 000 000 m s^{-1}) and the round trip time of laser pulse (Höglund and Large, 2005) (Fig. 5.1). Due to the short return times of the laser pulse even at long ranges, the instrument typically emits pulses at up to 20 kHz, progressively calculating an average distance until a predetermined standard deviation is achieved (Baltsavias, 1999). Given the time-based nature of this method, the quality of the onboard clock is the key to accurate measurements (Baltsavias, 1999). The best of these systems can achieve a measurement accuracy of ~0.015 m at ranges of up to 800 m (Riegl Laser Measurement Systems GmbH, 2005). TOF systems are widely used in long-range applications because they are capable of emitting considerable amounts of energy, although as range increases accuracy tends to decrease (Baltsavias, 1999).

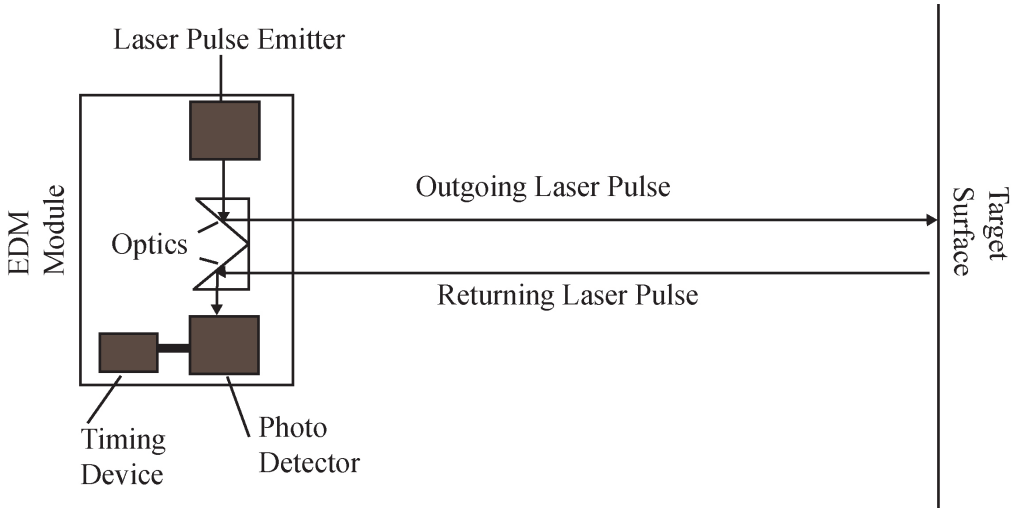

Figure 5.1. Schematic of a typical TOF EDM system. Note separate optical paths for laser pulse emission and collection (modified from: Höglund and Large, 2005; Bayoud, 2006).

By contrast, phase shift systems are indirect techniques that rely on precise knowledge of the frequency and phase of both the outgoing and returning laser energy (Höglund and Large, 2005; Bayoud, 2006). Since the frequency and phase of laser energy shifts at a known rate with increasing distance, those parameters of the returning energy are compared with the known values of the outgoing energy. This comparison allows the instrument to accurately determine the distance to target (Höglund and Large, 2005; Bayoud, 2006). Unlike TOF systems, a phase shift EDM cannot accurately estimate distance due to a cycle ambiguity produced by an insufficient number of full wavelengths returning to the instrument. The instrument resolves this ambiguity by modulating the frequency of the outgoing energy between 100 – 150 MHz to obtain a unique integer number of returning wavelengths (Baltsavias, 1999; Höglund and Large, 2005; Bayoud, 2006), thus making it possible to obtain highly accurate distance values. The best phase shift systems are capable of resolving distances much more accurately than TOF systems: typically ~0.003 m at ranges ≤ 500 m, and ~0.005 m at ranges > 500 m (Trimble Navigation Ltd., 2007b; Leica Geosystems AG, 2009b). However, total measurement times are somewhat longer than TOF systems because the cycle ambiguity must be resolved (Höglund and Large, 2005; Bayoud, 2006) (Fig. 5.2).

Airborne LiDAR consists of a TOF RL laser scanner mounted on an aircraft (Hopkinson *et al.*, 2001; Deems *et al.*, 2006; Deems and Painter, 2006). It is therefore imperative that the precise horizontal and vertical location, and pitch and roll of the aircraft be known at any given time during the scan so that the data is accurately placed in 3D space (Axelsson, 1999). Two systems are utilized to collect these data: first, known reference points on the ground are scanned by the aircraft which is fitted with a

high accuracy real-time kinematic (RTK) global positioning system (GPS) receiver, which can provide three-dimensional positional accuracy in the 0.015 m range (Trimble Navigation Ltd., 2007a) and fit the data to a real-world coordinate system.

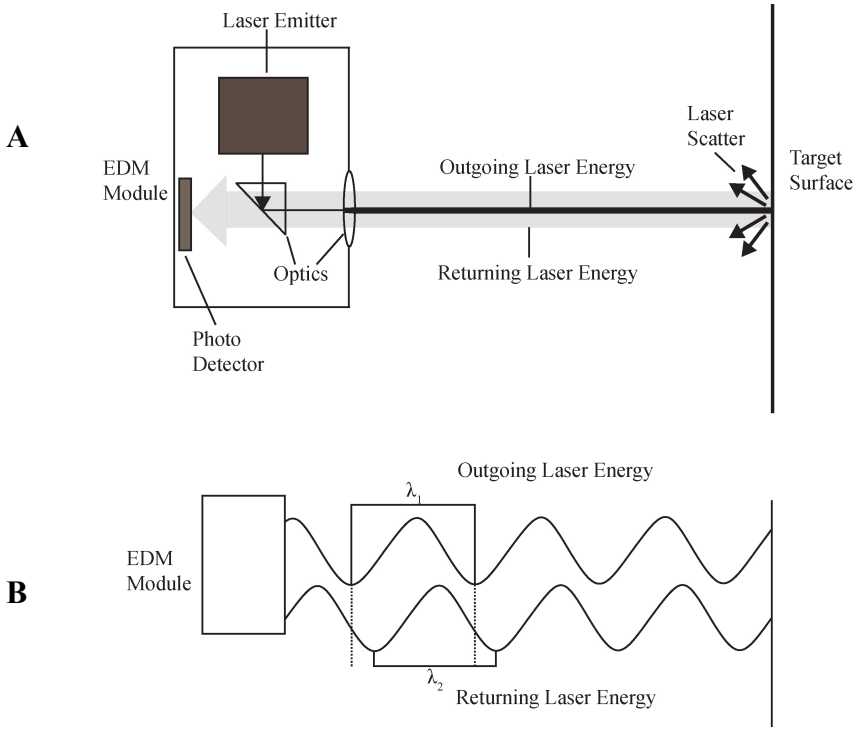

Figure 5.2. A. Schematic of a typical phase shift EDM system; B. Illustration of change in phase of returning energy (laser paths have been offset to illustrate change in phase). Dashed lines illustrate that λ_2 is shifted out of phase from λ_1 due to distance travelled from the instrument (modified from: Höglund and Large, 2005; Bayoud, 2006).

Second, the aircraft is fitted with an inertial navigation system that monitors pitch and roll and provides data on the orientation of the aircraft with respect to the ground. LiDAR produces large point cloud datasets and can receive pulse returns from vegetation cover, buildings, and other objects in addition to ground returns. These datasets place stress on computer storage media when storing either repeated scans or scans of complex surfaces. Processing of the point cloud requires high performance computers and specialized software to interpret point locations, filter anomalous points and produce useable digital models of the scanned area (Axelsson, 1999). Airborne LiDAR flights are

costly: $300 - $1000 CAD per square kilometre depending on factors such as resolution, post-processing, and time of year (Wulder *et al.*, 2008), which may prevent frequent use by researchers.

The most commonly used technology for remotely measuring snow depth is currently the TLS system (Jörg *et al.*, 2006; Prokop, 2008; Prokop *et al.*, 2008; Schaffhauser *et al.*, 2008), which consists of a scanning head that can rotate horizontally through 360°. Within this scanning head, an oscillating mirror or motorized telescope directs a narrow laser beam through the vertical plane, making the TLS system capable of collecting data in a hemisphere centred on the instrument. TLS systems use a RL TOF method and high accuracy timing devices to maximize distance accuracy, and can collect large amounts of data (up to 50 000 points s^{-1}), with point spacing as small as 0.005 m at the target (Leica Geosystems AG, 2009a) (Fig. 5.3). Known control points are scanned at the outset of the survey to locate the instrument with respect to a known coordinate system (Riegl Laser Measurement Systems GmbH, 2005; Leica Geosystems AG, 2009a). However, setting accuracy is typically not as high with the TLS as with traditional surveying instruments (i.e. theodolite, total station, etc.) resulting in uncertainty in instrument position relative to the coordinate system.

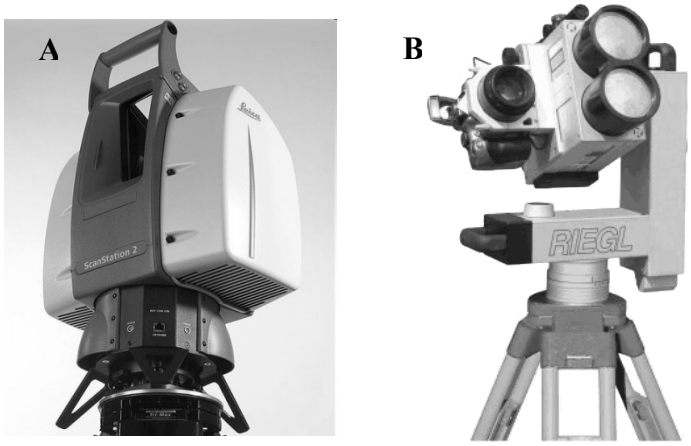

Figure 5.3. Two examples of terrestrial laser scanners illustrating the two primary designs: A. Leica Geosystems ScanStation with internal oscillating mirror; and B. Riegl LPM-i800ha with motorized telescope (Photos: A Leica Geosystems AG, B. Riegl Laser Measurement Systems GmbH).

Similar to airborne LiDAR, TLS systems collect large amounts of data and require similar data processing protocols. TLS systems start at ~$150 000 CAD, and have a narrow range of uses; this has largely prevented their widespread adoption by snow scientists.

The last current method is the hand-held distance meter (Hood and Hayashi, 2010) (Fig. 5.4). These devices are extremely light, compact, and inexpensive (~$5000 CAD), making them easily accessible to researchers. They use lower quality RL TOF systems with less precise timing devices, and typically achieve distance accuracies of ~0.100 m (LaserCraft Inc., 2007).

Figure 5.4. A typical hand-held distance meter (photo: LaserCraft Inc., 2007).

Some distance meters are capable of measuring inclination to a resolution of 0.1° (360”), and bearing to 0.5° (1800”) (LaserCraft Inc., 2007). This low resolution creates considerable uncertainty in the position of measured points (Hood and Hayashi, 2010). Unlike TLS, distance meters have no facility for forced centering over known control points, and no method to level the instrument, thus adding further uncertainty to the position of measured points.

The methods described above all determine snow depth in approximately the same way. Typically, a “snow-off” topographic survey is completed which provides the data input for a digital elevation model (DEM) which is produced through spatial interpolation of the point data. In the winter, a “snow-on” survey is completed where measurements are made to the snow surface rather than the ground surface from control points or from the aircraft. These points are interpolated to create a DEM of the snow surface. The elevation difference between these two surfaces is, therefore, the snow depth, so the ground DEM is subtracted from the snow DEM resulting in a surface of snow depth.

Although the methods described above have been used to good effect in numerous snow studies, their ability to repeatedly sample pre-determined points over time is limited due to low centering accuracy over control points, inability to accurately reproduce instrument orientation, and poor distance and angular resolution. The ability to repeatedly sample points allows the researcher to compare snow depth data between surveys, as snow accumulation at each measured point is driven by constant topographic and vegetation controls, with only snow accumulation and time varying. Accurately

sampling the same point could produce less noisy data, and results in simpler data analysis.

5.3 New Method: Robotic Total Station

Here we test an alternative method of remotely measuring snow depth using a modern robotic total station, which minimizes some of the limitations of other technologies. Specific advantages of the total station include greater angle and distance measurement accuracy, relatively simple data analysis and management, lower cost than TLS or airborne LiDAR, and a broad range of functionality that is useful for research beyond the snow science applications discussed here. Thus accurate measurements of snow depth can be repeated throughout the snow season to characterize snow accumulation. While Prokop *et al.* (2008) utilized a total station to provide a comparison with a TLS system; they neither characterized the errors in using this type of instrument, nor provided a comparison to TLS systems. Thus no previous studies have provided a detailed analysis of this method. Table 5.1 compares the technical specifications of the Leica and Trimble total stations, a common distance meter, and a TLS.

Table 5.1. Technical specifications of instruments used in this and other studies (Riegl Laser Measurement Systems GmbH, 2005; LaserCraft Inc., 2007; Trimble Navigation Ltd., 2007b; Prokop *et al.*, 2008; Leica Geosystems AG, 2009b).

	Leica TCRP 1201+	**Trimble S6**	**LaserCraft Contour XLRic**	**Riegl LPM-i800ha**
Laser Class	3R	1	1	1M
Wavelength Range (nm)	650 – 690	870	905	900
Beam Divergence (mrad)	0.2 x 0.3	0.41 x 0.81	3 x 3	1.3 x 1.3
Distance Accuracy	0 – 500m = 2 mm > 500 m = 4 mm	< 300 m = 3 mm > 300 m = 5 mm	±15 cm (to white target at 85 m)	Typically 15 mm
Maximum Range (Kodak White 90% reflective)	> 1000 m	> 800 m	800 m	800 m
Measurement Method	Hybrid TOF/Phase Shift	TOF	TOF	TOF
Angular Accuracy	1”	3”	360” vertical 1800” horizontal	32.4”
Weight	~ 6 kg	~ 6 kg	1.6 kg	15 kg
Approx. Cost	$37 000	$35 000	$5000	~ $100 000

This study compares two robotic total station instruments: (1) Leica Geosystems TCRP 1201+ (Fig. 5.5a); and, (2) Trimble Navigation S6 (Fig. 5.5b). These instruments are generally designed to be operated remotely by a single person, are capable of rotating vertically and horizontally utilizing servomotors, and can lock on to and track a moving retroreflector. The total station can turn to a specified angle with a higher degree of accuracy and precision than a traditional mechanical instrument, because it is operated by onboard software and digital inputs are used to calculate angles. This ability is critical for repeated point sampling over time. Data collected by the total station can be output in common text files (e.g., .csv) containing only point coordinates, or containing all raw data consisting of horizontal and vertical angles, slope and horizontal distances, and other information. This text-based format is economical of computer memory and processing power; files can also be imported to common spreadsheet software for analysis. The cost of a total station is typically 1/3 that of a basic TLS system: ~$35 000 - $40 000 CAD.

While this still represents a significant capital investment, the total station can be used year-round for a wide range of research, thus making it feasible to share the cost between several researchers with different applications.

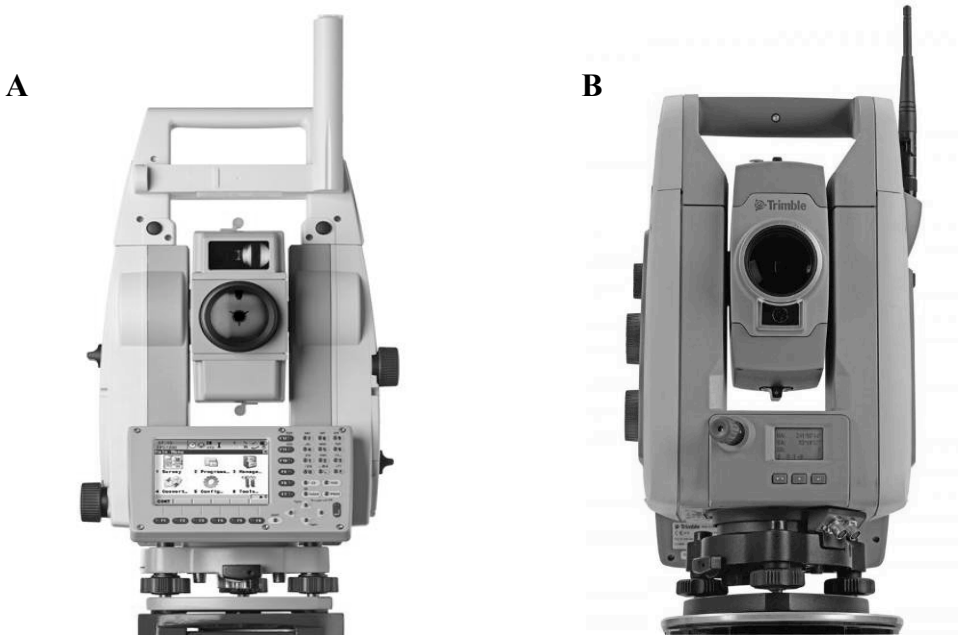

Figure 5.5. Robotic total stations used in this study: (A) Leica Geosystems TCRP 1201+ (photo: Leica Geosystems AG); (B) Trimble S6 (photo: Trimble Navigation Ltd.).

The Leica TCRP1201+ uses Leica's PinPoint R1000 system, which has an advertised range of >1000 m (Kodak white, 90% reflective, ideal conditions (Leica Geosystems AG, 2009b)), an advantage of more than 200 m compared to current RL EDM systems provided by other total station manufacturers. In RL mode, the R1000 system can measure distances to an accuracy of 0.002 m (+2 ppm) at ≤500 m, and 0.004 m (+2 ppm) at >500 m (Leica Geosystems AG, 2009b) (where ppm refers to an error of 0.001 m for every 1000 m measured along a survey traverse). Distance measurements are made using a collimated Class 3R red laser (650-690 nm) with an output of 5 mW (Leica Geosystems AG, 2009b). The PinPoint system is a hybrid of TOF and phase shift measurement technologies. Laser energy output is higher than traditional EDM systems,

and a proprietary signal analyzer algorithm is used to achieve longer ranges and higher accuracies than traditional TOF and phase shift methods (Bayoud, 2006). The PinPoint system also performs simultaneous onboard EDM calibration to account for thermal drift in the instrument, increasing confidence in measurements (Bayoud, 2006; Hosking, 2009). The Leica TCRP1201+ has angular measurement accuracy (horizontal and vertical) of 1" (0.0003°).

The Trimble S6 is comparable to the Leica and is based around Trimble's Direct Reflex EDM system. The instrument used in this study uses the DR300+ EDM, which is an RL-capable TOF system with a maximum advertised range of >800 m (Kodak white, 90% reflective, ideal conditions). A phase shift RL-capable EDM is also available, but with a significantly lower maximum range (Trimble Navigation Ltd., 2007b). The DR300+ system consists of an 870 nm infrared laser, coupled to proprietary signal processing algorithms and highly accurate timing devices, to produce a range accuracy of 0.003 m at ≤300 m, and 0.005 m at >300 m (Garget, 2005; Trimble Navigation Ltd., 2007b; Hosking, 2009). The total station used here has an angular accuracy (horizontal and vertical) of 3" (0.0008°).

5.2 Methods

5.2.1 Phase 1 – Lab Test

Phase 1 of this study consisted of a small-scale test under controlled conditions. The Trimble S6 total station was set up in a lab and aimed towards a slope analogue mounted on the wall at ceiling height. The slope analogue consisted of a 1.5 m^2 sheet of rigid cardboard that was attached to the wall at the top and propped out at the bottom

with two arms marked in 5° increments (Fig. 5.6); this allowed for an adjustable slope angle of 45° – 65°.

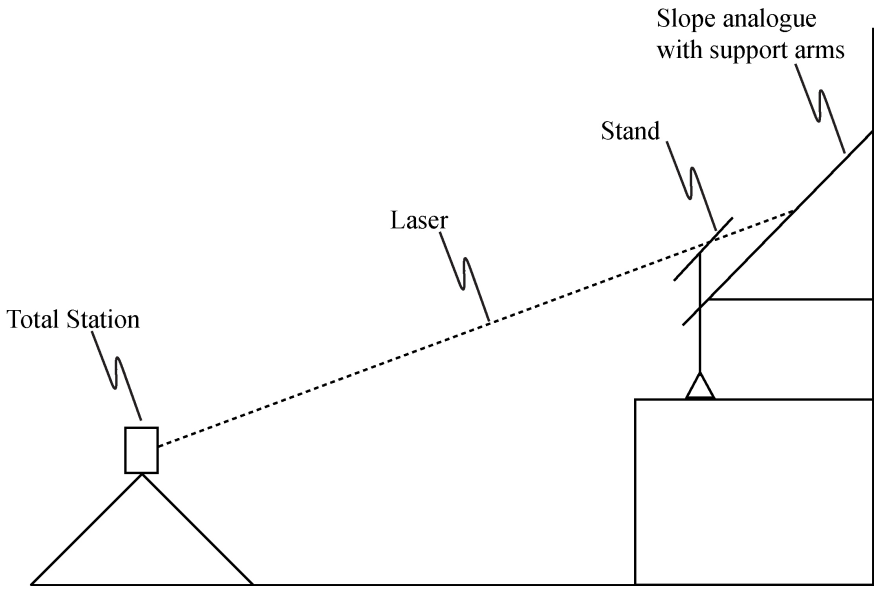

Figure 5.6. Adjustable slope used in phase 1 of the study. The slope analogue and adjustable support arms are visible.

A stand holding several sheets of white paper was used to simulate a snow surface; the angle of the stand was adjusted concurrently with that of the slope analogue to ensure that the surfaces were parallel. The height of the stand was also adjusted to simulate a range of snow depths (0.150 – 0.650 m). The total station was placed ~ 5.5 m from the slope analogue, and 45 measurements were collected with the vertical angle of the total station varying between 65.75° and 80°, and slope angle varying between 45° and 65° in 5° increments. The true "snow depth" was measured concurrently with a measuring tape. All measurements in this test were made perpendicular to the slope analogue.

Ground surface coordinates cannot be directly subtracted from snow surface coordinates to calculate snow depth, because the laser from the total station strikes the slope surface at an angle, while snow depth is conventionally measured perpendicular to

the slope (McClung *et al.*, 1984) (Fig. 5.7). Thus, trigonometric corrections are applied to each measurement using:

$$X = B \times \sin\theta \quad 5.1$$

$$\theta = a - \alpha \quad 5.2$$

and

$$\alpha = 90 - S \quad 5.3$$

where X is the calculated snow depth, B is the direct slope distance between the snow intercept and target ground point, θ is the angle between the slope angle and the vertical angle of the total station, α is the slope angle from zenith; S is the slope angle from horizontal; and a is the vertical angle of the laser beam from zenith as measured by the total station.

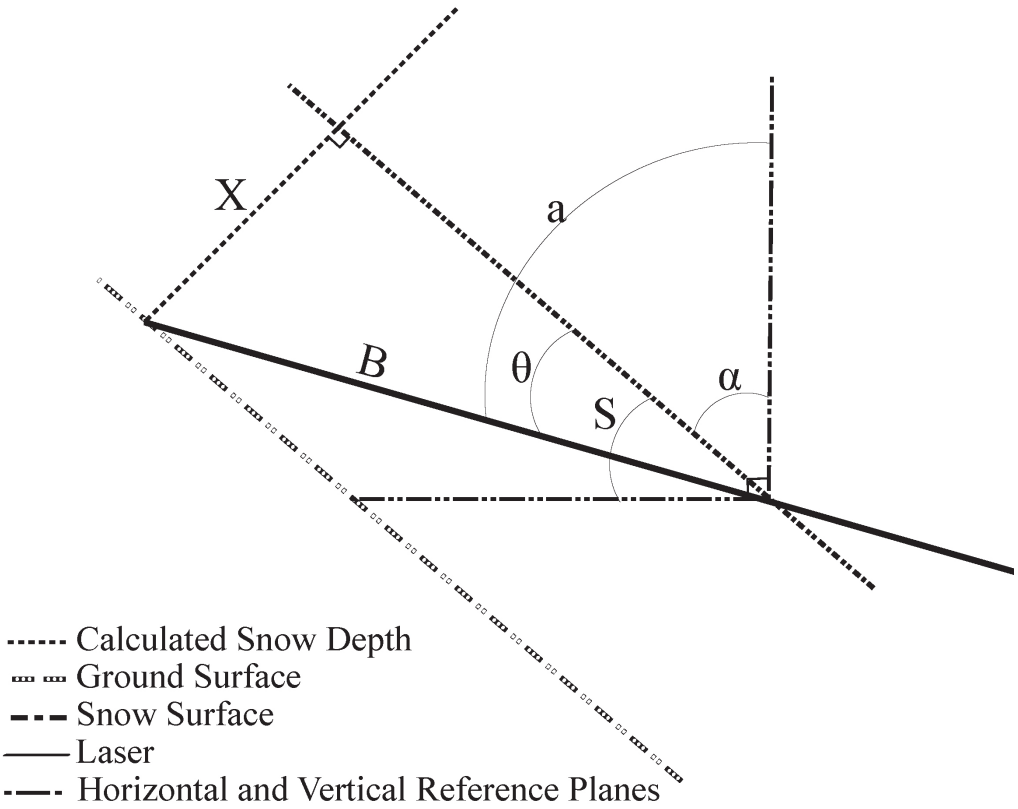

Figure 5.7. Schematic of laser interaction with snowpack, with variables from Equations 5.1 – 5.3 labelled.

Eq. 5.1 assumes that the slope is perpendicular to the face of the total station in the horizontal plane. However, as points move further from perpendicular, the laser intersects the snowpack progressively further down- and across-slope, increasing the length of *B* (Fig. 5.8) and resulting in overestimates of snow depth. An additional correction is thus applied to measurements that lie across-slope from this line:

$$B_{Calc} = \frac{B_{Meas}}{\cos((as - 180) - az} \qquad 5.4$$

where B_{Calc} is the cross-slope corrected *B* value, B_{Meas} is the measured *B* value from Eq. 5.1, *as* is the slope aspect, and *az* is horizontal angle measured by the total station. B_{Calc} can be directly substituted for *B* in Eq. 5.1. This method treats each measurement individually, and assumes that the snow and ground surfaces are parallel for each pair of ground and snow measurements.

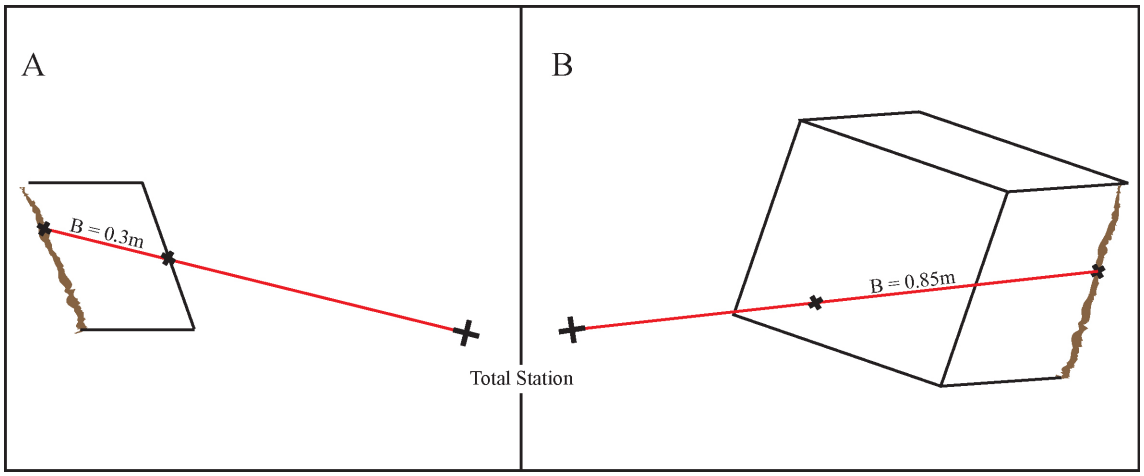

Figure 5.8. (A) Laser strikes snow surface perpendicular to slope. *B* is minimized, and represents the true value. (B) Laser strikes snow surface down- and across-slope because point is off perpendicular. This results in extension of *B*, and subsequent overestimation of snow depth. Eq. 5.4 corrects for this error.

5.2.2 Phase 2 – Field Test

Phase two was a field deployment, where the method was evaluated with the Trimble S6 robotic total station under natural conditions. Field measurements were collected in the Crowsnest Pass, Alberta, Canada, 2 km south of the town of Blairmore (Fig. 5.9).

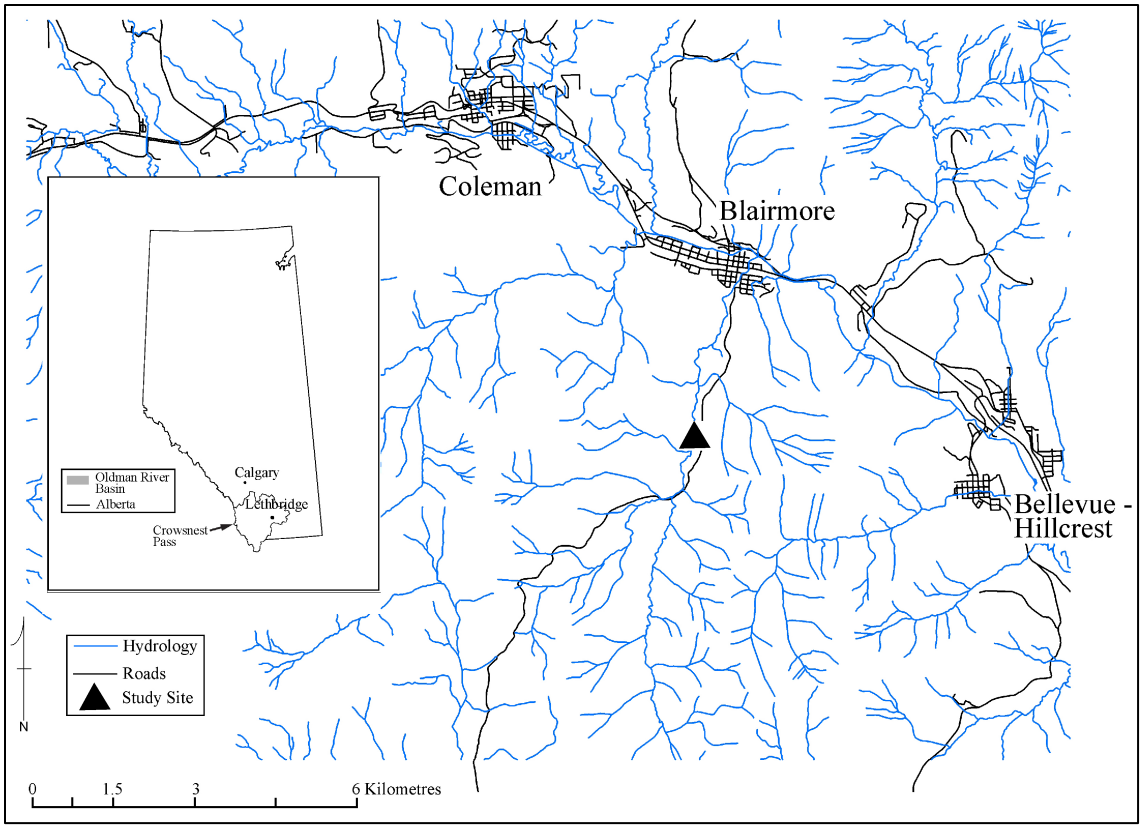

Figure 5.9. Map of measurement location for Phase 2 of the study.

The site was a deforested slope adjacent to a logging road, where a "snow-off" survey was performed on September 21, 2010. Slope angles ranged from 9.5° to 27°, and maximum measured distance from the total station to the slope was ~150 m. A "snow-on" survey was conducted on November 23, 2010, when measured snow depths ranged from 23 – 67 cm of fresh, low-density snow. The total station was deployed at angles ranging from perpendicular to the slope face to 55° off angle horizontally.

Two control points were established at the base of the logged slope and permanently marked with steel reinforcing bar to form a reference baseline, with a local coordinate system applied to the two control points. The initial "snow-off" topographic survey was performed with the Trimble S6 and Trimble MT1000 MultiTrack prism. A series of DEMs were then calculated for the study slope using ArcGIS 9.3.1 and several spatial interpolation methods: Inverse Distance Weighted, Spline, and Natural Neighbour; a triangulated irregular network (TIN) was also created. These DEMs were used to test the effect of the interpolation method on snow depth calculation, and determine which method gave the best fit with the measured snow depths.

For the "snow-on" survey, the measured topographic points from September were used as target points for the total station. The "Stakeout" program on the total station, which computes the correct horizontal and vertical angle required to point the instrument directly to an input coordinate, was used to locate these topographic points. The angle calculations are based on the point coordinate at which the instrument is set up, the height of the instrument above that point, and the relative change in X, Y, and Z coordinates between the two points. Once the angles are computed, the total station is automatically turned to the proper orientation, and a distance measurement is made to obtain a coordinate at the snow surface. Using the total station to determine the position of the desired measurement point, a field assistant was directed to the location indicated by the reticule in the telescope. Snow depth was manually measured perpendicular to the slope with a graduated avalanche probe at each point perpendicular to the local slope.

"Snow-on" data were corrected for cross-slope position using Eq. 5.4, and snow depth was calculated relative to the "snow-off" dataset using Eq. 5.1. Scatter plots of

measured vs. calculated depths were plotted to visually assess the degree of agreement between methods. Root mean squared error (RMSE) was calculated to quantify the error in snow depths calculated using the total station. Residuals were analyzed for normality, independent samples, and homoscedasticity.

A test was also performed to determine the effect of snow density and off perpendicular on the performance of each total station. Two control points were established ~25 m from a large container (0.500 x 0.370 m) of snow: one horizontally perpendicular to the container, the other ~25° off perpendicular. The surface area of the container was larger than the laser footprint. Distances to the snow surface from both controls points were accurately measured using the Trimble total station and a reflective target on the snow surface, near the centre of the container. Ten measurements to the bare snow surface were then performed with the Trimble total station for each combination of position (either perpendicular or off angle) and density (density 1 and density 2). Snow density was calculated by collecting density samples using a 250 cm^3 snow density cutter (Snow Metrics, Ft. Collins, CO), and weighing them on a calibrated balance (Ohaus Scout Pro 200 g). These data were plotted to visually assess any differences between perpendicular and off-angle measurements.

5.3 Results

Results from the lab study showed good agreement between calculated and measured snow depths. Root mean squared error (RMSE) of calculations was 0.034 m, with $r^2 = 0.98$, $p < 0.05$ (Fig. 5.10). Two outliers in the dataset were removed as erroneous measurements because the distance between the total station and snow surface

analogue was considerably shorter than the other measurements, indicating that the measurement was to some object other than the analogue surface. Calculated snow depths fall slightly below the 1:1 line, indicating that calculations are slightly underestimated. The y-intercept of the line of best fit is 0.007 m, and the slope is slightly less than 1, further indicating that the technique is accurately representing snow depth.

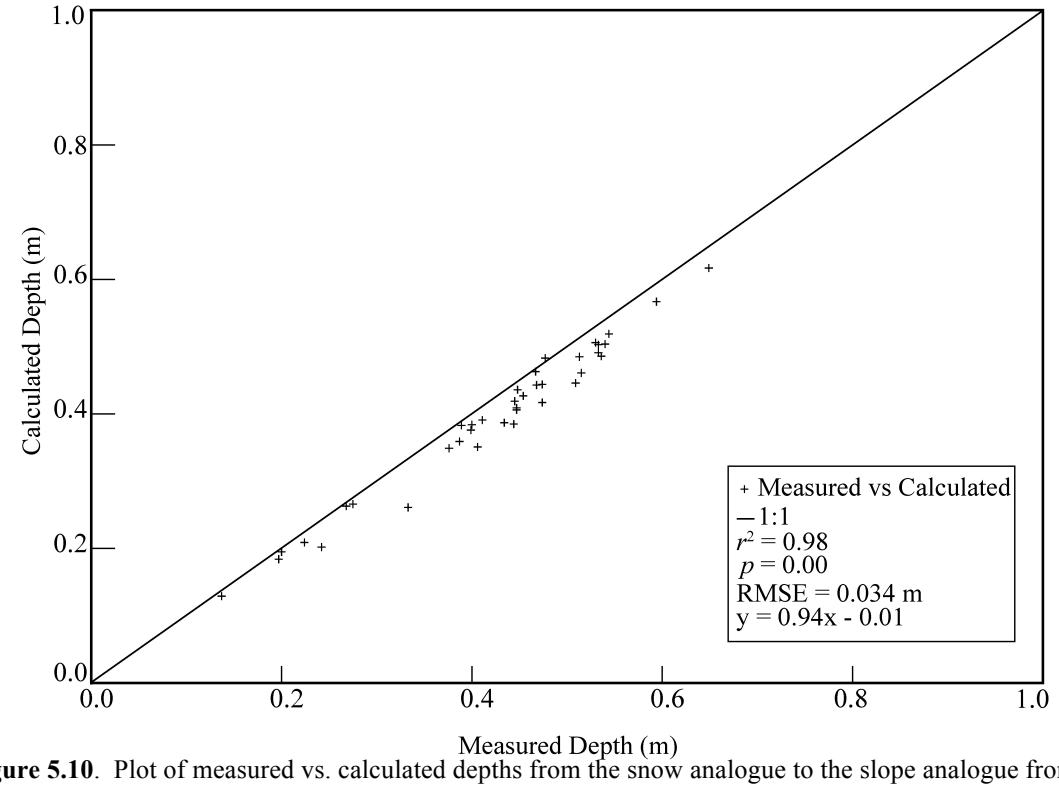

Figure 5.10. Plot of measured vs. calculated depths from the snow analogue to the slope analogue from the lab test. Solid line indicates 1:1 and the equation for the line of best fit is provided.

Analysis of the residuals (Fig. 5.11) shows that they are randomly distributed about the '0' line, which indicates that the linear model was appropriate for this dataset. This also shows that the samples are independent, and that the assumption of constant variance (i.e. homoscedasticity) is met. The residuals, and thus the sample data, are normally distributed (Shapiro-Wilk W = 0.947, p = 0.068). This indicates that the

predicted snow depths are robust. This success allowed progression to Phase 2 of the study.

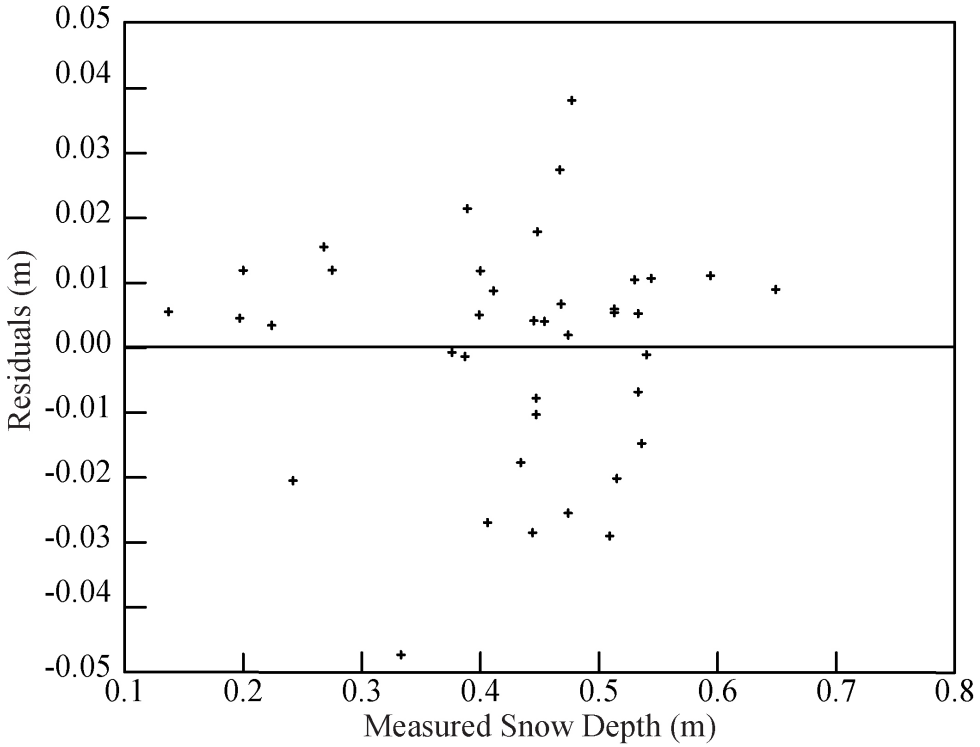

Figure 5.11. Measured depths vs. residuals for the lab tests. Residuals are well distributed above and below the 0 line, although the largest variability appears to occur when depths are 0.4 – 0.5 m.

Results from Phase 2 showed much greater variability in calculated snow depth under natural conditions. In this test, RMSE was 0.308 m, and $r^2 = 0.002$, $p = 0.684$, indicating no significant relationship (Fig. 5.12). Several methods of interpolating the original topographic survey data were tested to determine the bare-ground slope angles used in the calculation, but there was no difference in RMSE between interpolation methods. The slope of the line of best fit is much shallower than that of the lab test and the intercept is at 0.154 m, further evidence of error in the calculations. An interesting feature of the distribution in Fig. 5.12 is the range of calculated points at a measured snow depth of 0.300 m (the mode of the dataset), which have a range of over 1 m. This

variability is independent of location on the slope, indicating that it is a result of problems in the calculation rather than being driven by some unknown process.

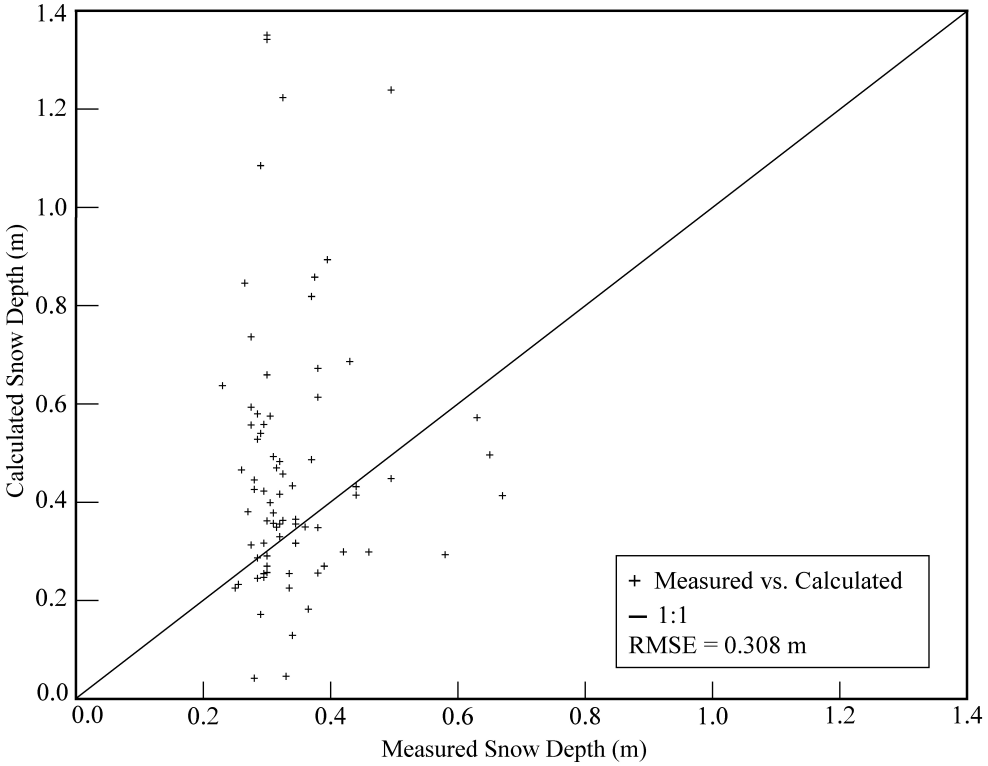

Figure 5.12. Plot of measured vs. calculated depths from the field test. No significant relationship was observed between measured and calculated snow depths. 1:1 line is provided.

An analysis of the residuals (Fig. 5.13) shows that although the points are randomly distributed and that a linear function is appropriate for this dataset, the clustering around measured depths of 0.300 m seen in Fig. 5.12 remains apparent. The residuals are not normally distributed (Shapiro-Wilks W = 0.85, p = 0.00), but are more clustered below the '0' line, indicating underestimation which is offset by fewer but larger overestimates. This clustering around one value indicates that variances are not constant (i.e. heteroscedastic), and that a systematic error exists in the data.

An analysis of residual distribution vs. distance between the total station and snow surface and residuals vs. slope angle showed no relationship, and the lab test produced excellent results. Thus, we hypothesize that the errors observed in the field

data are due to problems with the distance measurement, which may be affected by interactions between the laser and snow pack due to variations in snow density. Evidence of a systematic error seen in Fig. 5.13 further supports this hypothesis.

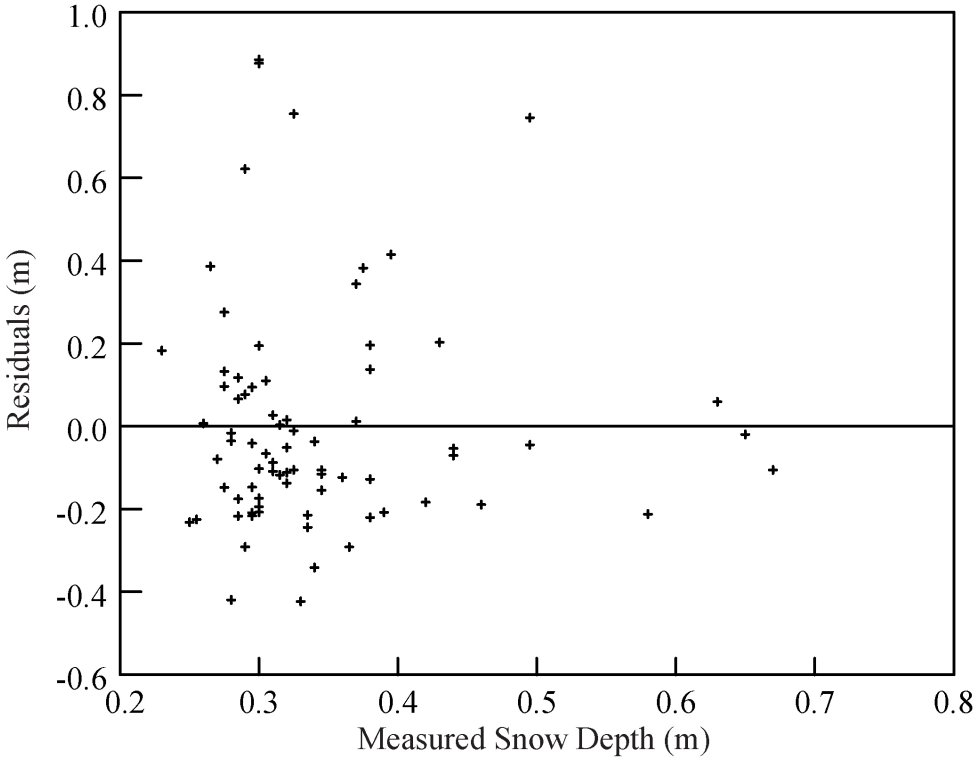

Figure 5.13. Measured depths vs. residuals for the field test. There is large variability in the residuals, particularly at shallow snow depths. The range of variability is ~ -0.5 – 0.8 m, which is often greater than the actual measured depth.

To test for the effects of snow density on EDM measurements, distance measurements from fixed control points to a fixed snow surface were collected. Two snow densities, 454 kg m^{-3} and 570 kg m^{-3}, were utilized for this test. The former is at the high end of the range expected of an alpine snowpack, while the latter is slightly above that range though it is consistent with densities encountered in avalanche deposits (Alford, 1967; McClung and Schaerer, 1993).

From the perpendicular position, the distance to the snow surface (true distance) was 20.278 m as measured by the Trimble to a reflective target on the snow surface in RL

mode. At density 1 (454 kg m^{-3}) the average distance to the snow surface (snow distance) was 20.297 m, an over estimate of 0.019 m. At density 2 (570 kg m^{-3}), snow distance was 20.291, an overestimate of 0.013 m. The average snow distances were determined from n = 10 measurements at each density. Within the 10 measurements, variability in snow distance was 0.001 m, indicating that the total station produces highly repeatable measurements when perpendicular to the snow surface.

From the off angle position, true distance was 27.590 m using the same reflective target and RL mode. At density 1 the snow distance was 27.582 m, an underestimate of 0.008 m. At density 2 the snow distance was 27.579 m, an underestimate of 0.011 m. Variability within the 10 measurements was again 0.001 m, indicating high repeatability when measuring off angle. The results from this test are summarized in Fig 5.14.

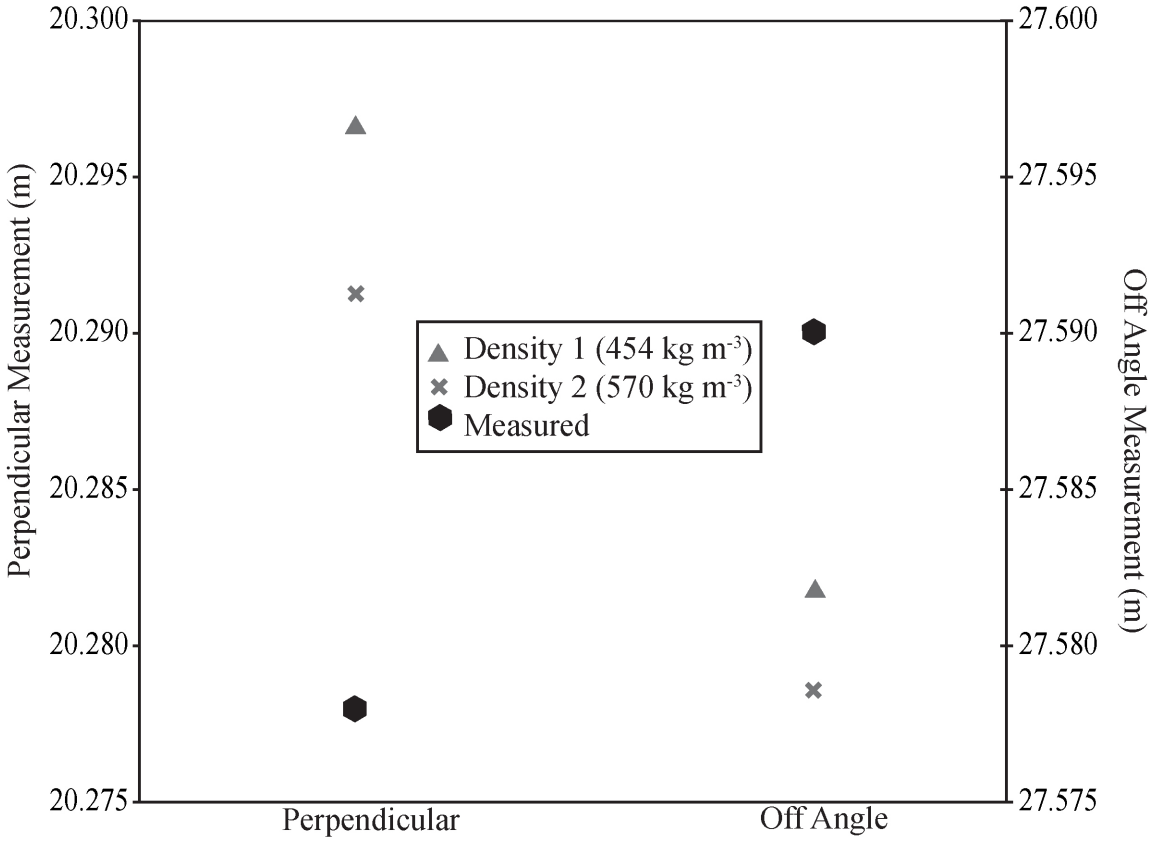

Figure 5.14. Comparison of mean distance measurements (n = 10 for each point) between perpendicular and off angle measurement stations to snowpack.

5.4 Discussion

Study results suggest that the total station may not provide a significant improvement in snow depth measurement, and may only perform as well as a TLS or distance meter. While the error in calculated snow depth of 0.300 m may not be a large portion of total measured depth in areas with deep snowpacks, it becomes significant in areas with a shallow snowpack.

However, the results from this study closely match results reported by Hood and Hayashi (2010), which raises the question of why the total station performs only similarly to the laser distance meter, and slightly worse than the TLS (Prokop, 2008; Prokop *et al.*, 2008). We would expect measurement uncertainty to be reduced, as the EDM used by the total station is considerably more advanced, with distance resolution approximately two orders of magnitude greater than the distance meter, and two times better than a TLS. Combined with the greater angular accuracy of the total station, the positional uncertainty at the target surface is minimal. This level of accuracy and precision is important for re-sampling points throughout a season, and is unattainable with either a TLS or distance meter.

Given the lack of literature on this topic, it is difficult to determine what is driving these results. These errors may apply to other described techniques, though their individual specifications may reduce the importance of error sources outlined below. Three potential sources of error relating to snow surface properties have been identified: (1) reflectivity; (2) permeability to laser beams; and, (3) microtopography. These sources of error may explain why the total station performs only similarly – as opposed to better

than – the other methods, and may indicate that there is a lower boundary to how well snow depth can be measured with total station systems.

The reflectivity of the snow is important to these technologies because they rely on returning energy in order to determine distance. The reflectivity of snow varies depending on the wavelength utilized by the instrument. The Leica total station operates in the visible wavelength range (650 – 690 nm) where snow is highly reflective (albedo = 85 – 90%), thus a large proportion of the emitted energy is likely returned to the instrument. The Trimble operates in the near infrared (870 nm), where snow is also highly reflective (albedo 70 – 90%). These albedo values may be higher than the surfaces typically measured by these instruments (e.g. concrete, asphalt, wood).

Hopkinson *et al.* (2011) highlighted an issue with high reflectivity that affected their measurements while using airborne LiDAR to map river channels in the Mackenzie Delta, Northwest Territories. They noted that laser pulses that are perpendicular to the surface saturate the sensor due to specular reflection of returning energy, and potentially introduce error into the estimation of distance (Urban *et al.*, 2008; Hopkinson *et al.*, 2011). Saturation of the sensor occurs when returning pulse intensities are near the upper limit of instrument sensitivity and tend to trigger the timing system early, resulting in underestimation of distance (i.e. the system interprets a shorter round-trip travel time, and calculates a shorter distance). Conversely, returning pulse intensities that are near the lower limit of sensitivity tend to trigger the timing system late, resulting in overestimation of distance. I hypothesize that sensor saturation may be responsible for some of the variability seen in our measurements. However, as total stations lack the ability to analyze the intensity of the returning signal like some LiDAR sensors can, we

cannot easily test for this. This may represent an issue for other remote techniques discussed here that are based on TOF methodology. However, at the longer wavelengths (~900 nm) used by the distance meter and TLS, snow quickly becomes much less reflective (O'Brien and Munis, 1975; Warren, 1982; Kuhn, 1985; Green *et al.*, 2002; Prokop, 2008), thus there is a lower probability of saturating the sensor. This may explain why the TLS and airborne LiDAR work well.

Another likely problem is the potential interaction between the laser energy from the EDM and the snow surface. The Leica total station uses a hybrid TOF/phase shift method to estimate range to a target, where the phase shift method is the primary component. The interaction of the laser with the crystalline snow surface may produce an additional phase shift in addition to the shift that occurs with distance. This would result from the millions of small, randomly oriented lenses on the snow surface that are each one refracting and reflecting the laser energy in unique ways (G. Walsh, pers. comm.). The TOF portion of this hybrid system is not a true TOF system, but rather uses a proxy for the flight time of the laser pulse that is derived from the full signal properties collected by the total station. Because the entire range calculation is based on the returning signal properties, interaction effects with the snowpack may cause erroneous estimates of distance, although in our test the errors are relatively small (G. Walsh, pers. comm.). Potentially, this could be due to the relatively small distances used in this test, as errors in EDM measurements increase with increasing distance to target. The effect of atmospheric conditions is likely not a contributing factor because there were no particulates (i.e., snow/dust) in the air on the day of survey, and the total station measures

barometric pressure and air temperature on the fly because they have a direct effect on the time of flight or phase change of the laser pulses.

Despite the assumption that there is no interaction between the snowpack and the laser or beam penetration into the snowpack (i.e. Prokop, 2008; Hood and Hayashi, 2010), the small scale test performed at the end of Phase 2 indicated a small interaction that is partially dependent on snow density. Deems (2007) analysed the interaction between laser energy from an airborne LiDAR system (1064 nm) and the snow surface, and determined that at least 97% of the interaction occurs in the top 0.010 m of the snowpack, depending on snow grain size and liquid water content. This is supported by the nadir measurements made at the end of Phase 2 that would simulate a LiDAR scanner directly overhead. Although this snow depth of 0.010 m is smaller than the distance resolution provided by distance meters or TLS systems, and significantly smaller than the 0.100 m distance resolution of a typical LiDAR EDM, it is approximately twice the distance resolution of a total station EDM (~ 0.005 m). Thus the instrument may be resolving data from multiple returns from different levels within the snowpack, and thus has to make a "best guess" at the true range to target. The TOF system used by TLS systems and Trimble total station may be less affected by this type of error, as they cannot analyze the waveform properties of the return signal.

Microtopography on the snow surface may also produce uncertainty in the measurements. The TOF method in the Trimble total station determines range by computing the standard deviation of returning measurements, then averaging those measurements that fall within it and rejecting those that fall outside. This effectively sets a "range gate" in the instrument. By default, the standard deviation is set to 0.003 m,

although this may be modified by the user. Unlike an airborne LiDAR TOF system, the Trimble system is unable to analyze and store multiple returns from a single laser pulse (Höglund and Large, 2005). Thus, microtopography on the snow surface (e.g. surface undulations, small-scale drifts etc.) may interact with the laser pulse before it reaches the intended target point. Outgoing laser pulses may strike microtopography on the snow surface and return to the instrument, thus the instrument will register returns at different distances. If enough returns are initially received from microtopography, this will incorrectly set the range gate, which may then cause rejection of measurements to the true target. This conclusion is supported by the off angle measurements from the end of Phase 2. Measurements made off angle are shorter than the true distance, which could result in the type of interaction described above. This is problematic as the vast majority of field measurements will not be perpendicular to a slope. A similar conclusion was reached by Hosking (2009), who evaluated the off-angle performance of a Trimble S6 using sheet steel targets set at varying angles off perpendicular and determined that measurement errors increase proportionally with increasing angle. This may result from the way the beam footprint spreads over the sloped target surface, causing one edge of the footprint to be further from the instrument than the other (Deems, 2007). Thus, returns from multiple distances are resolved by the instrument, potentially setting the range gate incorrectly. This may also be an issue with distance meters and TLS systems, which use the same TOF system as the Trimble S6. While the effect may be increased with the distance meters and TLS systems due to their wider laser footprint (see "Beam Divergence", Table 5.1), their lower distance resolution may negate this issue.

Despite these measurement errors, there remain advantages to using a robotic total station over a distance meter, TLS, or airborne LiDAR, particularly in areas with deep snowpacks. The primary advantage is that a robotic total station can place points on a snow surface with a high degree of accuracy and precision. Providing the control network remains intact, the total station can repeatedly sample the same set of points over time, allowing for an estimate of the change in alpine snow volume throughout the snow season. This level of repeatability is not possible with currently described distance meter techniques, and is impractical with TLS systems.

Although a total station is not as portable as a distance meter, it is considerably more portable than a TLS. A TLS system is typically contained within several, large, Pelican-type cases containing the instrument, computer, and battery packs. Additional required equipment includes a survey-grade tripod and potentially a portable generator if the instrument is expected to operate for extended periods. In total, a full TLS kit may weigh up to 30 kg, considerably increasing the effort required to transport the instrument. In contrast, a total station system is wholly contained within one relatively compact case. Additional equipment consists of a survey-grade tripod and reflector for backsighting. A robotic total station can typically run for 8 h on one "camcorder-type" lithium ion battery and space for extras are often included in the case; a full total station kit may weigh up to 10 kg.

Data collection on a TLS system is typically performed by a laptop computer, to which data is streamed in real time. Data may be stored onboard, but is limited by storage capacity. A total station may collect data either in on board memory, or on a hand-held, ruggedized, waterproof, solid-state computer, thus reducing the possibility of

data loss due to hardware failure. Additionally, total station data formats are extremely economical of storage space, increasing transfer speeds and allowing considerable quantities of data to be stored on limited computer memory.

5.6 Conclusion

This chapter presented the results of a project to develop and validate a new method of remotely capturing snow depth data in areas that have significant winter hazard, thus limiting access. Although large errors in the calculated snow depth data were observed, the errors were in the same range as previously described methods. Several potential issues with measurements based on electro-optical systems used by total stations were highlighted; however, more work is required in this area to better quantify these errors and develop solutions to mitigate them.

As the total station holds some advantages over the other methods, it is important to quantify these errors. Total stations offer increased angular resolution, which is key for repeatedly sampling points. They are also more portable and less expensive than TLS systems, and while not as inexpensive as distance meters, this is offset by the usefulness of this tool to several earth science sub-disciplines, allowing cost to be spread amongst many researchers. Remote measurements of snow depth using electro-optical technologies hold great promise for snow science by allowing for measurements in otherwise inaccessible areas.

6.0: Watershed-Scale Controls on Snow Accumulation

6.1 Introduction

6.1.1 Controls on Snow Accumulation

Snow accumulation is controlled by a number of interrelated processes that produce a range of spatiotemporally variable effects (see Chs. 2.3-2.5 for detailed discussion). Accumulation is most strongly controlled by elevation, which drives orographic precipitation. Lower air temperatures at high elevations also produce conditions where snowpack may persist throughout the year (McKay and Gray, 1981; Anderton *et al.*, 2004; Barry, 2008). Slope angle and aspect control snow accumulation through redistribution processes and exposure to incoming solar radiation. Redistribution encompasses wind and avalanche processes that are largely controlled by wind direction and slope angle, respectively (Elder *et al.*, 1998; Anderton *et al.*, 2004). Incoming solar radiation is strongly controlled by aspect, although slope angle may control radiation intensity at the snow surface, particularly in winter when the sun is at its lowest zenith angle (Pomeroy and Gray, 1995; Elder *et al.*, 1998; Barry, 2008).

At large scales (i.e. watershed-scale), the processes discussed above have the greatest effect on snow accumulation. However, at smaller scales (< 100 m) their effect is reduced, with the primary control being vegetation. A high proportion of snowfall may be intercepted by the forest canopy, particularly in coniferous forests (Pomeroy and Brun, 2001; Essery *et al.*, 2003; Varhola *et al.*, 2010). Depending on snowfall intensity, this snow may remain in the canopy to either sublimate back to the atmosphere, or blow away. Thus, shallower snowpacks are generally expected under dense forest canopies (Steppuhn, 1981; Troendle *et al.*, 1988). With high snowfall intensity the interception

capacity of the forest canopy may be exceeded, causing accumulated snow to fall to the ground via unloading.

Snow trapped in the canopy may also affect the underlying snowpack, as increased air temperatures may cause intercepted snow to melt and drip from the canopy. This process adds water and energy to the snowpack below, enhancing melt and increasing snowpack stratification if air temperatures drop again (Schmidt *et al.*, 1988; Schmidt and Gluns, 1991; Pomeroy and Gray, 1995; Pomeroy *et al.*, 1998; Storck *et al.*, 2002).

6.1.2 Snow Surveying

When manually measuring the snowpack to quantify SWE, data are most commonly collected by performing a snow survey along an established snow course (Woo, 1997). Snow courses are transects that have been designed to allow repeated measurement of snow properties to monitor snow accumulation over a season and between years. The spatial distribution of the snow courses, areal extent of snow cover, and accumulation patterns due to topographic and vegetative features should all be considered when designing the snow course network (Goodison *et al.*, 1981; Woo, 1997). Snow courses are generally permanently marked with five to ten sampling locations so that repeated measurements can be made in close proximity (Goodison *et al.*, 1981) (Fig. 6.1).

In hilly or mountainous terrain, a snow course is generally between 120 - 270 m long, with marked measurement points spaced at 30 m intervals. In areas of low relief, the length of the snow course may be extended and intervals between measurements may range from 100 - 500 m (Goodison *et al.*, 1981; Pomeroy and Gray, 1995).

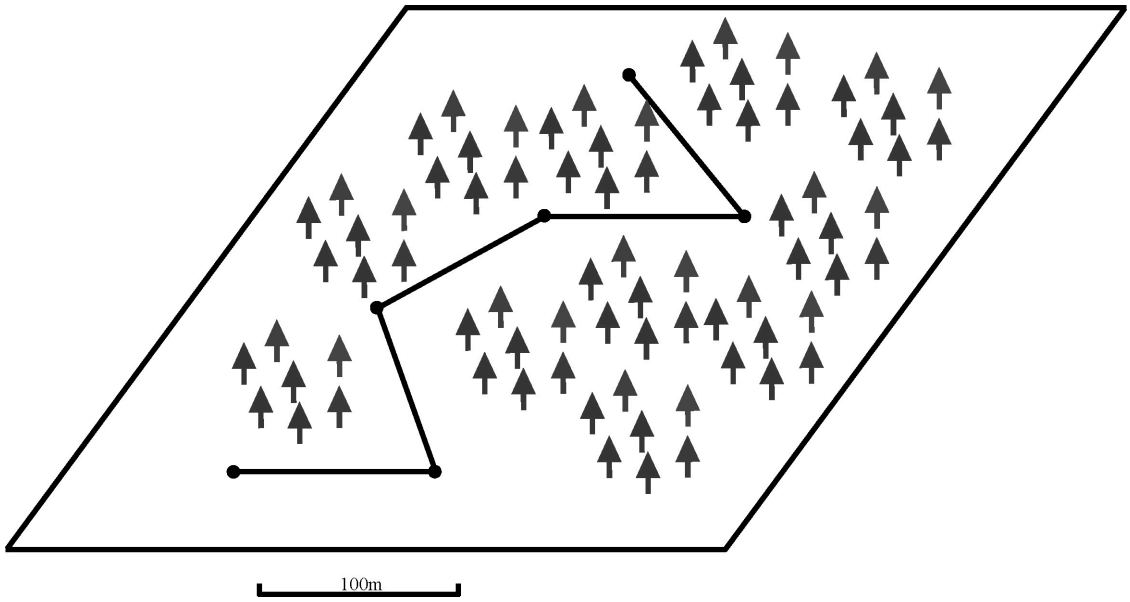

Figure 6.1. Schematic of a snowcourse. Density samples are taken at fixed intervals at permanently marked locations (filled circles), 100 m intervals in this case. Multiple depth samples are taken between density samples to capture the greater spatial variability. The course need not be straight, taking any shape required to capture the required terrain.

Fixed sampling points allow collection of subsequent measurements within a small area, thus reducing the possibility that confounding factors such as differing terrain or vegetation cover will affect later analysis. This system also allows a lower sampling intensity, reducing the workload of the snow surveyor. However, snow surveying is destructive to the snowpack, and once a particular location has been sampled it cannot be sampled again. The permanent stakes along the snow course simply mark the general location and samples are collected within a specified radius of that point (Adams and Barr, 1974b).

With small sample populations, statistical significance becomes an important factor in designing a snow survey, as they likely do not have the ability to provide the researcher with adequate statistical power to detect small differences in SWE (Goodison *et al.*, 1981). For example, a snow course with 10 sample points will fail to detect a 6 cm difference in SWE 90% of the time at $p = 0.05$ (Spittlehouse and Winkler, 1996). This

failure to detect small differences in SWE may become important if low snow accumulation conditions are encountered.

Dickinson and Whiteley (1972) found the lowest standard error of SWE when depth and density samples were taken in a 1:1 ratio. However, they also found that for a population of 41 depth samples, the standard error of SWE increases by only a factor of 1.5 when density sampling was reduced to ten measurements. This represents an increase of only 10% in the coefficient of variation and substantially reduces the workload of the snow surveyor, as density is much more difficult and time consuming to measure than depth (Dickinson and Whiteley, 1972; Goodison *et al.*, 1981). To further reduce sampling requirements, a sample population of 30 depth measurements provides similar statistical power as $n = 41$ depth samples, allowing a researcher to detect differences in SWE of 4 cm at $p = 0.05$ (Spittlehouse and Winkler, 1996).

Due to time and cost constraints, it is often not possible to measure snow properties at a sufficiently high resolution to determine basin-wide SWE values using traditional snow surveys (Erxleben *et al.*, 2002). Complicating matters further, safety concerns often make it impossible to access some areas in mountainous terrain in winter due to high avalanche risk. Although modern technologies may reduce this limitation (e.g. Prokop, 2008; Prokop *et al.*, 2008; Hood and Hayashi, 2010), they have not yet overcome some technical issues that limit their utility. This results in an incomplete picture of snow properties across the entire watershed.

Thus, recent studies have investigated techniques to collect spatially distributed measurements of snow depth in these inaccessible areas (see Ch. 5). We have used a robotic total station to remotely measure snow depth in alpine regions, which allows for

high measurement repeatability, a key requirement for studies investigating snow through time. Pre-selected sampling points (X, Y, Z) are measured in the field to record the distance of the snow surface from a fixed measurement location, from which snow depth relative to the underlying rock surface is calculated (see Ch. 5). Snow density values for alpine snowpacks are derived from the literature and used to calculate SWE for each measurement point, thus extending the basin-wide snow survey network.

6.1.3 Spatial Interpolation of Point Snow Measurements

In order to quantify spatial patterns of snow accumulation or to make comparisons with other continuous datasets, a continuous surface of snow depth or SWE must be calculated from the point measurements. In many cases, interpolation methods are applied to predict the value of unsampled points, using an algorithm that estimates a continuous dataset over the entire study area based on the sampled point data (Meijerink *et al.*, 1994; Burrough and McDonnell, 1998). The accuracy of the modelled surface is highly affected by the distribution of sampled points, with greater accuracy when sampling points are evenly distributed rather than when they are clustered (Chang and Li, 2000). Inverse distance weighting (IDW), spline, linear regression, and regression tree methods are the most common spatial interpolation techniques used in studies of snow accumulation.

IDW and spline are considered local interpolators because they use the nearest measured values to calculate each interpolated point. These methods rely on the assumption that there is a progressive change in interpolated values with increasing distance between measured points. Local interpolation techniques have low predictive capability in mountain watersheds: coefficient of determination (r^2) values generally

range from 0.098 - 0.205 for IDW, and as low as 0.07 for splines (Erxleben *et al.*, 2002; López-Moreno and Nogués-Bravo, 2006). Because local methods rely on the assumption of continuous change between predictor variables across space, López-Moreno and Nogués-Bravo (2006) postulate that the low predictive values reported are the result of the topographical complexity that is characteristic of mountainous areas, where values of predictor variables may vary widely over small spatial scales.

Chang and Li (2000) found that a multiple regression approach performed better than other common types of spatial interpolation. They achieved r^2 values of ≥ 0.6 in all watersheds studied, with half of the watersheds achieving an r^2 of ≥ 0.9. Similar results were reported by Jost *et al.* (2007) ($r^2 = 0.83$ and 0.89 for both study years), and López-Moreno and Nogués-Bravo (2006) and Stähli *et al*. (2001) ($r^2 = 0.51 – 0.58$). Multiple regression works best when a stratified snow sampling scheme is applied, which likely accounts for the difference in r^2 values between these studies. The sampling design used by Jost *et al.* (2007) divides the study area into strata with similar characteristics (e.g. elevation, slope, aspect, vegetation cover, etc.). This sampling strategy ensures that samples are collected along gradients of the most important predictor variables and, when combined with random sampling within each stratum, is considered a more robust method than traditional transect sampling when performing statistical analyses (Jost *et al.*, 2007). The primary drawback to multiple regression is the assumption of linear relationships between the predictor and response variables. All variables measured by Chang and Li (2000) and Jost *et al.* (2007) met this assumption, but other studies (i.e. Erxleben *et al.*, 2002; Anderton *et al.*, 2004) found only non-linear relationships, precluding the use of this technique.

Non-linear estimation techniques have, therefore, received considerable attention in recent literature, as they can detect non-linearity, which is often observed between the commonly used predictor variables and snow depth or SWE (Elder *et al.*, 1995; Elder *et al.*, 1998; Balk and Elder, 2000; Anderton *et al.*, 2004; Molotch *et al.*, 2005; López-Moreno and Nogués-Bravo, 2006; López-Moreno and Stähli, 2008). The most common non-linear technique is classification and regression tree analysis (C&RT, Breiman *et al.*, 1984). This method makes no assumption of data normality and can be applied to any combination of continuous or categorical data. A regression tree is grown by recursively splitting the input data into 'nodes' based on hierarchical relationships (Fig. 6.2).

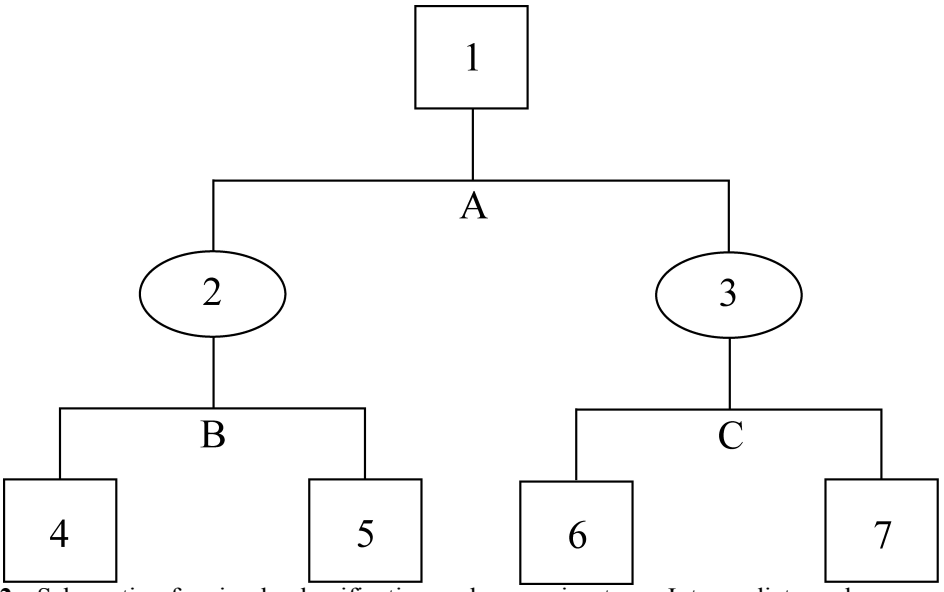

Figure 6.2. Schematic of a simple classification and regression tree. Intermediate nodes are represented by ellipses, terminal nodes by squares, and splits by lines. Node 1 contains the full dataset, which is split on a critical value of Variable A. Input values that are < A go to Node 2, while values > A go to Node 3. The splitting occurs again with Variables B and C, which routes input values to Terminal Nodes 4 – 7.

The C&RT algorithm begins with all response variable data (i.e. SWE) paired with predictor variables (i.e. elevation, slope, etc.) in the initial node (1 in Fig. 6.2). All predictor variables are analyzed to determine which split results in the greatest reduction of within-node variance (Breiman *et al.*, 1984). At each split (A, B, C in Fig. 6.2), one

variable is chosen, and a critical value determined. All values above or below this criterion are routed to the next node (either 2 or 3 in Fig. 6.2) along with the remaining variables. Splitting continues in this manner until any further splits produce minimal reductions in node variance, or the terminal nodes become 'pure' (i.e. one value per node). As all response variable values that fall within a terminal node are averaged, all input data falling into a terminal node are assigned the mean value for that node (Breiman *et al.*, 1984).

C&RT has the potential to considerably overfit the input data, such that each individual input value is classified into its own terminal node. Thus, trees are generally fully grown, and then pruned back one branch at a time. After each pruning step, the effect on the predictive power of the tree is assessed by calculating statistical deviance and r^2, then selecting the tree that minimizes deviance, maximizes r^2 and provides the simplest interpretation of relationships (i.e. fewest terminal nodes) (Elder *et al.*, 1995; Elder *et al.*, 1998; Balk and Elder, 2000; Molotch *et al.*, 2005). For a comprehensive discussion of C&RT, see Breiman *et al.* (1984).

6.1.4 Accounting for Sample Errors

With all measurements, error inherent with the sampler or sensor must be quantified in order to better understand and qualify the resulting dataset (Beaumont and Work, 1963; Goodison *et al.*, 1981). We therefore quantified the sampling error of the SnowHydro snow tube used in this study (SnowHydro, Fairbanks, AK), by comparing it with two existing designs: the Standard Federal and the Meteorological Service of Canada (MSC) tubes (see Ch. 4). All samplers produced density values that were not statistically different from high-resolution density data collected in collocated snow pits

in a forested environment. Additionally, the SnowHydro sampler performed better than the two other designs in this environment, which represents the dominant sampling conditions for this study.

The robotic total station remote measurement technique was rigorously validated with collocated manual depth measurements. An irreducible observed error of ± 0.35 m was attributed to interaction between the laser and the snow surface. Hopkinson *et al.* (2011) observed similar patterns in over- and under-estimation of measurements from airborne Light Detection and Ranging (LiDAR) surveys over water, which was dependent on the intensity of the returning laser pulse. Testing of two different instruments indicates that this is only a serious problem for instruments with a time of flight electronic distance meter (EDM); instruments with phase-shift EDMs do not appear as strongly affected (see Ch. 5).

6.2 Methods

6.2.1 Predictor Variables

Predictor variables selected for the C&RT analysis include elevation, slope, aspect, and canopy closure. The elevation variable represents controls on orographic precipitation and air temperature, while the slope angle variable represents radiation receipt and likelihood of avalanching and/or downslope snow creep. The aspect variable represents radiation receipt and wind exposure, and the canopy closure variable represents interception and radiation transmission to the snowpack. Other studies have also used radiation and wind field surfaces as predictor variables, in addition to topographic and vegetation surfaces. In the absence of field data against which to test GIS-derived radiation surfaces, we use slope and aspect as proxies for radiation. As we

do not have wind data from which to derive wind surfaces, aspect is used as a proxy for wind redistribution. Winds are predominantly from the west (Nkemdirim, 1996), thus we expect snow removal from westerly slopes and deposition on easterly slopes.

Topographic data were derived from a LiDAR digital elevation model (DEM) created for Alberta Sustainable Resources Development (ASRD). These data were collected to provide a highly accurate bare earth elevation surface for the Alberta government (Alberta Sustainable Resource Development, 2008). Elevation data were processed to 1 m horizontal (0.45 m RMSE) and vertical (0.30 m RMSE) resolution (Alberta Sustainable Resource Development, 2008). From this dataset, 1 m resolution maps of slope angle and aspect were produced using ArcGIS 9.3.1 (ESRI, Redlands CA).

Forest data were initially provided from the Alberta Vegetation Index (AVI) (ASRD, Edmonton, AB). While this dataset includes a number of forest parameters, the categorical canopy closure data was at too coarse a resolution to be meaningfully applied in this study. Thus, LiDAR point cloud data provided by ASRD was processed by the Alberta Terrestrial Imaging Centre (ATIC) to derive 15 m resolution continuous datasets of stem density (stems per pixel), canopy height (dm), canopy closure (%), and location and height of individual trees (ATIC, 2010; McGaughey, 2010).

LiDAR canopy data were ground-truthed to ensure that it was representative of natural conditions in the watershed. Hemispherical photographs were taken using a full-frame, Canon EOS 5D digital SLR camera and Sigma 8 mm *f*/3.5 circular fisheye lens oriented north, on a levelled tripod at a height of 1.5 m above the ground surface. Photographs were processed using edge detection software (SideLook 1.1.01, retrieved from www.appleco.ch, Nobis and Hunziker, 2005), and Gap Light Analyzer (GLA)

(Institute of Ecosystem Studies, Simon Fraser University, Burnaby, British Columbia, Frazer *et al.*, 1999) was used to calculate the fraction of sky and canopy. Photographs were collocated with the density sampling stakes described in Ch. 6.2.1, and provided the % canopy closure above each sampling point for comparison with the LiDAR-derived values from the nearest pixel to each stake. Results indicate that the LiDAR canopy data accurately represented forest cover in the watershed, and could be utilized as a continuous predictor for analysis (Fig. 6.3).

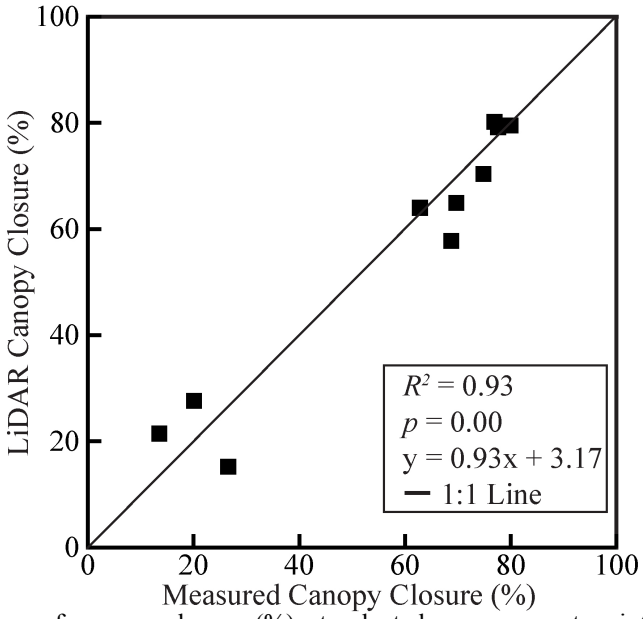

Figure 6.3. Comparison of canopy closure (%) at selected measurement points with canopy closure derived from a LiDAR point cloud dataset of Star Creek.

6.2.2 Snow Sampling Strategy

Snow courses were established below treeline in the Star Creek watershed (see Ch. 3). Each transect was 500 m long, with snow density measurement sites permanently marked at 100 m intervals (n = 54) using 1.5 m long sections of white PVC tubing affixed to 0.5 m long steel reinforcing bar (rebar) driven into the ground. White PVC was selected in order to reduce any differential melting effects caused by the presence of the tube. Snow depth measurements were paced off at 10 m intervals (n = 462) between

density markers. While pacing leads to some variability in location of sampling points, tracks from previous surveys were often visible, adding confidence that samples were repeatedly collected within ~1 m of each other. Three transects were installed in the West Fork sub-basin, and two in each of the East Fork and McLaren Creek sub-basins. An additional 1000 m long snow course was installed near the basin outlet, below the confluence of the East and West Forks, to capture lower elevations and lower slope angles. All transects ran approximately perpendicular to the stream channel, thereby encompassing a wide range of topographic and vegetation variability (Fig. 6.5).

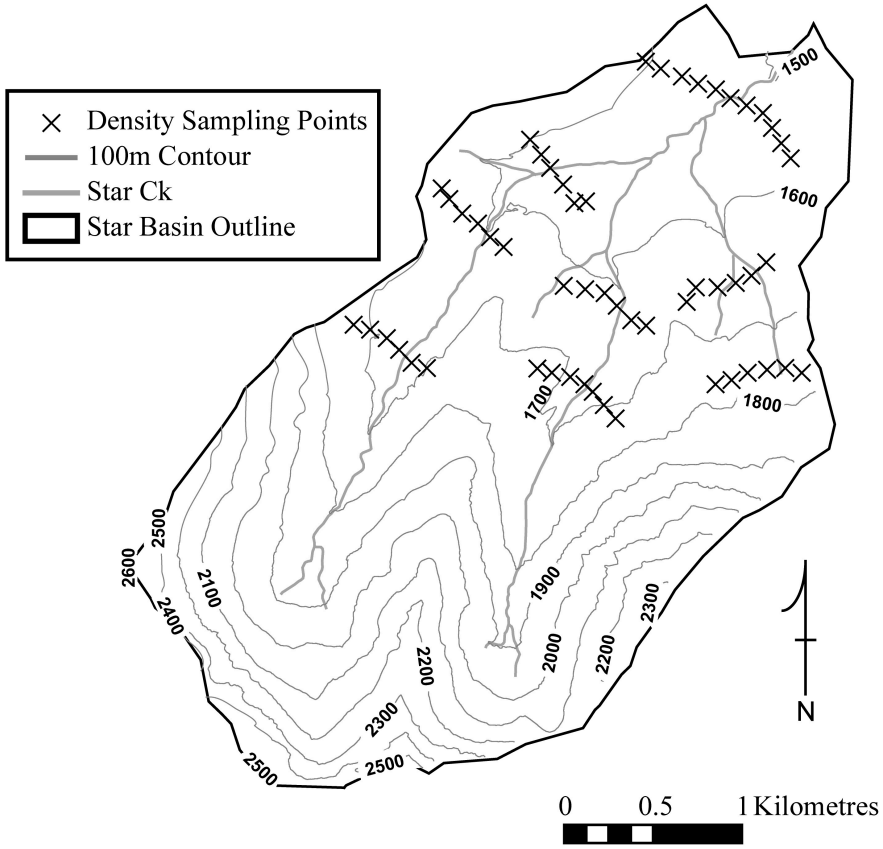

Figure 6.4. Location of transects in Star Creek. Crosses indicate location of density sampling points, spaced at 100 m intervals.

The full topographic variability of the watershed was not adequately represented by the existing points. Therefore, to capture steeper slopes and high elevations, a

network of remotely measured points was established above treeline in the West Fork (See Ch. 5 for details of remote measurements) (Fig. 6.6). No remote points could be established in the East Fork because areas that provide the required sightlines for the total station were not sufficiently safe from avalanche hazard due to forest and slope conditions. Additionally, access to this portion of the watershed is considerably more difficult than into the West Fork. Thus, relationships between topography and snow accumulation derived from the West Fork points were assumed to be representative of alpine accumulation in the watershed, and were thus also applied to the East Fork. The alpine zone in the McLaren Creek sub-basin consists of the flank of Mt. McLaren (which forms the southeast watershed boundary) with very steep to vertical slopes and no alpine bowl as in the East or West Forks. Field observations indicated that these slopes did not accumulate deep snowpacks, due to consistent sloughing of accumulated snow. Thus, no remote sampling points were established in this area.

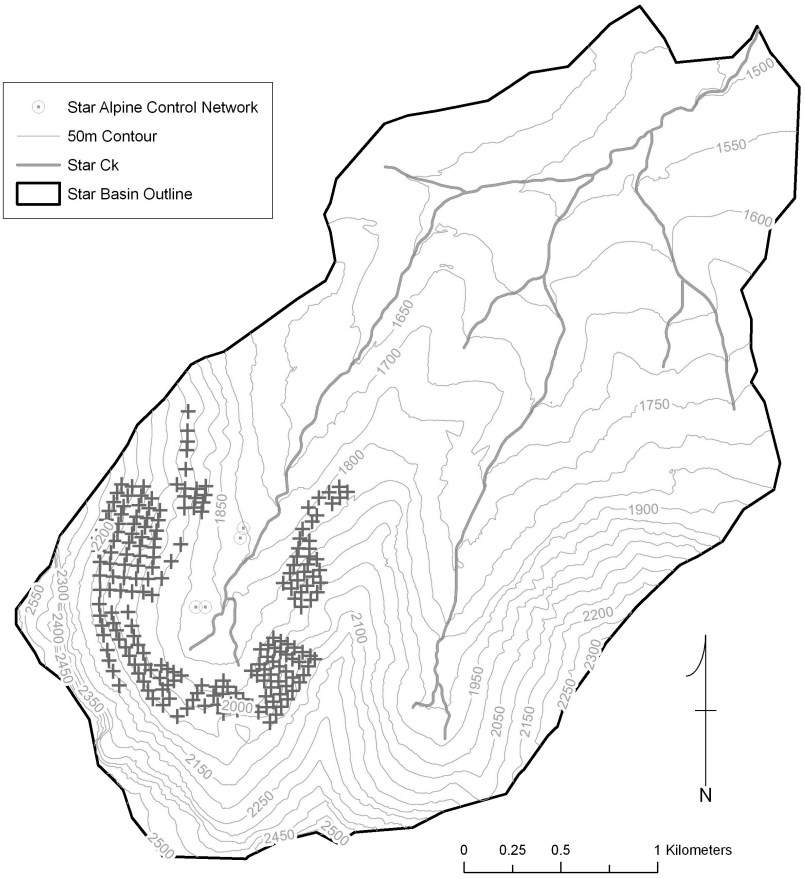

Figure 6.5. Location of remote snow depth measurement points in the alpine region of Star Creek West Fork. Crosses show sampling point locations; circles mark location of control points established with RTK GPS.

Remote measurements were based on a network of control points surveyed with a Trimble R7 differential GPS. Control points were marked with 0.5 m long rebar driven into the ground, leaving ~10 cm exposed, to reduce the possibility of control point drift. The initial measurement consisted of a 6 h static survey of the first control point. Static survey data were post-processed with Natural Resources Canada's Precise Point Positioning service to achieve high point accuracy. A subsequent survey with a Trimble R7 real time kinematic (RTK) GPS was performed to establish the remaining control points. These control points were registered to UTM zone 11U, and have a positional error of ± 4 cm in the X, Y, and Z directions. High control point accuracy is essential for

this technique, as small positional errors propagate as distance to target increases, causing considerable positional uncertainty at the target point. This potentially leads to large errors in the calculated snow depths produced by the technique. When deployed in the field in 2010, large errors were observed in the dataset, resulting in unusable data. Thus, the remaining results and discussion focuses on data collected below treeline.

Remote measurements were collected in 2010 with either a Trimble S6 or Leica TCRP 1201+ robotic total station (see Ch. 5 for details). However, when the data were processed to calculate snow depth, unrealistic values (> 3 m) were produced. This was likely driven by low positional accuracy of the control points (± ~3.5 m), as these surveys were performed prior to the high accuracy GPS survey. Additionally, above-average snow accumulation in 2011 produced severe winter avalanche hazard throughout the Crowsnest Pass region, preventing access to the alpine areas of the watershed for the duration of the field season. When the alpine region was accessed during the April survey, a large avalanche (> 100 m wide) had run through an area where the lower elevation control point was established. This point was buried under an ~ 2 m avalanche deposit and likely destroyed, thus the remote measurement technique was not used in 2011, either. Thus, snow depth measurements above treeline are not available for either field season, so C&RT analysis for the whole basin was completed with only the traditional snow survey data from below treeline.

A histogram analysis of topographic and vegetation parameters was performed for the basin below treeline, and compared to the distributions of the same parameters for all sampling points. Basin-wide values were derived from pixel counts falling within each class calculated from the LiDAR DEM (Fig. 6.4). Generally, there is good agreement

between the basin-wide and sample point distributions. Canopy closures of ≤ 10% are underrepresented, as few sampling points were located in large clearings. The remaining canopy closures, however, are well represented. The distribution of aspect is highly representative. Elevation is well represented: a very small area of the watershed that falls below 1480 m.a.s.l is not represented, and the highest elevation class (1850 m.a.s.l.) approximately representing treeline is underrepresented as no transect coincides with treeline. The range of slope angles below treeline is well represented, given the low avalanche risk on these densely forested slopes.

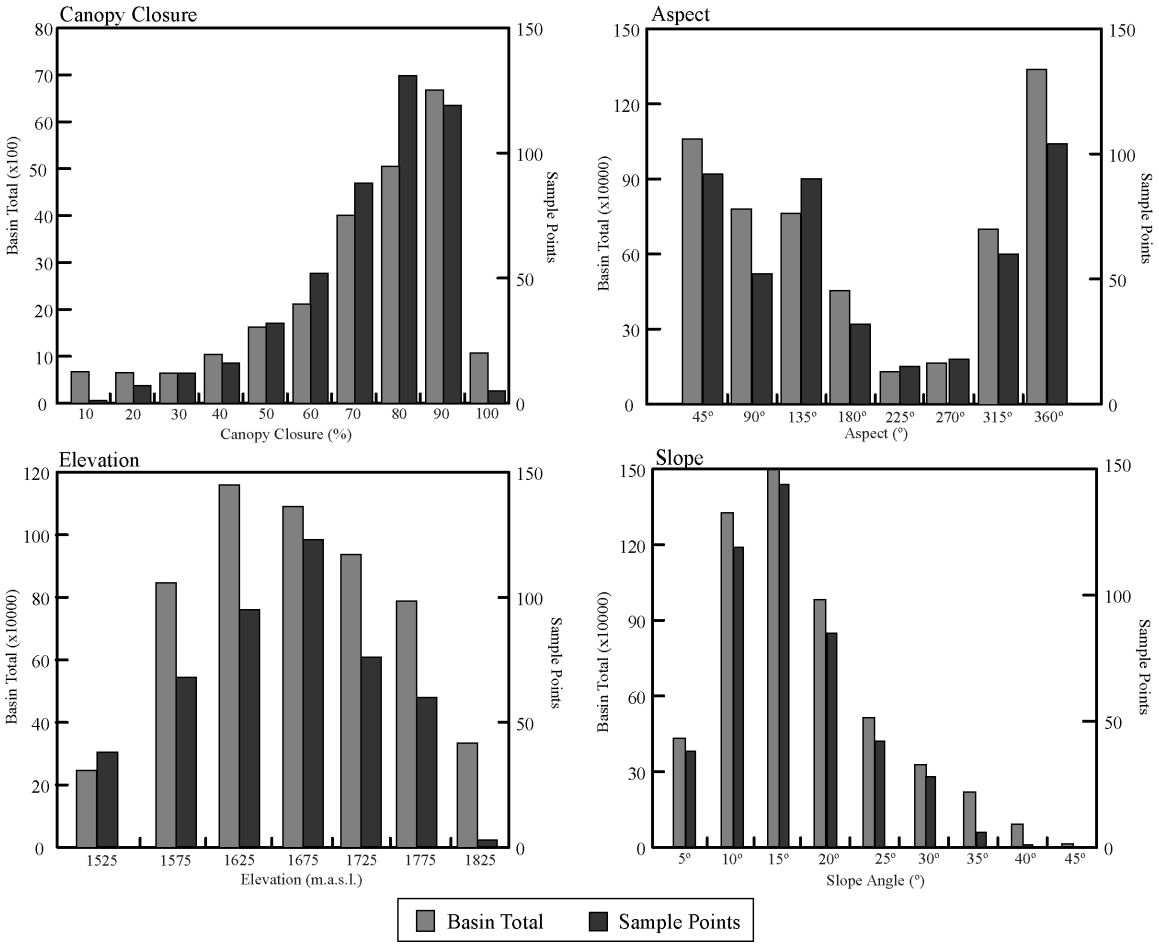

Figure 6.6. Histograms of sampling points and total basin values (number of pixels) including 462 depth sampling points below treeline, and 200 remote sampling points above treeline. Sampling point distributions generally match the distribution of pixel values derived from the DEM, indicating that the sample points are representative of basin values

Snow surveys were performed using standard techniques (Goodison *et al.*, 1981). Three snow surveys (manual and remote measurements) were scheduled in each of 2010 and 2011. Surveys were conducted on approximately the same dates between years, in February, March, and April, and required on average 3.5 days to complete. Unfortunately, the February 2011 survey did not include the 1000 m transect due to extreme cold weather.

For each survey, snow depths were measured with a graduated avalanche probe perpendicular to the local slope angle. The Standard Federal and SnowHydro snow samplers were used for density measurements depending on snow conditions: the Federal only when snow conditions warranted (i.e. wind hardened, deep), and the SnowHydro for all other conditions as it provides superior performance (See Ch. 4). The Standard Federal was used for only two snow surveys: February 2010 and February 2011, where it was used for all samples; the SnowHydro was used for all other surveys. Snow tube sampling error tests indicate similar results from each of these tubes, with no significant statistical difference observed between them. SWE was calculated from the snow depth measurements made between density stakes using Eq. 6.1:

$$SWE = d_s \frac{\rho_s}{\rho_w} \quad 6.1$$

where d_s is snow depth (cm), and ρ_s and ρ_w are the density of snow and water (g cm^{-3}), respectively. ρ_s was taken as the average of the density measurements collected at the two stakes bracketing the 10 depth measurements. Using the high-resolution snow depth measurements allowed me to estimate SWE at a finer scale, thus incorporating a much larger range of topography and vegetation.

Scatterplots of each predictor variable versus SWE and snow depth for each sample point were created to quantify relationships between the two, and to assist in interpreting regression trees.

6.2.3 Statistical Analysis of Snow Measurements

Multiple linear regression was initially used to determine the effect of topography and vegetation on basin-wide SWE, given its good performance in similar studies. However, strong non-linear relationships between predictor and response variables were observed in both years, precluding the use of linear techniques to predict SWE across the basin. As C&RT analysis has been effectively used to explain a high proportion of the variance in non-linear datasets similar to the one collected here, it was a more appropriate technique for interpolating snow depths across the watershed.

C&RT requires a large number of samples (n = 200 – 400) to make reasonably accurate predictions, although it is less sensitive to input variable resolution than linear models (López-Moreno *et al.*, 2010). The accuracy of C&RT models also tends to increase with increasing DEM resolution. High resolution DEMs (i.e. 1 m, 5 m) are better able to capture the topographic variability of a study area (Kienzle, 2004). This supplies more information about predictor variables for the C&RT algorithms to process, thereby potentially producing more accurate predictions of SWE. For this study, the use of 1 m resolution predictor variables and n = 462 samples provides confidence that SWE predictions are accurate. Snow depth measurements were converted to SWE as outlined above and were paired with topographic and canopy parameters (predictor variables) derived from the LiDAR datasets: elevation (m), slope angle (degree), aspect (categorized into the 8 ordinal compass directions), and canopy closure (%).

The high number of input values increases tree complexity, as a greater range of variability must be explained by the C&RT algorithms. Using the 462 snow depth measurements – rather than the 54 density measurements – as the basis of SWE calculations incorporates much higher spatial variability into the regression tree. With only 54 density measurements, the regression trees would have been substantially less complex because: (1) density is much less spatiotemporally variable, thus fewer tree splits (resulting in fewer terminal nodes) would be required to explain the observed variability; and, (2) density was measured at a much lower resolution than depth (100 m vs. 10 m). This effectively decreases the resolution of predictor variables, resulting in loss of variability compared with the higher resolution depth measurements. Thus there is a trade-off between low complexity trees based on a limited subset of the predictor variability, and more complex trees based on a greater range of topographic variability. Although the simpler explanation of a phenomenon is generally favoured in the sciences, using the smaller density dataset would not provide the required information to adequately explain the spatiotemporal variability of SWE observed across the watershed.

All data analysis was performed using Statistica DataMiner software (StatSoft, Tulsa, OK). Regression trees were grown for each snow survey date to investigate variations on the controls on snow accumulation between months and between years. The optimally sized tree for each survey was defined as being within one standard error of the maximum r^2 and having minimum statistical deviance (Elder *et al.*, 1995; Elder *et al.*, 1998; Balk and Elder, 2000). Simple linear regression of measured and predicted values for each tree was used to calculate r^2, and generalized linear modelling using a normal distribution and identity link function was used to calculate statistical deviance

(Stokes *et al.*, 2006). Normality was assessed graphically using normal probability plots. Data that appeared non-normal was analyzed with a Tukey-Lambda test to determine the best distribution to represent these data, based on the lambda value (λ) with the largest correlation to the input dataset (Joiner and Rosenblatt, 1971). A dataset that is highly correlated with $\lambda = 0.14$ indicates that a normal distribution is appropriate (Vasicek, 1976).

Importance plots of each regression tree were used to assess the relative role of predictor variables in controlling SWE. In these plots, the variable most commonly used for splitting in a given tree is assigned a value of 1, and the remaining variables are represented as proportion of the initial variable. It is important to note that these plots do not suggest hierarchy in the tree structure.

6.2.4 Spatial Distribution of SWE

Regression trees are similar to decision trees, in that they are interpreted as a series of conditional statements derived from each split. These conditional statements classify input data (raster cells in this case) based on the characteristics of each given cell in all input raster surfaces. The trees grown in Statistica DataMiner were imported to ENVI 4.8 (ITT Visual Information Solutions, Boulder, CO), an image analysis software package, using the built-in Decision Tree module. This module allows the user to build a regression tree or import a pre-existing tree developed in other software. Once the tree is built, it is applied to a set raster surfaces of the predictor variables to create a new raster surface, in which cells are iteratively assigned terminal node values as the rasters are processed by the tree. The output of this module is a raster surface at the same resolution as the input data (i.e. 1 m). Unfortunately, Decision Tree cannot store fractional

numbers, but rather outputs raster cell values as labels: Cat1, Cat2, etc. The ENVI outputs were thus saved as raster files and imported into ArcGIS 9.3.1.

Predicted SWE values produced in Statistica are real numbers with decimal values, which are represented in GIS as floating point rasters. The SWE values from the original trees were converted to integers by multiplying by 100 (e.g. 4.56 cm SWE x 100 = 456 cm SWE). The ENVI rasters were then reclassified in ArcGIS so that each category (e.g. Cat1, Cat2, etc.) was assigned the appropriate integer SWE value derived from the original regression tree. Each raster was then divided by 100 to create floating point rasters of SWE for each regression tree.

6.3 Results and Discussion

6.3.1 Snow Conditions

2010 and 2011 produced considerably different snow accumulation patterns in SWE and snow covered area. 2010 was a low snow accumulation year, with peak SWE measuring 86% of normal at the nearest snow pillow station (Alberta Environment, 2010). In Star Creek, this low accumulation was quite pronounced, with low elevation areas of the watershed remaining snow-free throughout the winter: bare ground was encountered on low elevation transects during each of the three surveys. Snow depth and SWE increased minimally from March to April, although April depth values were lower than those measured in February (Fig. 6.7).

Local meteorological conditions likely contributed to this low accumulation pattern, as mean monthly air temperatures were 3 – 4°C above normal from January to March at the nearest Environment Canada meteorological station (Coleman, AB; 1341 m.a.s.l), enhancing ablation rates (Fig. 6.8).

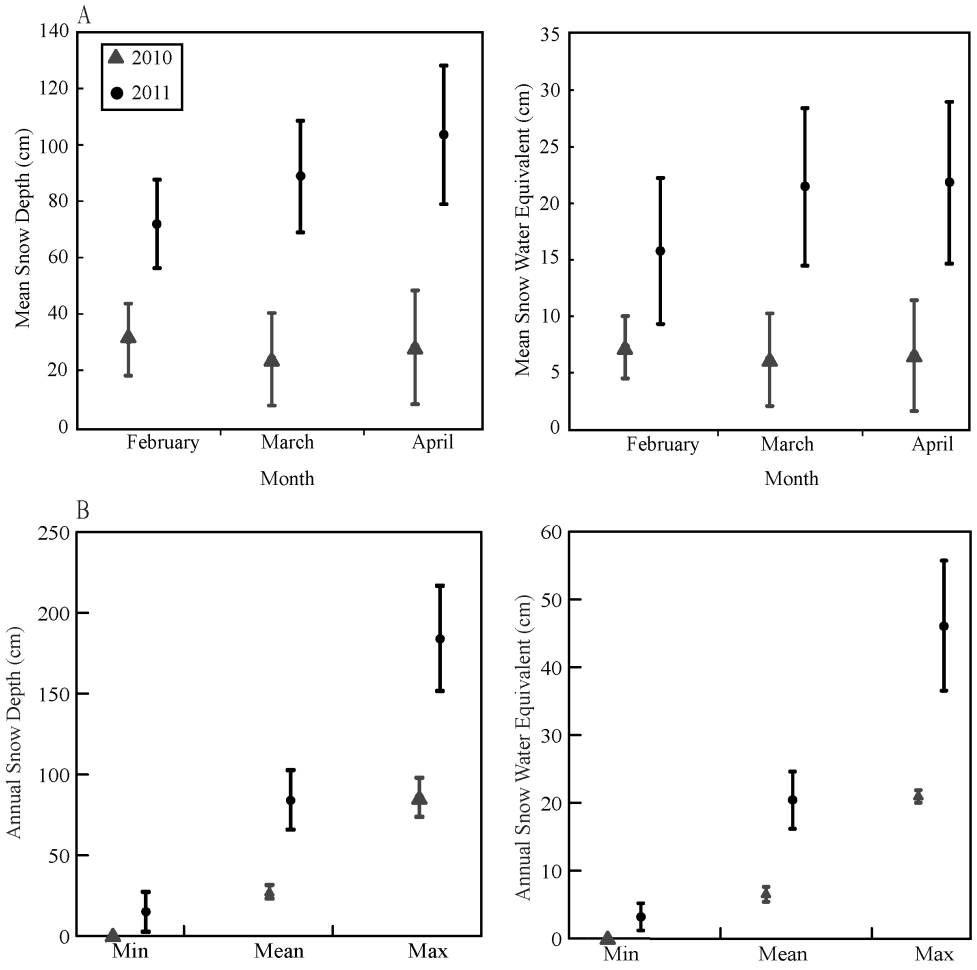

Figure 6.7. Snow accumulation in each year: (A) Measured mean snow depth and SWE from February to April 2010 and 2011. (B) Comparison of measured minimum, mean, and maximum snow depth and SWE in 2010 and 2011. Minimum values for snow depth and SWE in 2010 were 0 cm, measured repeatedly throughout the season. Mean, min and max snow depth and water equivalent are calculated from n = 462 depth measurements.

2011 had considerably more snow accumulation than 2010, with peak SWE measuring 312% of average at the nearest snow pillow station (Alberta Environment, 2011b). No bare ground was encountered during any survey in 2011. A strong increasing trend in depth and SWE was observed throughout 2011 (Fig. 6.7): mean snow depth and SWE from 2011 was nearly 5 times higher than 2010 values. Air temperatures at Coleman in 2011 were closer to 30-year normals (Fig. 6.8), and likely promoted snow accumulation rather than the ablation conditions of 2010.

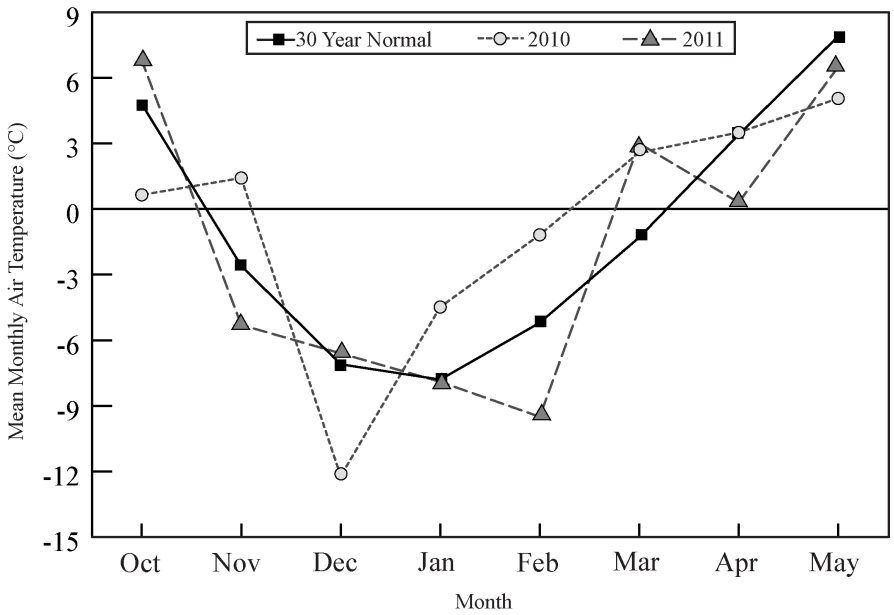

Figure 6.8. Mean monthly air temperatures at Coleman, AB (1341 m.a.s.l.). Solid line indicates 30-year normal (1971 – 2000) (Environment Canada, 2011).

Predictor variables were plotted against SWE measurements for both 2010 and 2011 to observe SWE response to each variable individually (Fig. 6.9). Across all 2010 scatterplots, SWE generally decreased from February to April. Although accumulation generally increased with elevation, plots of elevation versus measured SWE show a large number of 0 cm SWE values that extend up to ~1680 m. Also visible is a step change to higher SWE near 1630 m. Approximately similar snow amounts accumulated on both low and high angle slopes, thus there is no definitive radiation intensity signal, as lower SWE values would be expected on higher angle slopes due to receipt of more intense incoming solar radiation.

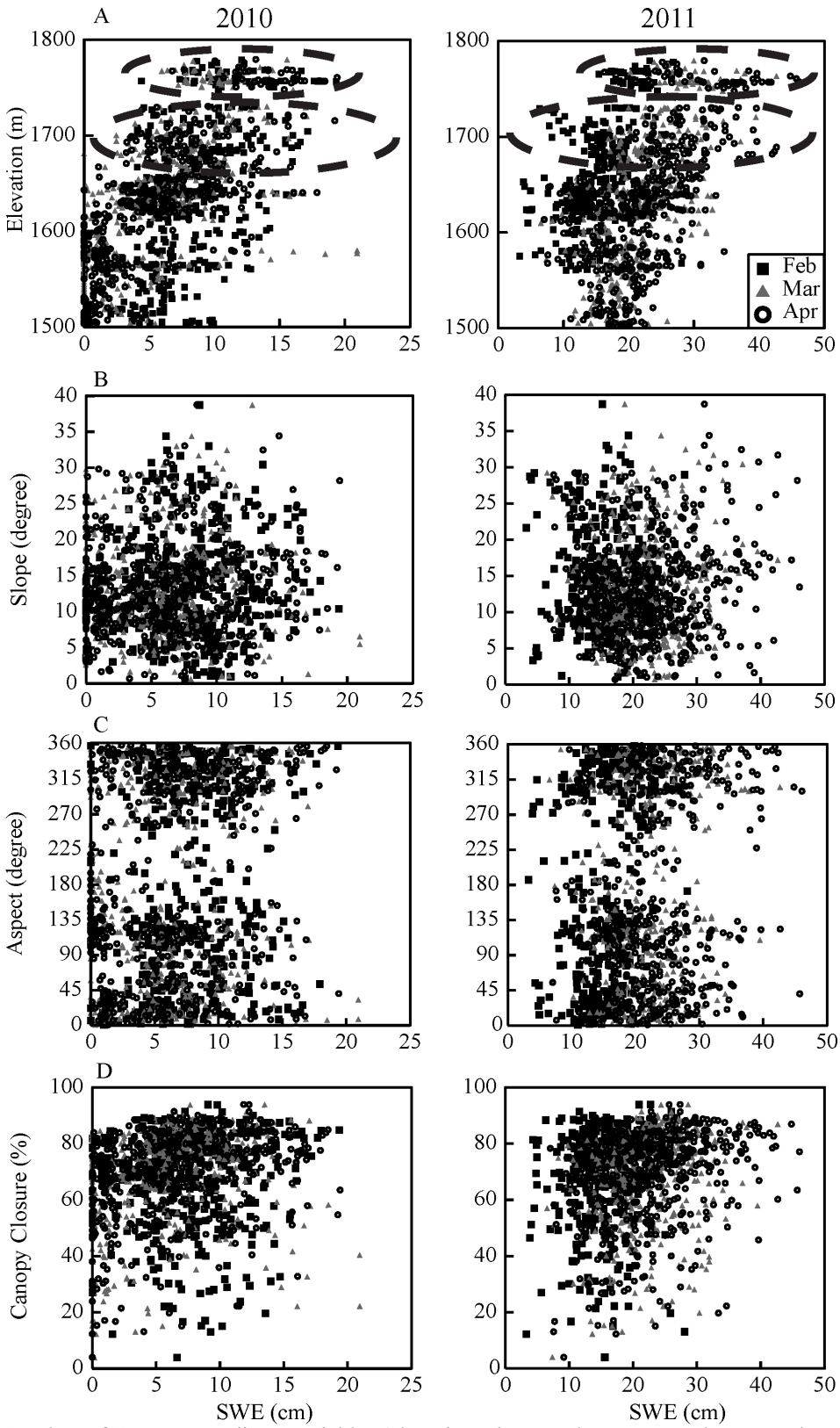

Figure 6.9. Plots of SWE vs. predictor variables (elevation, slope angle, aspect, and canopy closure) for all sampling points in 2010 (left) and 2011 (right). Dashed ellipses highlight step changes observed in elevation vs. SWE plots.

Measured SWE varied minimally with aspect during all surveys in 2010, even at locations with 0 cm SWE values. Slightly more SWE was measured on north- than on south-facing aspects, as northerly aspects receive considerably less radiation than southerly aspects. Measured SWE showed little variation across a range of canopy closures, with 0 cm SWE measured under all canopy conditions, including very low canopy closures. Similar to scatter plots for the other predictor variables, total SWE declined as the season progressed. Overall, less SWE was measured in clearings in 2010, which may suggest that they were subject to greater solar radiation fluxes or higher rates of wind redistribution.

SWE increased throughout the season in 2011 (Fig. 6.9), and also increased with elevation, with a step change to higher SWE at ~1630 m and again at ~1740 m. The distribution of data points observed in all four 2011 scatter plots correspond well with patterns observed in the 2010 plots, but with a shift in magnitude to higher overall SWE. As the season progressed, more snow accumulated on steeper slopes than in 2010. Additionally, the range of canopy closures with the same SWE decreased as the season progressed, with greater SWE at higher closures.

6.3.2 Classification and Regression Trees

Normal probability plots for the 2010 data suggest that the tails of the distribution are 'heavy' (i.e. a large number of samples fall in the tails of the distribution; Fig. 6.10). This is particularly evident at the '0' end of the distribution due to a considerable number of 'no-snow' samples, and suggests that the data are not normally distributed. Probability plots for 2011, however, show distributions consistent with a normally distributed dataset, with only minor deviations (Fig. 6.11).

Results from the Tukey-Lambda test show that both the 2010 and 2011 datasets were highly correlated with $\lambda = 0.14$, which suggests that the data are best represented by a normal distribution (Table 6.1). Therefore, the parametric statistical tests used for these analyses were deemed appropriate (Wessa, 2008).

Table 6.1. Correlation coefficients with $\lambda = 0.14$ calculated with Tukey's lambda distribution. High correlation indicates data are normally distributed. Results in the table are all significant at $p = 0.05$

	Measured	***Predicted***
February 2010	0.996	0.989
March 2010	0.973	0.975
April 2010	0.967	0.962
February 2011	0.998	0.992
March 2011	0.998	0.987
April 2011	0.994	0.983

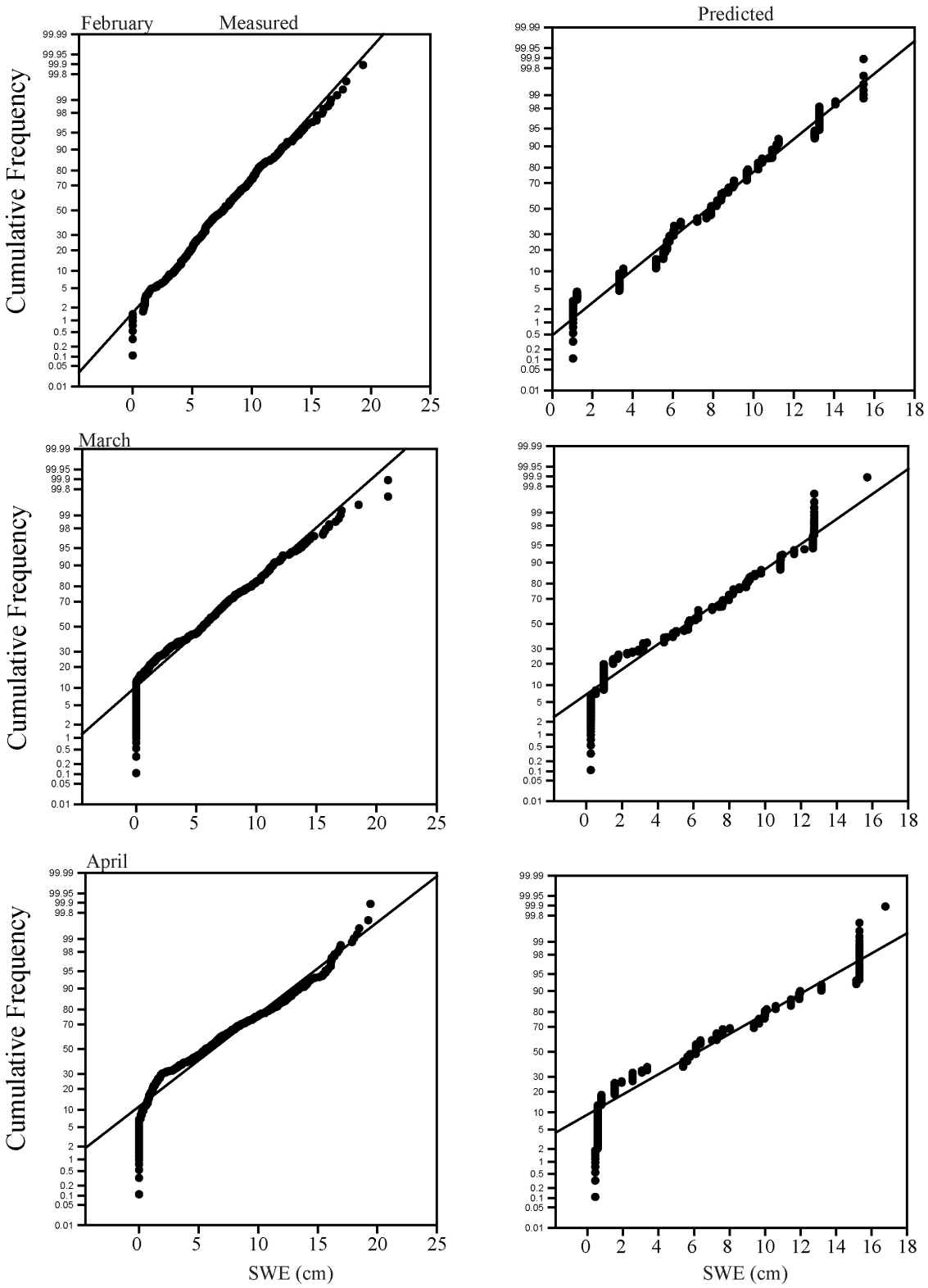

Figure 6.10. Normal probability plots of measured and modelled SWE data for 2010. Heavy tails in the March and April distributions suggest non-normality.

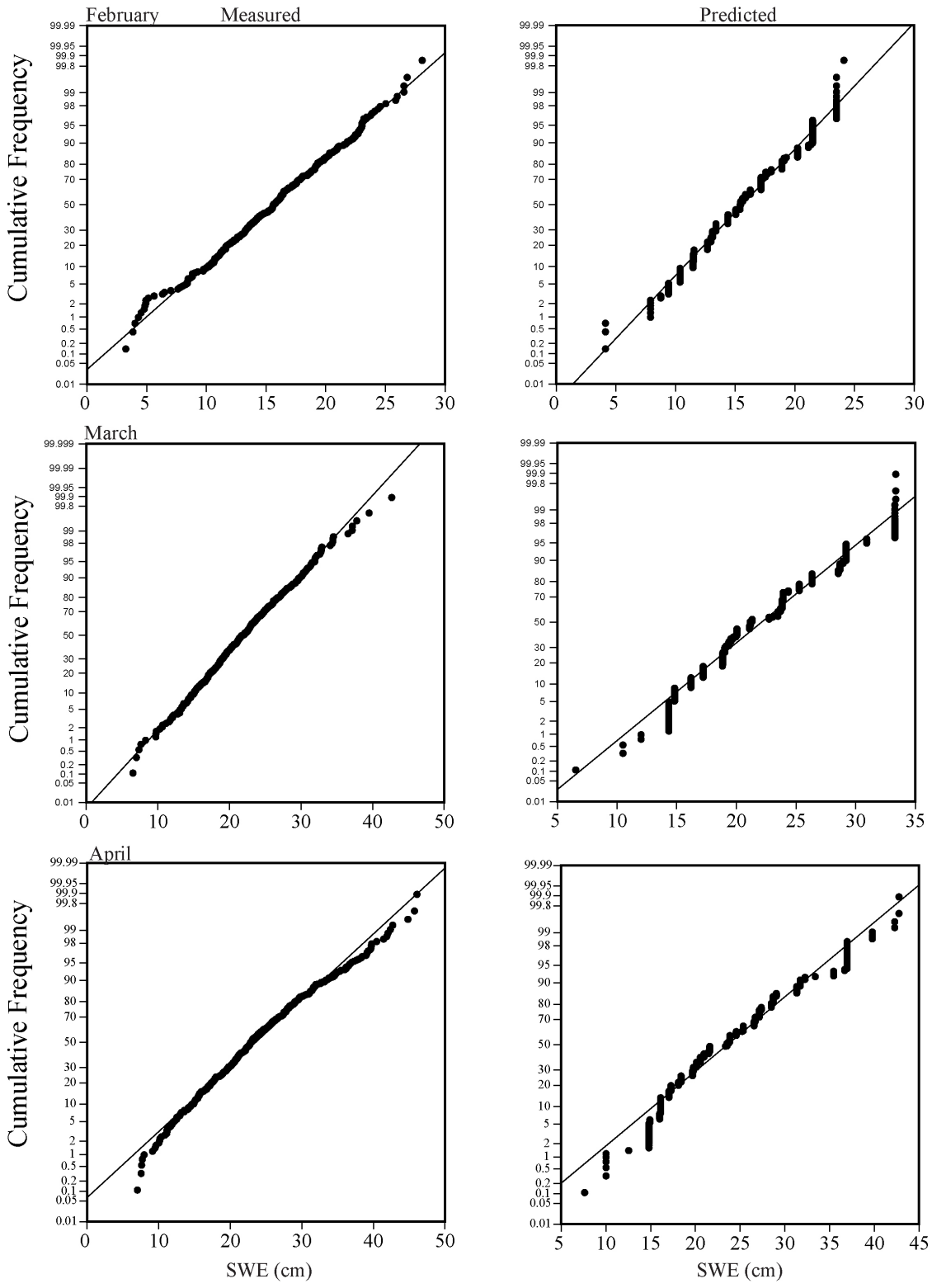

Figure 6.11. Normal probability plots of measured and modelled SWE data for 2011. Deviations from normality were considered small.

Optimal tree sizes were chosen based on an analysis of statistical deviance and r^2 produced by the C&RT algorithm (Fig. 6.12). As the tree grows from an initial two terminal nodes to its maximum size, r^2 increases rapidly until the tree reaches a threshold size (~30 terminal nodes) beyond which r^2 increases asymptotically. Low r^2 values are expected with small, low complexity trees, as the classification of data points is too coarse to provide a strong relationship between measured and predicted values. With increasing tree complexity, the classification becomes finer and r^2 increases.

Data from 2010 produced deviance statistics of a lower magnitude than 2011 data; however, the relative magnitude of deviance in comparison to other tree sizes is more important than the magnitude of the deviance statistic itself. For most of the snow surveys modelled in this study, deviance is initially quite low, but increases to a threshold of ~8 terminal nodes beyond which it decreases again. I hypothesize that this reduction in deviance results from small numbers of unique predicted values in the predicted population with low complexity trees. The deviance statistic follows an approximate Pearson χ^2 distribution, the assumptions of which break down with a small number of unique values within a sample population (McCullagh and Nelder, 1989).

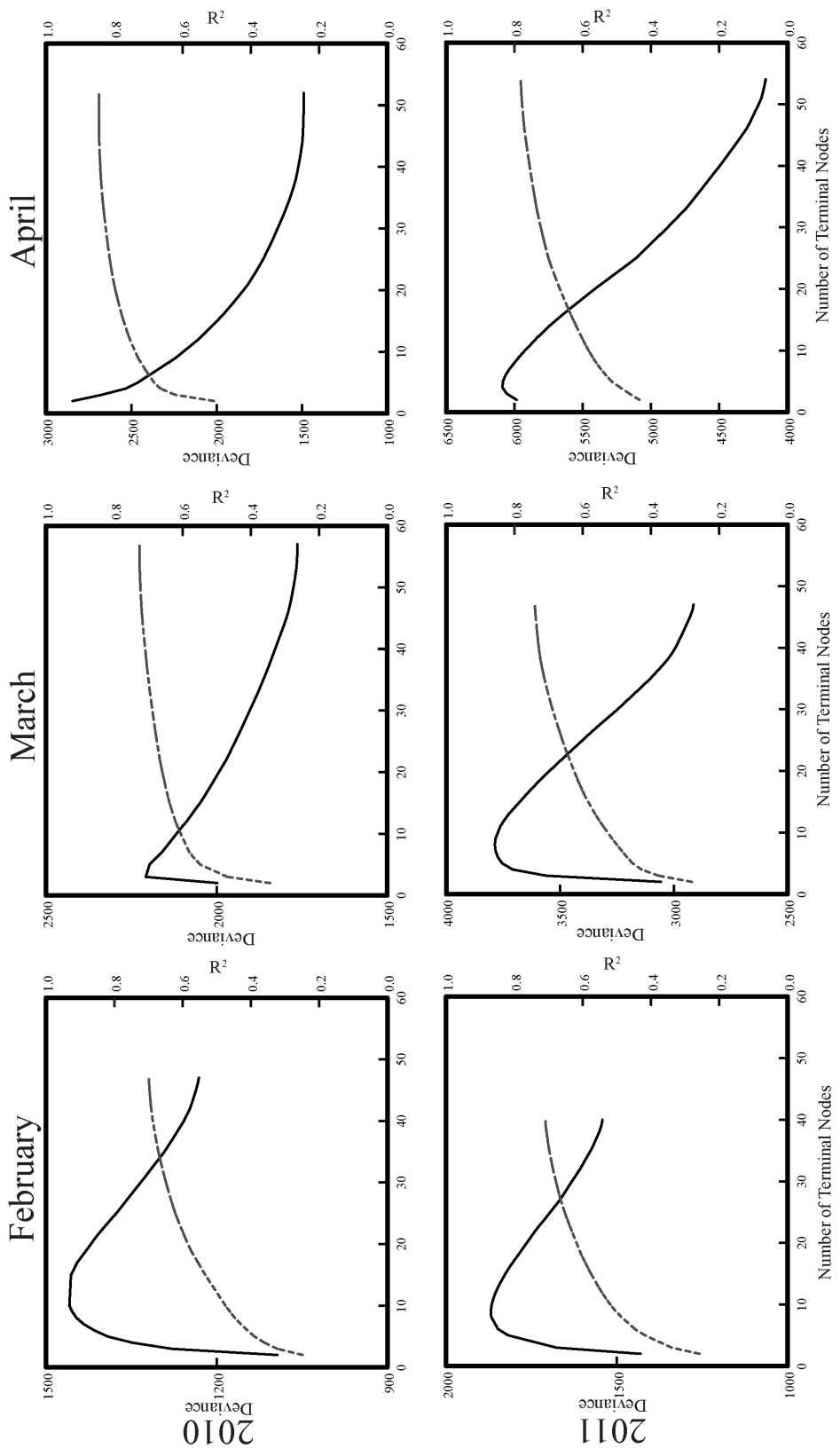

Figure 6.12. Plots of statistical deviance (solid lines) and r^2 (dashed lines) for each tree grown for 2010 and 2011 snow surveys using SWE calculated from snow depths

Thus, reported deviance statistics below 8 terminal nodes may be based on the invalid assumptions of this distribution, and are thus incorrect. However, as a larger number of unique predicted values are introduced to the sample population, deviance decreases with increasing tree complexity. This would not have a large effect on the tree selection process used here, as the low deviance statistics calculated for low complexity trees are associated with low r^2 values, making it unlikely that these trees would be selected for use.

Between years, maximum tree size was approximately similar. However, once optimal trees were selected for each snow survey, tree complexity decreased for 2010 data and increased for 2011 data as the season progressed (Table 6.2).

Table 6.2. Attributes of regression trees selected for analysis of SWE. All r^2 values reported are significant at $p = 0.05$

	Month	***No. of Terminal Nodes***	***r^2***	***Deviance***	***No. of Samples in Terminal Nodes***
2010	Feb	40	0.68	1257.5	5 – 10
	Mar	44	0.72	1801.8	3 – 13
	Apr	32	0.83	1611.5	1 – 20*
2011	Feb	33	0.69	1579.5	1 – 18*
	Mar	37	0.72	3052.7	3 – 24
	Apr	43	0.76	4396.7	5 – 19

*Note: In these cases less than three terminal nodes contain a single sample.

For 2010, this likely represents an increasingly simple interaction between the predictor variables and snowpack as the season progressed, as no accumulation was measured between February and April. In contrast, the 2011 snowpack increased by consistently large amounts during the same February to April period, resulting in more complex interactions between the controls and snowpack. To adequately explain these

complex interactions, therefore, increasingly complex regression trees were required as the season progressed, resulting in the increasing number of terminal nodes observed in 2011.

The selected trees do not significantly overfit the data, which would be evidenced by relatively few samples within each terminal node; extreme overfitting would be indicated by a tree with only one sample in each terminal node. The majority of terminal nodes for selected trees contain ≥ 15 samples; while several terminal nodes have < 15 samples, only a few within each tree contain ≤ 5 samples.

Spatial autocorrelation is often visible in tree structure, particularly in the lower levels of the tree. This manifests as repeated splitting on the autocorrelated variable (e.g. elevation) within one branch as the tree grows (Anderton *et al.*, 2004). Examination of the selected trees shows that a range of variables are used throughout each branch of each tree, thus autocorrelation is not affecting the results of this analysis.

6.3.3 Controls on Snow Accumulation 2010

It is difficult to interpret the importance plots produced by the C&RT algorithm as each of the predictor variables integrate a number of physical processes. Below, I identify the processes represented by each predictor variable and attempt to define the effects on snow accumulation in the context of field data.

In 2010, elevation was the single largest driver of snow accumulation (Fig. 6.13), while importance values for the remaining predictor variables decreased as the season progressed.

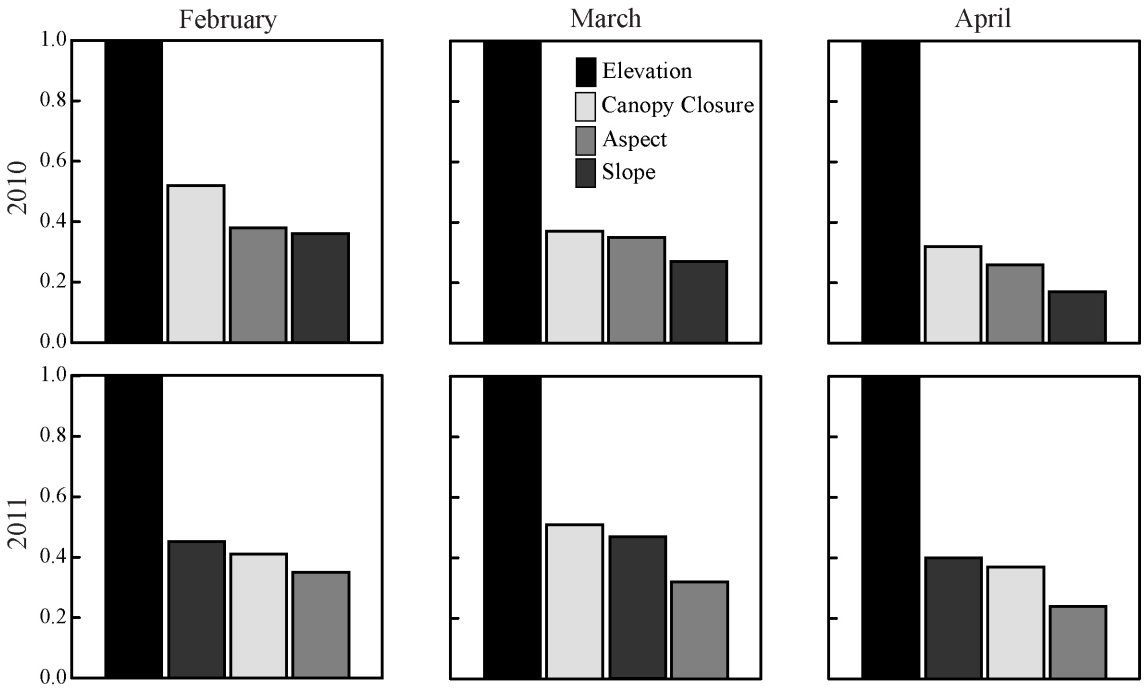

Figure 6.13. Importance plots for the selected trees from Table 6.1. These plots indicate how often each variable was used in splitting in the specified tree, and do not indicate a hierarchy of variables within the tree. The most commonly used variable is assigned a value of 1, and the remaining variables are represented as a proportion of that value.

Field observations revealed a strong elevational gradient in snow depth and SWE throughout the season. Large areas of bare ground were encountered on all of the low elevation transects during all surveys, while higher elevation transects retained greater snow depths. 2010 was warm relative to the 30-year normal (1971-2000), thus differential melt is most responsible for the elevation signal. During snow surveys, higher air temperatures were observed at lower elevations, where the snowpack was actively melting during all surveys. However, air temperatures decreased with increasing elevation, resulting in lower melt rates or even continued accumulation at higher elevations.

All selected trees initially divide the data into low and high elevation areas, and each of these initial splits are within an elevation band ~20 m wide centred on ~1630 m,

with the exception of February 2011 which split at 1730 m. The low elevation area is represented by the 1000 m transect, the mid and low transect in the West Fork, and the two lowest in the East Fork and McLaren Ck., while the high area is represented by the three highest transects in each sub-watershed. This is interpreted as a pure elevation signal rather than some combination of the other variables that could be accounted for by elevation. There are no substantial changes in forest type, structure, or species composition within this band and it is ~150 m below treeline in all sub-watersheds. No transects were divided by this band, thus a large range of slope angles and aspects are incorporated in each of these groups. As SWE is typically 5 – 10 cm higher above than below this band, it is interpreted as a threshold between accumulation regimes driven by orographic versus meteorological processes. Archived regional avalanche forecasts from 2010 and 2011 indicated that the 0°C isotherm fluctuates around this elevation band throughout the winter (Canadian Avalanche Centre, 2011). This represents a transition from cold conditions above, which suppresses snowpack ablation and increases the likelihood of precipitation falling as snow rather than rain, to warm conditions below, which encourages snowpack ablation. The above-average air temperatures of 2010, combined with snow line consistency between years, suggests that differential melting is likely driving the elevation signal. Below the first split, however, there are few similarities between trees.

Canopy closure was the second most important predictor of SWE in 2010 (Fig. 6.13). This suggests that vegetation effects, such as interception and longwave radiation fluxes from, and attenuation by, the canopy were important for snow accumulation. The effect of canopy closure was greatest in February, when it was ~50% as important as

elevation; it declined in importance as the season progressed, becoming only 30% by April. This may be explained by the low snow accumulation conditions observed in 2010, as infrequent snowfalls would negate any canopy interception effects.

Aspect was the third most important predictor in 2010 (February: 39%, March: 35%, April: 25% of elevation), which was not observed in the scatterplots. Unlike canopy closure, aspect declined only minimally as the season progressed, likely due to increasing incoming solar radiation. The shallow, dense snowpack may have prevented any redistribution and may explain why the 2010 aspect vs. SWE plot (Fig. 6.9) shows minimal variation between westerly and easterly aspects, despite the prevailing westerly wind direction in this basin.

Slope was least important in predicting accumulation in 2010 (February: 38%, March: 28%, April: 18%) and also showed no relationship in the scatterplots. The shallow snow conditions were certainly below the threshold for avalanching, and were probably also below the threshold where downhill snowpack creep would occur on the steep slopes adjacent to some stream reaches (McClung and Larsen, 1989; Exner and Jamieson, 2009). Steep slopes that would allow more direct radiation inputs did not accumulate substantial snowpacks in this year, negating this effect.

Overall, importance values decreased as the season progressed. This is interpreted as representing both the reduction in SWE observed between surveys, and the increasing importance of elevation through differential melting processes

6.3.4 Controls on Snow Accumulation 2011

Elevation was also the strongest predictor of accumulation in 2011 (Fig 6.13), with snow depths and SWE were observed to increase with elevation. No bare patches

were observed in 2011, and the snowpack was generally much more uniformly distributed. Given the consistency of snow line between years as noted above, it is likely that below-average air temperatures in January and February, and large snowfall events from February to April, created conditions that allowed the snowpack to consistently increase in depth and SWE through the field season. Although there was a large increase in mean snow depth between March and April, SWE only increased slightly, which can be accounted by a large, low-density snowfall event that occurred just prior to the April surveys (Fig. 6.7).

Slope angle was consistently more important in 2011, as the second-most dominant control in February (45% of elevation) and April (40% of elevation) though this relationship was not observed in the scatterplots. In March, however, slope and canopy closure had approximately similar rankings (Fig. 6.13).

Canopy closure was ranked third in February (40% of elevation) and April (35% of elevation). Scatterplots show approximately similar SWE under the range of canopy closures sampled. This supports field observations, which suggested that snowfall in 2011 was characterized by frequent events that likely exceeded the interception capacity of the canopy and caused large-scale canopy unloading of intercepted snow throughout the basin, which would tend to reduce the relative importance of this variable in snow accumulation patterns. Canopy closure increased to 50% importance in March, which had above average air temperatures. Interception of snowfall from the event just prior to the survey may also be responsible for this result.

Aspect was ranked last in 2011 (February: 35%, March: 30%, April: 15%), which corresponds with the lack of relationships observed in the scatterplots. Based on field

observations, wind transport did not appear to be a substantial driver of snow accumulation. However, higher importance values in February suggest that transport was more important earlier in the season, prior to the initiation of snow surveys. Field observations of minimal wind transport may thus explain the low importance value for the remainder of the season.

The regression tree analysis identified relationships between SWE and the indices selected to represent processes driving snow accumulation. In some cases, however, the scatter plots of measured data suggest that there is no strong relationship. This may be due to two potential factors: 1) the regression tree algorithm is developing spurious relationships to explain unrealistic patterns in the data, or 2) three of the indices account for radiation processes (slope, aspect, canopy closure), thus splitting the radiation effect across these variables and thus resulting in a weak response when each variable is evaluated separately. The latter is the most likely, given that some patterns in the observed data that are mirrored in the regression trees (e.g., elevation, canopy).

6.3.5 Spatial Distribution of Snow Water Equivalent

Accumulation patterns across the basin produced by the regression trees approximately matched accumulation patterns observed in the field in 2010 (Fig. 6.14). Large clearings and stands of trembling aspen in the northernmost areas of the basin showed consistently higher accumulation throughout the year due to low interception rates, as observed in the field.

Higher SWE values were observed on east-facing slopes, which are in the lee of the prevailing wind direction (westerly in this watershed). These areas are expected to experience greater deposition of wind-transported snow – patterns that emerge in the

February and March maps. Slope was not a major control in 2010, and prediction maps do not contain any features that appear to be slope related. The April prediction map is closest to observed field conditions, as this survey was completed shortly after a high-magnitude snowfall event, which drove the small increase in mean snow depth and SWE in Figure 6.7a. Despite this storm, negligible snow amounts accumulated at the bottom of the watershed, represented by a wedge of low SWE values at the lowest elevations.

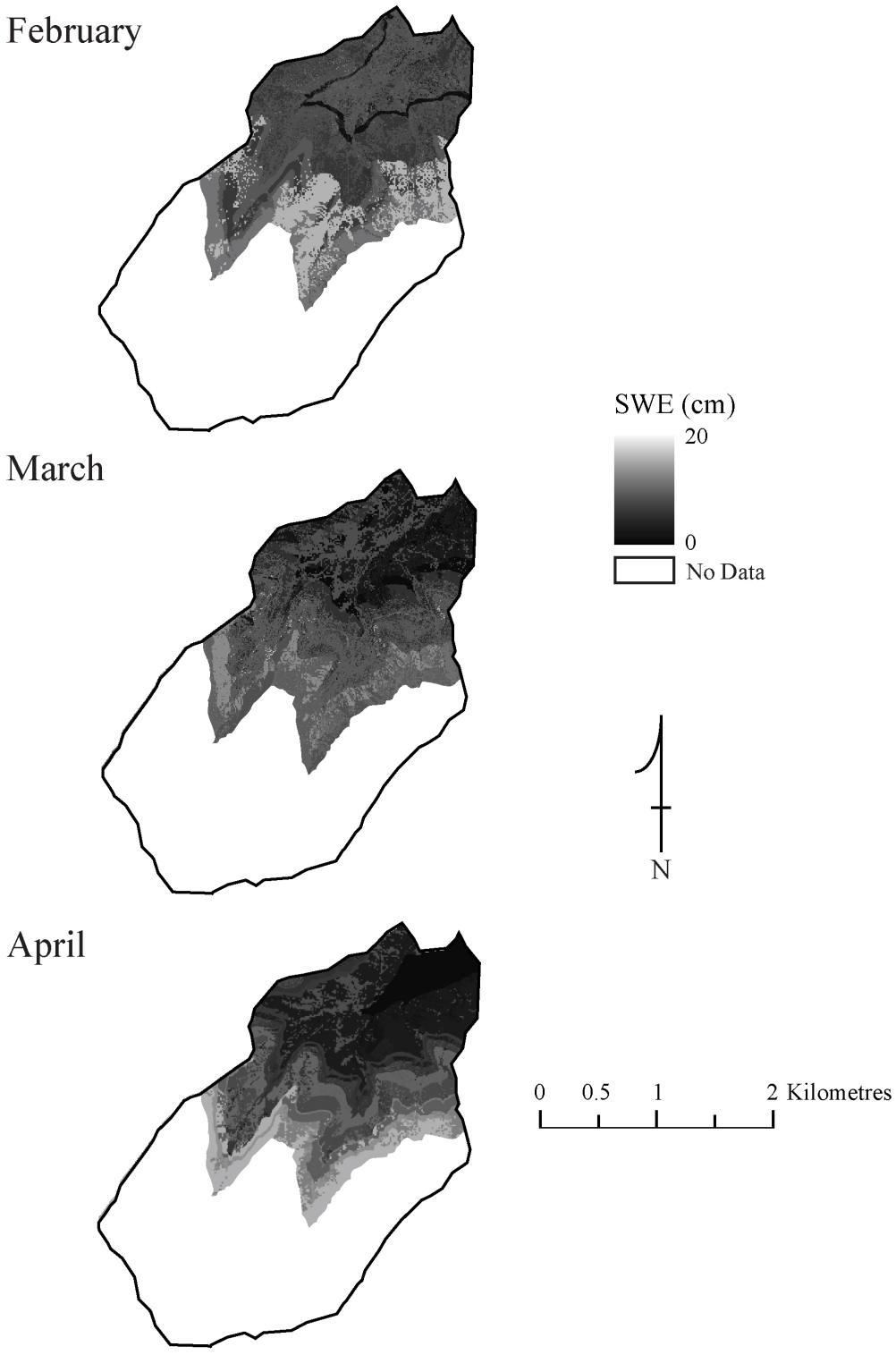

Figure 6.14. SWE prediction maps produced from regression tree analysis for 2010 snow surveys.

Prediction maps produced for 2011 show different accumulation patterns than seen in the 2010 maps (Fig. 6.15). The prediction map for February produces an odd alternating pattern of SWE values with elevation. The lowest of these bands is attributed to lack of low elevation data, as the 1000 m transect was not sampled in February 2011 due to extreme cold conditions. Thus any low elevation splitting in the regression tree for that month would be based on the lowest transect that was sampled, which is located in the West Fork. However, the banding above this elevation shows increasing snow accumulation with elevation. This is likely caused by orographic effects driving snow accumulation processes rather than the differential melt that drove elevational dependence in 2010. The prediction map for March, which includes all transects, produces a similar banding pattern, although the magnitudes are higher. The banding is absent in the April map, which shows more uniform snow accumulation in the lower portions of the watershed.

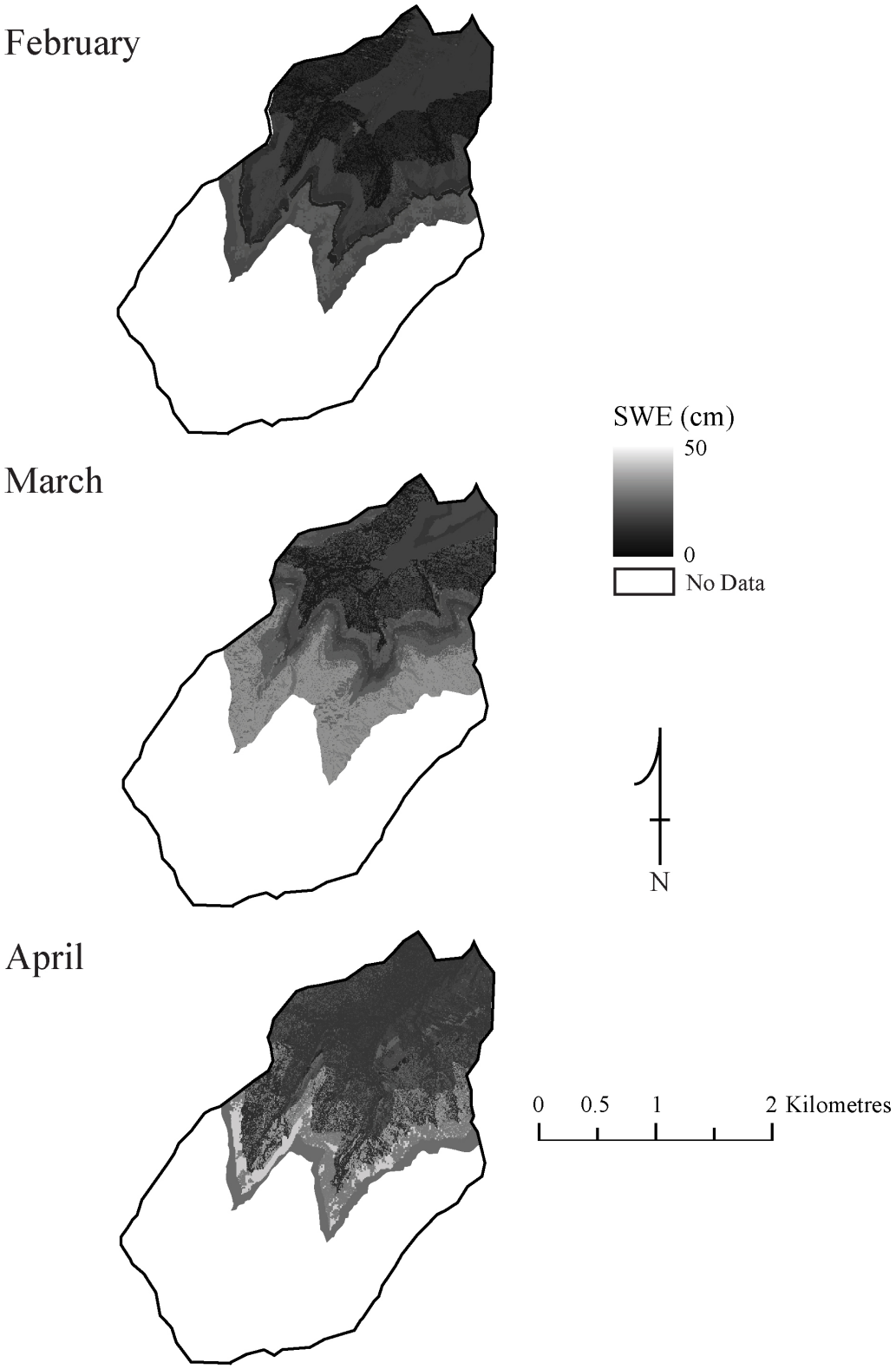

Figure 6.15. SWE prediction maps produced from regression trees for 2011 snow surveys.

Aspect effects, represented by strong transport and deposition features, are absent from the 2011 prediction maps. Faint scour and deposition features are observed in the March map, though they are not as strong as those observed in 2010. This is expected, given that wind transport was not observed to be a major control on snow distribution in 2011.

6.3.6 Summary

Similar to most other studies of snow accumulation and distribution, elevation was shown to be the strongest predictor of snow accumulation throughout both the 2010 and 2011 snow seasons (e.g. Elder *et al.*, 1998; Erxleben *et al.*, 2002; Jost *et al.*, 2007; López-Moreno and Stähli, 2008; Grünewald *et al.*, 2010). As noted in Ch. 6.1.1, the controls discussed here operate most effectively at different scales. Topographic controls typically operate at large scales (> 100 m), and vegetation at smaller scales (< 100 m). However, this analysis showed that canopy closure was often very important in controlling snow accumulation. The sampling strategy used here effectively incorporated both small- and large-scale variability. The short spacing of sampling points along the transects was effective at detecting the small scale variability driven by canopy closure, and the distribution of transects across a range of elevation bands, slope angles and aspects integrated that small scale variability with the effects of larger scale processes.

Although the regression tree analysis agreed fairly well with field observations, there are several areas where this study could be improved. First, there is considerable difficulty in interpreting specific processes driving snow accumulation when using integrated predictor variables such as those applied here. The snowpack response to variables such as incoming radiation and redistribution are tied with other variables (e.g.

slope, aspect), making it difficult to extract individual effects. The addition of wind- and radiation-based predictor variables would provide additional information on drivers of snow accumulation tat would assist in identifying individual processes. Additionally, meteorological data such as air temperature and temperature lapse rates would be useful for validating tree results, particularly regarding the role of melt versus accumulation in driving elevational changes in snow accumulation. Finally, data from the alpine portion of the watershed are required to improve coverage over the watershed, and improve basin-wide estimates of SWE. This is particularly important given the high proportion of watershed area that the alpine region represents. Additional years of data with more snow accumulation variability would be useful as we only collected data from two extreme years.

6.4 Conclusion

This study investigated the topographic and vegetation controls on snow accumulation below treeline in a small, montane watershed in the Crowsnest Pass, Alberta, Canada, where minimal research has been done to quantify snow accumulation patterns and controls. Snow surveys were performed between two years, capturing two snow accumulation regimes: low accumulation in 2010 and high accumulation in 2011. While controls on snow accumulation were different between years, within years the relative proportion of controls remained similar throughout the season. In 2010, the most important variable controlling snow accumulation was elevation. Canopy closure, aspect, and slope angle were considerably less important in this year. In 2011, elevation was again the most important control, followed by slope angle, canopy closure, and aspect.

Although elevation was the strongest predictor in both years, different processes are likely responsible: differential melting caused by higher air temperatures at low elevation and strong lapse rates under the warm conditions of 2010, and orographic precipitation generation under the colder conditions of 2011. Canopy closure remains important between years, controlling interception and therefore the amount of snow reaching the ground, and reducing shortwave radiation fluxes that drive melting. To reiterate, however, no SWE samples from above treeline were included in this analysis. Thus, although accumulation patterns may broadly resemble patterns observed in the field, the magnitude of predictions is likely overestimated.

Quantification of snow water availability is currently based on statistical relationships between snowpack and streamflow that are difficult to apply given climate non-stationarity. A more process-based understanding of the factors controlling snow accumulation is thus essential to maintain accurate predictions of annual water supply from snowmelt-dominated systems. As the regression tree method is based on physical indices driving snow water storage in a watershed, it is able to incorporate the interaction between snow accumulation and key predictor variables as opposed to measuring SWE at a point, providing a more robust estimate of water storage. Used in conjunction with snow survey and snow pillow SWE data to validate predictions, regression tree models can provide spatially distributed, high resolution estimates of SWE throughout the eastern Rockies, which will give water supply forecasters the data required to provide improved estimates of annual water supply.

7.0: Summary and Outlook

7.1 Summary

Southern Alberta is a water stressed environment where surface water resources provide the majority of the water supply (Byrne *et al.*, 2006; Rock and Mayer, 2007; Rood *et al.*, 2008). These surface water resources are largely fed by melting annual snowpacks in the eastern Rocky Mountains, which contribute up to 80% of the annual flow recorded in western rivers (Elder *et al.*, 1998; Jost *et al.*, 2007).

Ongoing climate change is expected to contribute to increasing water stress given its substantial effects on snow processes. Forecasts indicate a reduction in the amount and extent of snow accumulation, a shift to rain rather than snow as the dominant form of precipitation, and a shift to earlier spring melt (Groisman *et al.*, 2004; Mote *et al.*, 2005; Stewart *et al.*, 2005; Lemke *et al.*, 2007; McCabe *et al.*, 2007; Trenberth *et al.*, 2007).

Climate change may also contribute to large-scale changes in forest structure in the headwater basins that accumulate snow. Warming temperatures could allow large areas of alpine tundra to be colonized by lower elevation species, reducing snow accumulation due to increased interception losses (Soja *et al.*, 2007). Warmer and drier conditions overall may create large areas of existing forest that are more susceptible to destructive insect infestations, and increase the probability, frequency, and severity of wildfire (Hélie *et al.*, 2005; Stahl *et al.*, 2006; Fischlin *et al.*, 2007; Aukema *et al.*, 2008; Littell *et al.*, 2009). Beetle infestation and wildfire open the forest canopy, reducing interception, and increasing snowpack depth and water equivalent. However, the open canopy also exposes the snowpack to increased surface wind speeds and radiation fluxes

which contribute to increased melt rates and shorter melt seasons (Winkler *et al.*, 2005; Boon, 2007; Burles and Boon, 2011).

Given the importance of snow accumulation to annual water supply in water stressed environments, and the possibility of large changes in snow processes with climate change, it is important to understand the interactions between topography, vegetation, and snow accumulation. The purpose of this research was to quantify the role of topography and vegetation in controlling snow accumulation at the watershed scale over two consecutive years. The specific objectives for this research were outlined in Chapter 1:

1) Establish a comprehensive snow survey network that incorporates terrain and vegetation variability within the watershed.
    a. Perform an error analysis of the snow samplers used for snow surveys
    b. Develop and validate a new method to remotely measure snow depth at high elevations and in hazardous terrain.
2) Quantify peak SWE across the watershed from the snow survey data and a range of interpolation methods
3) Quantify the primary controls on snow accumulation across the watershed using statistical approaches

The study area for this project was located in the Crowsnest Pass, southwestern Alberta. This small, montane watershed (~1050 ha) has very low levels of forest disturbance and is, therefore, representative of undisturbed forest conditions throughout the headwaters of the Oldman River basin. Vegetation cover is characterized by mature, lodgepole pine dominated forest at lower elevations and subalpine forest, alpine meadow, and exposed bedrock and talus at higher elevations.

This thesis was structured so that foundational information and research required for completing Objective 3 was presented and discussed prior to a discussion of controls on snow accumulation. Chapter 1 introduced the research objectives and discussed the motivation for this study. Chapter 2 introduced the thesis topic and placed the research in the context of previous work. Chapter 3 provided a detailed description of the study watershed and a discussion of the regional research context. Chapters 4 and 5 outlined studies dealing with Objectives 1a and 1b, respectively, which provided necessary background information for understanding data produced for Chapter 6. Objectives 2 and 3 were addressed in Chapter 6.

Chapter 4 outlined a study to evaluate the performance of the snow samplers used for this thesis. This study utilized two sampling grids that were established in the Star Creek watershed: one in a mature pine forest and the other in a clearcut. The objective was to quantify sampler performance under different snow conditions caused by differences in forest cover. This project performed the first rigorous evaluation of the SnowHydro snow tube, a new design developed by M. Sturm (Fairbanks, AK). For comparison, the Standard Federal and Meteorological Service of Canada (MSC) snow tubes were also tested, as there is considerable literature on their performance. This study found a highly stratified snowpack in both stands that was representative of early-spring snow conditions throughout the Crowsnest Pass region. Under these conditions the SnowHydro, the primary sampler for the research related to Objectives 2 and 3, produced the most consistent measurements of snow density when compared with density measurements from two snow pits. This research also highlighted that the calibration of the spring scale provided with the Standard Federal sampler is temperature dependent, an

issue that is often overlooked in the literature. In contrast with previous literature, which determined that all snow samplers overestimated density by 5 – 10%, I observed < 10% underestimates of snow density, similar to results recently reported by Sturm *et al.* (2010). These data allow researchers to make more informed decisions on the type of sampling equipment to use given the snow and meteorological conditions in their study areas. This also allows current users to have a better understanding of the sampling errors they are likely to encounter when using these snow tubes.

Chapter 5 discussed the development and validation of a new method for remotely measuring snow depth in terrain where considerable avalanche risk prevents traditional snow surveys. Existing methods described in the literature utilize terrestrial and airborne LiDAR equipment, which are extremely expensive to purchase and operate, and require specialized knowledge for data processing. Hand-held laser distance meters are also described in the literature, but lack the accuracy required to repeatedly sample a snowpack throughout a season and between years. The method developed in Chapter 5 utilized a modern, robotic total station that provides a considerable improvement in repeatability of surveys over existing methods. Although the total station provides a considerable improvement in measurement accuracy in theory, measurement errors could not be reduced beyond ± 30 cm snow depth, approximately similar to depth accuracies produced with airborne LiDAR and TLS equipment. An interaction between the laser measurement system of the total station and the snowpack was inferred. The highly reflective snowpack produces stronger reflections of the laser energy than the instrument expects, and triggers the photo detectors early or late depending on angle of incidence at snow surface. This interaction may have produced a considerable effect on the

measurement accuracy, producing large over- and underestimates of the range to target. However, this may not be as large an issue with other techniques, as it is with a total station. Considerable research and validation of this method remains before it can be operationally deployed. Although this technique could not be used to address Objectives 2 and 3, there is still great promise for this technology. Current manual methods of measuring snow depth are not well suited for high alpine environments, given the danger to snow surveyors. However, these areas are highly important accumulation areas that store large quantities of water. To be used effectively though, a greater understanding of the interaction described above, and a method of correcting for it is required, whether that is a hardware solution or a simple correction in the calculations of snow depth.

Chapter 6 addressed Objectives 2 and 3: quantifying snow accumulation and distribution across a montane watershed, and quantifying the processes responsible for the observed accumulation and distribution patterns. This research was accomplished with traditional snow surveys over the February to April field seasons of 2010 and 2011. Field sampling was completed on a network of eight snow courses (54 snow density, 462 snow depth measurements) that represented the range of topographic and vegetation variability below treeline in Star Creek. Remote snow depth measurements were attempted above treeline in 2010, with a network of 200 points. However, highly inaccurate control point coordinates may have contributed to unrealistic estimates of snow depth, thus measurements could not be used. In 2011, high avalanche risk throughout the season prevented access to the alpine, thus remote measurements were not collected. Data were analyzed using classification and regression tree modelling (C&RT), which splits data on hierarchical relationships between predictor and response

variables (Breiman *et al.*, 1984). This method is non-linear, and works with any combination of continuous and categorical data, making it ideally suited for snow studies as snow often responds non-linearly to predictor variables. Four primary predictor variables are highlighted in the literature as the dominant controls on snow accumulation: elevation, slope angle, aspect, and forest canopy closure, and were therefore used in the C&RT analysis.

Snow conditions varied greatly between years: 2010 was characterized by above average air temperatures and low snow accumulation, with large areas of the watershed having no snow accumulation throughout the field season. 2011 had near average air temperatures, but snow accumulation was considerably above average. These two disparate years provided ideal datasets with which to evaluate the role of topography and vegetation under two very different snow accumulation regimes.

In both years, elevation was the strongest control on snow accumulation in Star Creek; however, very different processes produced this elevation dependence between years. An investigation of archived regional avalanche bulletins suggested that snowline elevation in the Crowsnest Pass occurs at approximately the same elevation between years. However, in 2010 above average air temperatures at low elevations in the watershed may have contributed to melting in these areas. Strong temperature gradients across the watershed may have reduced melt with increasing elevation, allowing continued accumulation at the highest elevations measured. In 2011, average air temperatures were closer to normal, and likely did not contribute to this differential accumulation pattern though snow accumulation appeared to be strongly driven by

orographic processes. Instead, snow accumulation increased with elevation due to orographic processes.

Canopy closure, slope angle, and aspect played different roles in controlling snow accumulation between years. In 2010, the variables as ranked in importance relative to elevation were: canopy closure, aspect, and slope angle. This reflects snow accumulation conditions observed in 2010. Infrequent, low magnitude snowfall events increased the importance of interception, and above average temperatures contributed to an isothermal snowpack that melted with increasing radiation inputs. In 2011, the ranking relative to elevation was slope angle, canopy closure, and aspect. High snow accumulation contributed to downhill creep of snowpack on steep slopes where there was no evidence of avalanche activity. Consistent high-magnitude snowfall events reduced the importance of canopy closure by overwhelming interception capacity. Cold air temperatures resulted in a cold snowpack that was less sensitive to radiation inputs, thus minimizing the effect of aspect. However, it should be noted that the results described here are currently applicable only to Star Creek, as the relationships were derived from a specific set of topographic, vegetation and SWE data collected there. Addition of these data from other watersheds would allow a wider range of conditions to be considered, and produce large-scale SWE estimates.

The C&RT results allowed me to examine modelled snow accumulation and distribution across the watershed. The relationships derived from the snow survey data, when mapped, produced results that provided a good match to observations that were made in the field, and explained considerable amounts of variance in the survey datasets.

Using this technique, snowpack for large areas of mountain headwater basins could be predicted, allowing for more accurate predictions of water yield.

7.2 Outlook

Overall, this thesis accomplished the aims set out in Chapter 1 by quantifying the sampling errors of several snow tubes, developing and testing a new remote snow depth measurement technique, and quantifying the controls on snow accumulation and distribution across the study watershed.

However, several areas of this study warrant additional investigation to expand on this work:

1) Additional snow conditions should be assessed for snow tube performance. This study only investigated early-spring snow conditions where the pack was nearly isothermal and exhibited strong internal stratification, and at only one elevation. To provide a better understanding of the performance of the SnowHydro snow tube, a wider range of conditions need to be assessed. This could include conditions such as cold, mid-winter snowpacks, and late spring isothermal packs, as these conditions were represented in sampling for Chapter 6. This could be expanded to include snowpacks in different elevation ranges (i.e. alpine snowpacks) as different internal snowpack processes and external meteorological controls operate at those elevations.
2) The measurement error produced in the remote snow depth measurement technique should be addressed. My research showed that a total station is a practical and cost efficient alternative to laser scanners, and a field deployment in

2010 showed that error ranges similar to those reported for laser scanners are achievable. However, a measurement error of ±30 cm may represent a significant proportion of snow depth on exposed alpine slopes. A solution is likely to be more of an engineering exercise, and therefore out of the scope of this research. However, a first step would be to reduce the sensitivity of the photo detectors to prevent them being overloaded by the high intensity returns, which appears to be an underlying mechanism of these errors (Hopkinson *et al.*, 2011). This could be accomplished via the hardware by installing a filter over the detectors to physically reduce the intensity, or by rewriting the instrument firmware to correct for high intensity returns.

3) A side-by-side comparison with hand-held distance meters and terrestrial laser scanners should be completed. Currently, these technologies are used independently (terrestrial LiDAR predominantly in the Swiss Alps, hand-held distance meters in the central Canadian Rocky Mountains, and total stations in the southern Canadian Rocky Mountains), meaning that results from studies are not easily intercomparable due to differences in snow processes and accumulation amounts. Measuring a snowpack from the same set of control points, and over a short time period would remove the variability in snow properties and make data directly comparable. This proposed study site should have low avalanche risk to allow a snow surveyor to directly measure snow depth without risk of triggering an avalanche. Therefore, low elevation or low angle slopes are likely to be the best location to perform such a test.

4) Better alpine snow accumulation data are required for more robust estimations of snow accumulation above treeline. I attempted to use the remote technique described in Ch. 5, however, unrealistic values produced in 2010 and high avalanche hazard in 2011 prevented us from collecting and utilizing the data. Remote techniques are the best option for collecting alpine snow data given the hazard to snow surveyors, so I recommend that these methods be used once the measurement errors are reduced.
5) An improved method for accounting for wind redistribution of snow should be investigated, as the Crowsnest Pass is a windy environment (Nkemdirim, 1996), with effects on snow distribution. Aspect was used as a proxy for wind transport, as prevailing westerly winds in the study area produce scour on windward slopes and deposition on lee slopes. Although this approach produced accumulation patterns similar to those observed in the field, improved modelling of wind fields in the study area would provide a more accurate and robust estimate of snow distribution. Winstral et al.'s (2009) upwind slope algorithm, which models topographic shelter or exposure to wind, and could be a useful tool; unfortunately, time constraints prevented its application to this study.
6) Use of meteorological data (e.g. wind speed and direction, temperature, incoming radiation, etc.) would help to improve predictions of snow accumulation by providing a wider range of explanatory variables. In this project, meteorological controls are tied to topographic or vegetation variables (e.g. radiation inputs and wind exposure are tied to slope angle and aspect, temperature lapse rates and snowfall generation are tied to elevation) making it difficult to determine which

control is most responsible for accumulation. Quantifying these relationships would help clarify the underlying processes responsible for the melt controlled elevation dependence in 2010, and the orographic precipitation controlled dependence observed in 2011. Additionally, meteorological data would greatly improve predictions of snow accumulation by accounting for mid-winter melt driven by Chinook events. Distributing sensors along an elevation gradient to measure these variables throughout the watershed would allow creation of meteorological data surfaces, which could be used as additional predictor variables.

7) Additional years of data and a wider range of study areas would help broaden our understanding of snow accumulation processes. Although I collected data from two extreme years, data from more average years would allow prediction of snow accumulation across a range of snowfall regimes. Inclusion of additional watersheds would incorporate a greater range of topographic and vegetation variability, provided these watersheds were selected to address the gaps in predictor variables from this study by including a wider elevation range, different vegetation covers and species compositions, and varying treeline elevations. Although data from multiple watersheds would likely increase generalization in SWE predictions, because a broader range of interactions between controls and snowpack would be included in the predictions, this limitation would be offset by the increased spatial coverage. Large-scale maps of high resolution SWE data would be very useful in predicting annual water supply.

7.3 Conclusion

This thesis provided several contributions to snow science. The first test of the SnowHydro snow sampler performance was completed, and it was found to outperform two existing designs under the specific conditions described. A new method of remotely measuring snow depth in hazardous terrain that improves survey repeatability and costs considerably less than other approaches was described and tested. However, this research also highlighted some limitations of this laser-based technique that has not previously been described in the literature. Finally, this study quantified the topographic and vegetation controls on snow accumulation in the headwaters of the Oldman River basin of southern Alberta.

The regression tree models produced statistically based estimates of SWE, in contrast to snow survey and snow pillow based measurements that report the amount of snow measured at a point. Estimates based on predictor variables that represent a range of accumulation processes are likely more useful than the current operational measurement methods because the underlying mechanisms that explain snow accumulation are incorporated, rather than simply measuring snow accumulation. Using this knowledge allows researchers to establish relationships between topography, vegetation, local meteorology, and snow accumulation, which may then be used to estimate SWE across a range of watersheds.

This technique may be of interest to any agency that regularly collects snow data (e.g. Alberta, British Columbia, most western U.S. states) as an alternate means of predicting the amount of water stored as snow in the headwater basins. Data from existing snow survey programs could be incorporated into the framework developed here

given the appropriate topographic and vegetation variables for the sampling points. These regression trees could potentially be used to provide large-scale estimates of water storage throughout the Rocky Mountains.

To this point, there has been little research on snow processes in this portion of the Canadian Rocky Mountains (e.g. Pigeon and Jiskoot, 2008; Burles and Boon, 2011). A set of snowpack controls similar to that reported in the literature for other watersheds was observed. This is important due to large amounts of mid-winter snowpack ablation driven by high Chinook frequency, and downstream areas that are highly dependent on snow accumulation for their annual water needs. However, additional studies on snow accumulation processes could improve models to forecast annual snow accumulation in this region, and therefore improve water supply forecasts in an area dependent on mountain snowpack.

References

Adams, W.P., 1976. Areal differentiation of snow cover in eastern central Ontario. *Water Resources Research*, **12**: 1226-1234.

Adams, W.P. and Barr, D.R., 1974a. *The study of snow*, 44-76 pp.

Adams, W.P. and Barr, D.R., 1974b. *Techniques and equipment for measurement of snowcover, including stratigraphy*, 11-26 pp.

Alberta Environment, 2010. Rankings for June 2010 Mountain Snow Courses for Oldman River Basin. Last Updated: June 7, 2010,. Accessed: May 31, 2010. http://environment.alberta.ca/forecasting/data/snow/jun2010/oldscrank.pdf

Alberta Environment, 2011a. Alberta River Basins, Snow Data. Last Updated: July 7, 2011. Accessed: July 7, 2011. http://www.environment.alberta.ca/apps/basins/Map.aspx?Basin=10&DataType=4

Alberta Environment, 2011b. Rankings for June 2011 Mountain Snow Courses for Oldman River Basin. Last Updated: June 3, 2011. Accessed: June 28, 2011. http://www.environment.alberta.ca/forecasting/data/snow/jun2011/oldscrank.pdf

Alberta Sustainable Resource Development, 2008. LiDAR Digital Elevation Model Metadata (XML), Edmonton, AB.

Alberta Terrestrial Imaging Centre, 2010. *Characterization of Forest Attributes in the North York and Star Ck Watersheds Using LiDAR Data*, Lethbridge AB, 11 pp.

Alford, D., 1967. Density variations in alpine snow. *Journal of Glaciology*, **6**: 495-503.

AMEC, 2007. *Water for Life: current and future water use in Alberta*. Alberta Enivronment, Queen's Printer for Alberta, Edmonton, Alberta. pp. 627

Anderton, S.P., White, S.M. and Alvera, B., 2004. Evaluation of spatial variability in snow water equivalent for a high mountain catchment. *Hydrological Processes*, **18**: 435-453.

Aukema, B.H., Carroll, A.L., Zheng, Y., Zhu, J., Raffa, K.F., Moore, R.D., Stahl, K. and Taylor, S.W., 2008. Movement of outbreak populations of mountain pine beetle: influences of spatiotemporal patterns and climate. *Ecography*, **31**: 348-358.

Axelsson, P., 1999. Processing of laser scanner data - algorithms and applications. *ISPRS Journal of Photogrammetry & Remote Sensing*, **54**: 138-147.

Bagnold, R.A., 1941. *The Physics of Blown Sand and Desert Dunes*, ed. London, England, Methuen, 265 pp.

Balk, B. and Elder, K.J., 2000. Combining binary decision tree and geostatistical methods to estimate snow distribution in a mountain watershed. *Water Resources Research*, **36**: 13-26.

Baltsavias, E.P., 1999. Airborne laser scanning: basic relations and formulas. *ISPRS Journal of Photogrammetry & Remote Sensing*, **54**: 199-214.

Barnett, T.P., Adams, J.C. and Lettenmaier, D.P., 2005. Potential impacts of a warming climate on water availability in snow-dominated regions. *Nature*, **438**: 303-309.

Barry, R.G., 2008. *Mountain Weather and Climate, 3rd Edition*, ed. Cambridge, Cambridge University Press, 506 pp.

Bayoud, F., 2006. Leica's Pinpoint EDM technology with modified signal processing and novel optomechanical features TS24.3, XXIII International FIG Congress - Shaping the Change, Munich, Germany, pp. 16pp.

Bayrock, L.A. and Reimchen, T.H.F., 2007. Surficial Geology, Alberta Foothills and Rocky Mountains DIG 2007-0077. Alberta Geolgical Survey, Edmonton, pp. ArcGIS digital vector data.

BC Ministry of Environment, 1981. *Snow Survey Sampling Guide*. Water Management Branch, Surface Water Section. SS13-81. Queen's Printer for British Columbia, Victoria. pp. 28

Beaumont, R.T., 1967. Field accuracy of volumetric snow samplers at Mt. Hood, Oregon. *Physics of Snow and Ice*, **1**: 1007-1013.

Beaumont, R.T. and Work, R.A., 1963. Snow sampling results from three samplers. *Bulletin of the International Association of Hydrological Sciences*, **8**: 74-78.

Bernhardt, M., Zängl, G., Liston, G.E., Strasser, U. and Mauser, W., 2009. Using wind fields from a high-resolution atmospheric model for simulating snow dynamics in mountainous terrain. *Hydrological Processes*, **23**: 1064-1075.

Berry, O., 1981. Snow and Climate. In: D.M. Gray and D.H. Male (Editors), Handbook of Snow: Principles, Processes, Management and Use. The Blackburn Press, Caldwell, New Jersey, pp. 32-59.

Bindon, H.H., 1964. The design of snow samplers for Candian snow surveys, Proceedings of the 21st Annual Meeting of the Eastern Snow Conference, Utica, New York, pp. 23-28.

Bladon, K.D., Silins, U., Wagner, M.J., Stone, M., Emelko, M.B., Mendoza, C.A., Devito, K.J. and Boon, S., 2008. Wildfire impacts on nitrogen concentration and production from headwater streams in southern Alberta's Rocky Mountains. *Canadian Journal of Forest Research*, **38**: 2359-2371.

Boon, S., 2007. Snow accumulation and ablation in a beetle-killed pine stand in northern interior British Columbia. *B.C. Journal of Ecosystems and Management*, **8**: 1-13.

Bray, D.I., 1973. A report on the variability of snow water equivalent measurements, Proceedings of the 30th Annual Meeting of the Eastern Snow Conference, Amherst, Massachusetts, pp. 20-31.

Breiman, L., Friedman, J.H., Olshen, R.A. and Stone, C.J., 1984. *Classification and Regression Trees*, ed. London, Chapman and Hall/CRC, 358 pp.

Brooks, K.N., Folliott, P.F., Gregersen, H.M. and Thames, J.L., 1991. *Hydrology and the Management of Watersheds*, ed. Ames, Iowa, Iowa State University Press, 392 pp.

Burles, K., 2010. Snowmelt Energy Balance in a Burned Forest Stand, Crowsnest Pass, Alberta. M.Sc. Thesis, University of Lethbridge, Lethbridge Alberta, 143 pp.

Burles, K. and Boon, S., 2011. Snowmelt energy balance in a burned forest plot, Crowsnest Pass, Alberta, Canada. *Hydrological Processes*. DOI: 10.1002/hyp.8067

Burrough, P.A. and McDonnell, R.A., 1998. *Principles of Geographical Information Systems*, ed. Oxford U.K., Oxford University Press, 333 pp.

Butler, D.R., 1979. Snow avalanche path terrain and vegetation, Glacier National Park, Montana. *Arctic and Alpine Research*, **11**: 17-32.

Buttle, J.M. and Metcalfe, R.A., 2000. Boreal forest disturbance and streamflow response, northeastern Ontario. *Canadian Journal of Fisheries and Aquatic Sciences*, **57**: 5-18.

Buttle, J.M., Oswald, C.J. and Woods, D.T., 2005. Hydrologic recovery of snow accumulation and melt following harvesting in northeastern Ontario, Proceedings of the 62nd Annual Meeting of the Eastern Snow Conference, Waterloo Ontario, pp. 83-91.

Byrne, J., Kienzle, S., Johnson, D., Duke, G., Gannon, V., Selinger, B. and Thomas, J., 2006. Current and future water issues in the Oldman River Basin of Alberta, Canada. *Water Science and Technology*, **53**: 327-334.

Canadian Avalanche Centre, 2011. South Rockies: Bulletin Archive. Last Updated: May 25, 2011. Accessed: August 4, 2011. http://www.avalanche.ca/cac/bulletins/archive/south-rockies

Cayan, D.R., Kammerdiener, S.A., Dettinger, M.D., J.M., C. and Peterson, D.H., 2001. Changes in the onset of spring in the western United States. *Bulletin of the American Meteorological Society*, **82**: 399-415.

Chambers, J.M., Cleveland, W.S., Kleiner, B. and Tukey, P.A., 1983. *Graphical Methods for Data Analysis*, ed. Boston, Massachusetts, Duxbury Press: Wadsworth & Brooks/Cole, 395 pp.

Chang, M., 2003. *Forest Hydrology, An Introduction to Water and Forests*, ed. London, U.K., CRC Press, 373 pp.

Chang, T. and Li, Z., 2000. Modelling snow accumulation with a geographic information system. *International Journal of Geographical Information Science*, **14**: 693-707.

Church, J.E., 1933. Snow surveying: Its principles and possibilities. *The Geographical Review*, **23**: 529-563.

Claus, B.R., Russell, S.O. and Schaerer, P.A., 1984. Variation of ground snow loads with elevation in southern British Columbia. *Canadian Journal of Civil Engineering*, **11**: 480-493.

Clyde, G.D., 1931. A new spring balance for measuring water content of snow. *Science*, **73**: 189-190.

Clyde, G.D., 1932. *Circular 99 - Utah snow sampler and scales for measuring water content of snow*. Utah State Agricultural College, Utah Agricultural Experiment Station. Paper 90. Logan, Utah. pp. 9

Coops, N. and Waring, R., 2011. A process-based approach to estimate lodgepole pine (*Pinus contorta* Dougl.) distribution in the Pacific Northwest under climate change. *Climatic Change*, **105**: 313-328.

Deems, J.S., 2007. Quantifying scale relationships in snow distributions. Ph.D. Thesis, Colorado State University, Fort Collins, CO, 134 pp.

Deems, J.S., Fassnacht, S.R. and Elder, K.J., 2006. Fractal distribution of snow depth from LiDAR data. *Journal of Hydrometeorology*, **7**: 285-297.

Deems, J.S. and Painter, T., 2006. LiDAR measurement of snow depth: accuracy and error sources, International Snow Sciences Workshop, Telluride, CO, pp. 331-338.

Dickinson, W.T. and Whiteley, H.R., 1972. A sampling scheme for shallow snowpacks. *Bulletin of the International Association of Hydrological Sciences*, **17**: 247-258.

Dingman, S.L., 2002. *Physical Hydrology*, 2nd ed. Upper Saddle River New Jersey, Prentice Hall, 600 pp.

Duncan, D.B., 1955. Multiple range and multiple F tests. *Biometrics*, **11**: 1-42.

Dyunin, A.K. and Kotlyakov, V.M., 1980. Redistribution of snow in the mountains under the effect of heavy snow-storms. *Cold Regions Science and Technology*, **3**: 287-294.

Easterling, D., 2002. Recent changes in frost days and the frost-free season in the United States. *Bulletin of the American Meteorological Society*, **83**: 1327-1332.

Elder, K., Dozier, J. and Michaelsen, J., 1991. Snow accumulation and distribution in an alpine watershed. *Water Resources Research*, **27**: 1541-1552.

Elder, K., Michaelsen, J. and Dozier, J., 1995. Small basin modelling of snow water equivalence using binary regression tree methods, Biogeochemistry of Seasonally Snow-Covered Catchments. IAHS Publication No. 228. International Association of Hydrological Sciences, Wallingford, U.K., pp. 129-139.

Elder, K., Rosenthal, W. and Davis, R.E., 1998. Estimating the spatial distribution of snow water equivalence in a montane watershed. *Hydrological Processes*, **12**: 1793-1808.

Ellis, C.R., Pomeroy, J.W., Essery, R.L.H. and Link, T., 2011. Effects of needleleaf forest cover on radiation and snowmelt dynamics in the Canadian Rocky Mountains. *Canadian Journal of Forest Research*, **41**: 608-620.

Environment Canada, 2011. National Climate Data and Information Archive, Canadian Climate Normals, 1971-2000 - Coleman, Alberta. Last Updated: May 18, 2011. Accessed: May 30, 2011. http://www.climate.weatheroffice.ec.gc.ca/climate_normals/index_e.html

Erxleben, J., Elder, K. and Davis, R., 2002. Comparison of spatial interpolation methods for estimating snow distribution in the Colorado Rocky Mountains. *Hydrological Processes*, **16**: 3627-3649.

Essery, R.L.H., Pomeroy, J.W., Parviainen, J. and Storck, P., 2003. Sublimation of snow from coniferous forests in a climate model. *Journal of Climate*, **16**: 1855-1864.

Exner, T. and Jamieson, B., 2009. The effect of daytime warming on snowpack creep, International Snow Science Workshop, Davos, Switzerland, pp. 271-275.

Farnes, P.E., Peterson, N.R., Goodison, B.E. and Richards, R.P., 1982. Metrication of manual snow sampling equipment, Proceedings of the 50th Annual Meeting of the Western Snow Conference, Reno, Nevada, pp. 120-132.

Field, C.B., Mortsch, L.D., Brklacich, M., Forbes, D.L., Kovacs, P., Patz, J.A., Running, S.W. and Scott, M.J., 2007. North America. In: M.L. Parry, O.F. Canziani, J.P. Palutikof, P.J.v.d. Linden and C.E. Hanson (Editors), Climate Change 2007: Impacts, Adaption and Vulnerability. Contribution of Working Group II to the Fourth Assessment Report of the Intergovernmental Panel on Climate Change. Cambridge University Press, Cambridge, U.K., pp. 617-652.

Fischlin, A., Midgley, G.F., Price, J.T., Leemans, R., Glopal, B., Turley, C., Rounsevell, M.D.A., Dube, O.P., Tarazona, J. and Velichko, A.A., 2007. Ecosystems, their properties, goods and services. In: M.L. Parry, O.F. Canziani, J.P. Palutikof, P.J.v.d. Linden and C.E. Hanson (Editors), Climate Change 2007: Impacts, Adaption, and Vulnerability. Contribution of Working Group II to the Fourth Assessment Report of the Intergovernmental Panel on Climate Change. Cambridge University Press, Cambridge, U.K., pp. 211-272.

Flannigan, M.D., Amiro, B.D., Logan, K.A., Stocks, B.J. and Wotton, B.M., 2005. Forest fires and climate change in the 21st century. *Mitigation and Adaption Strategies for Global Change*, **11**: 847-859.

Frazer, G.W., Canham, C.D. and Lertzman, K.P., 1999. *Gap light analyzer (GLA), Version 2D0: Users manual and program documentation*, Simon Fraser University and Millbrook Institute of Ecosystem Studies, Burnaby, B.C., 40 pp.

Freeman, T.G., 1965. Snow survey samplers and their accuracy, Proceedings of the 22nd Annual Meeting of the Eastern Snow Conference, Hanover, New Hampshire, pp. 1-10.

Garget, D., 2005. Testing of robotic total stations for dynamic tracking. B.S.S. Thesis, University of Southern Queensland, Toowoomba, Queensland, Australia, 131 pp.

Germain, D., Filion, L. and Hétu, B., 2005. Snow avalanche activity after fire and logging disturbance, northern Gaspé Peninsula, Quebec, Canada. *Canadian Journal of Earth Sciences*, **42**: 2103-2116.

Gillan, B.J., Harper, J.T. and Moore, J.N., 2010. Timing of present and future snowmelt in from high elevations in northwest Montana. *Water Resources Research*, **46**. DOI: 10.1029/2009WR007861

Golding, D.L. and Swanson, R.H., 1986. Snow distribution patterns in clearings and adjacent forest. *Water Resources Research*, **22**: 1931-1940.

Goodison, B., 1978. Accuracy of snow samplers for measuring shallow snowpacks: an update, Proceedings of the 35th Annual Meeting of the Eastern Snow Conference, Hanover New Hampshire, pp. 36-49.

Goodison, B., Glynn, J.E., Harvey, K.D. and Slater, J.E., 1987. Snow surveying in Canada: A perspective. *Canadian Water Resources Journal*, **12**: 27-42.

Goodison, B.E., Ferguson, H.L. and McKay, G.A., 1981. Measurement and Data Analysis. In: D.M. Gray and D.H. Male (Editors), Handbook of Snow: Principles, Processes, Management and Use. The Blackburn Press, Caldwell, New Jersey, pp. 191-274.

Graumlich, L.J., 1993. Response of tree growth to climatic variation in the mixed conifer and deciduous forests of the upper Great Lakes region. *Canadian Journal of Forest Research*, **23**: 133-143.

Gray, D.M., Norum, D.I. and Dyck, G.E., 1970. Densities of Prairie Snowpacks, Proceedings of the 38th Annual Meeting of the Western Snow Conference, Victoria, British Columbia, pp. 24-30.

Green, R.O., Dozier, J., Roberts, D. and Painter, T., 2002. Spectral snow-reflectance models for grain-size and liquid-water fraction in melting snow from the solar-reflected spectrum. *Annals of Glaciology*, **34**: 71-73.

Groisman, P.Y., Knight, R.W., Karl, T.R., Easterling, D.R., Sun, B. and Lawrimore, J.H., 2004. Contemporary changes of the hydrological cycle over the contiguous United States: trends derived from *in situ* observations. *Journal of Hydrometeorology*, **5**: 64-85.

Grünewald, T., Schirmer, M., Mott, R. and Lehning, M., 2010. Spatial and temporal variability of snow depth and SWE in a small mountain catchment. *The Cryosphere*, **4**: 215-225.

Hedstrom, N.R. and Pomeroy, J.W., 1998. Measurements and modelling of snow interception in the boreal forest. *Hydrological Processes*, **12**: 1611-1625.

Hélie, J.F., Peters, D.L., Tattrie, K.R. and Gibson, J.J., 2005. *Review and Synthesis of Potential Hydrologic Impacts of Mountain Pine Beetle and Related Harvesting Activities in British Columbia* Natural Resources Canada, C.F.S.P.F. Centre. Mountain Pine Beetle Initiative Working Paper 2005-23. Queen's Printer for Canada, Victoria. pp. 26

Hennessy, K., Whetton, P., Smith, I., Bathols, J., Hutchinson, M. and Sharples, J., 2003. *The impact of climate change on snow conditions in mainland Australia*. Australian Commonwealth Scientific and Industrial Research Organization (CSIRO), Atmospheric Research Department. Aspendale, Victoria, Australia. pp. 50

Hiemstra, C.A., Liston, G.E. and Reiners, W.A., 2002. Snow redistribution by wind and interactions with vegetation at upper treeline in the Medicine Bow Mountains, Wyoming, U.S.A. *Arctic, Antarctic, and Alpine Research*, **34**: 262-273.

Hiemstra, C.A., Liston, G.E. and Reiners, W.A., 2006. Observing, modelling, and validating snow redistribution by wind in a Wyoming upper treeline landscape. *Ecological Modelling*, **197**: 31-51.

Hjulstrøm, F., 1935. Studies of the morphological activity of rivers as illustrated by the River Fyris. *Bulletin of the Geological Institute University of Uppsala*, **25**: 221-527.

Höglund, R. and Large, P., 2005. *Trimble White Paper: Direct Reflex EDM Technology for the Surveyor and Civil Engineer*, Trimble Engineering and Construction Group, Dayton OH, 13 pp.

Hood, J.L. and Hayashi, M., 2010. Assessing the application of a laser rangefinder for determining snow depth in inaccessible alpine terrain. *Hydrology and Earth Systems Science*, **14**: 901-910.

Hopkinson, C., Crasto, N., Marsh, P., Forbes, D. and Lesack, L., 2011. Investigating the spatial distribution of water levels in the Mackenzie Delta using airborne LiDAR. *Hydrological Processes*. DOI: 10.1002/hyp.8167

Hopkinson, C., Sitar, M., Chasmer, L., Gynan, C., Agro, D., Enter, R., Foster, J., Heels, N., Hoffman, C., Nillson, J. and Pierre, R.S., 2001. Mapping the spatial distribution of snowpack depth beneath a variable forest canopy using airborne laser altimetry, Proceedings of the 58th Annual Meeting of the Eastern Snow Conference, Ottawa, Ontario, Canada, pp. 253-264.

Hosking, A., 2009. Investigation into the effectiveness of reflectorless technologies on structural surveillance monitoring. B.S.S. Thesis, University of Southern Queensland, Toowoomba, Queensland, Australia, 88 pp.

Howe, H., 2006. Temperature extremes and the snow scale, Proceedings of the 74th Annual Meeting of the Western Snow Conference, Las Cruces, NM, pp. 147-148.

Johnson, E.A., 1987. The relative importance of snow avalanche disturbance and thinning on canopy plant populations. *Ecology*, **68**: 43-53.

Joiner, B.L. and Rosenblatt, J.R., 1971. Some properties of the range in samples from Tukey's Symmetric Lambda Distributions. *Journal of the American Statistical Association*, **66**: 394-399.

Jones, J.A., 2000. Hydrologic processes and peak discharge response to forest removal, regrowth, and roads in 10 small experimental basins, western Cascades, Oregon. *Water Resources Research*, **36**: 2621-2642.

Jörg, P., Fromm, R., Sailer, R. and Schaffhauser, A., 2006. Measuring snow depth with a terrestrial laser ranging system, International Snow Science Workshop, Telluride, CO., pp. 452-460.

Jost, G., Weiler, M., Gluns, D.R. and Alila, Y., 2007. The influence of forest and topography on snow accumulation and melt at the watershed scale. *Journal of Hydrology*, **347**: 101-115.

Judson, A. and Doesken, N., 2000. Density of freshly fallen snow in the central Rocky Mountains. *Bulletin of the American Meteorological Society*, **81**: 1577-1587.

Kienzle, S., 2004. The effect of DEM raster resolution on first order, second order, and Compound Terrain derivatives. *Transactions in GIS*, **8**: 83-111.

Kind, R.J., 1981. Snow Drifting. In: D.M. Gray and D.H. Male (Editors), Handbook of Snow: Principles, Processes, Management, and Use. The Blackburn Press, Caldwell, New Jersey, pp. 338-359.

Kuhn, M., 1985. Bidirectional reflectance of polar and alpine snow surfaces. *Annals of Glaciology*, **6**: 164-167.

Kukla, G.J. and Kukla, H.J., 1974. Increased surface albedo in the Northern Hemisphere. *Science*, **183**: 709-714.

Langham, J., 1981. Physics and Properties of Snowcover. In: D.M. Gray and D.H. Male (Editors), Handbook of Snow: Principles, Processes, Management and Use. The Blackburn Press, Caldwell, New Jersey, pp. 275-337.

LaserCraft Inc., 2007. *Contour Specifications*, Norcross, GA., 1 pp.

Leica Geosystems AG, 2009a. *Leica ScanStation C10 Datasheet*. Rep. 776241en-IX.09-RDV, Heerbrugg, Switzerland, 2 pp.

Leica Geosystems AG, 2009b. *Leica TPS1200+ Series Technical Data.* . Rep. 738601en-V.09, Heerbrugg, Switzerland, 16 pp.

Lemke, P., Ren, J., Alley, R.B., Allison, I., Carrasco, J., Flato, G., Fujii, Y., Kaser, G., Mote, P., Thomas, R.H. and Zhang, T., 2007. Observations: Changes in Snow, Ice, and Frozen Ground. In: S. Solomon, D. Qin, M. Manning, Z. Chen, M. Marquis, K.B. Averyt, M. Tignor and H.L. Miller (Editors), Climate Change 2007: The Physical Science Basis. Contribution of Working Group I to the Fourth Assessment Report of the Intergovernmental Panel on Climate Change. Cambridge University Press, Cambridge, U.K., pp. 337-383.

Lillquist, K. and Walker, K., 2006. Glacier and climate flucuations at Mount Hood, Oregon. *Arctic, Antarctic, and Alpine Research*, **38**: 399-412.

Littell, J.S., McKenzie, D., Peterson, D.L. and Westerling, A.L., 2009. Climate and wildfire area burned in western U.S. ecoprovinces, 1916-2003. *Ecological Applications*, **19**: 1003-1021.

Logan, L.A., 1973. Basin-wide water equivalent estimation from snowpack depth measurements, Role of Snow and Ice in Hydrology, IAHS Publication 107.

International Association of Hydrologic Sciences, Wallingford, U.K., pp. 864-884.

López-Moreno, J.I., 2005. Recent variations of snowpack depth in the central Spanish Pyrenees. *Arctic, Antarctic, and Alpine Research*, **37**: 253-260.

López-Moreno, J.I., Latron, J. and Lehmann, A., 2010. Effects of sample and grid size on the accuracy and stability of regression-based snow interpolation methods. *Hydrological Processes*, **24**: 1914-1928.

López-Moreno, J.I. and Nogués-Bravo, D., 2005. A generalized additive model for the spatial distribution of snowpack in the Spanish Pyrenees. *Hydrological Processes*, **19**: 3167-3176.

López-Moreno, J.I. and Nogués-Bravo, D., 2006. Interpolating local snow depth data: an evaluation of methods. *Hydrological Processes*, **20**: 2217-2232.

López-Moreno, J.I. and Stähli, M., 2008. Statistical analysis of the snow cover variability in a subalpine watershed: Assessing the role of topography and forest interactions. *Journal of Hydrology*, **348**: 379-394.

MacDonald, M.K., Pomeroy, J.W. and Pietroniro, A., 2010. On the importance of sublimation to an alpine snow mass balance in the Canadian Rocky Mountains. *Hydrology and Earth Systems Science*, **14**: 1401-1415.

Magono, C., 1953. On the growth of snow flake and graupel. *Science Reports of the Yokohama National University*, **Series I**: 18-40.

Magono, C. and Lee, C., 1966. Meteorological classification of natural snow crystals. *Journal of the Faculty of Science, Hokkaido University, Series VII*, **2**: 321-335.

Male, D.H. and Gray, D.M., 1981. Snowcover Ablation and Runoff. In: D.M. Gray and D.H. Male (Editors), Handbook of Snow: Principles, Processes, Management and Use. The Blackburn Press, Caldwell, New Jersey, pp. 360-436.

Matzinger, N., Andretta, M., Van Gorsel, E., Vogt, R., Ohmura, A. and Rotach, M.W., 2003. Surface radiation budget in an Alpine valley. *Quarterly Journal of the Royal Meteorological Society*, **129**: 877-895.

McCabe, G.J., Clark, M.P. and Hay, L.W., 2007. Rain-on-snow events in the western United States. *Bulletin of the American Meteorological Society*, **88**: 319-328.

McClung, D. and Schaerer, P., 1993. *The Avalanche Handbook*, 2nd ed. Seattle Washington, The Mountaineers, 271 pp.

McClung, D.M. and Larsen, J.O., 1989. Snow creep pressures: Effects of structure boundary conditions and snowpack properties compared with field data. *Cold Regions Science and Technology*, **17**: 33-47.

McClung, D.M., Larsen, J.O. and Hansen, S.B., 1984. Comparison of snow pressure measurements and theoretical predictions. *Canadian Geotechnical Journal*, **21**: 250-258.

McCullagh, P. and Nelder, J.A., 1989. *Generalized Linear Models, 2nd Edition*, ed. London, Chapman and Hall/CRC, 532 pp.

McGaughey, R.J., 2010. *FUSION/LDV: Software for LiDAR Data Analysis and Visualization. FUSION Version 2.80*, United States Department of Agriculture, Forest Service, Pacific Northwest Research Station, 150 pp.

McKay, G.A. and Gray, D.M., 1981. The Distribution of Snowcover. In: D.M. Gray and D.H. Male (Editors), Handbook of Snow: Principles, Processes, Management and Use. The Blackburn Press, Caldwell, New Jersey, pp. 153-190.

Meijerink, A.M.J., de Brouwer, H.A.M., Mannaerts, C.M. and Valenzuela, C.R., 1994. *Introduction to the Use of Geographic Information Systems for Practical Hydrology*. Publication Number 24. International Institute for Aerospace Survey and Earth Science (ITC), Enschede. pp. 243

Meiman, J.R., 1970. Snow accumulation related to elevation, aspect and forest canopy, Snow Hydrology, Proceedings of a Workshop Seminar, 1968. Canadian National Committee for the International Hydrological Decade, Queen's Printer for Canada, Ottawa, Ottawa, pp. 35-47.

Molotch, N.P., Blanken, P.D., Williams, M.W., Turnipseed, A.A., Monson, R.K. and Margulis, S.A., 2007. Estimating sublimation of intercepted and sub-canopy snow using eddy covariance systems. *Hydrological Processes*, **21**: 1567-1575.

Molotch, N.P., Colee, M.T., Bales, R.C. and Dozier, J., 2005. Estimating the spatial distribution of snow water equivalent in an alpine basin using binary regression tree models: the impact of digital elevation data and independent variable selection. *Hydrological Processes*, **19**: 1459-1479.

Montesi, J., Elder, K., Schmidt, R.A. and Davis, R.E., 2004. Sublimation of intercepted snow within a subalpine forest canopy at two elevations. *Journal of Hydrometeorology*, **5**: 763-773.

Mote, P.W., Hamlet, A.F., Clark, M.P. and Lettenmaier, D.P., 2005. Declining mountain snowpack in western North America. *Bulletin of the American Meteorological Society*, **86**: 39-49.

Murray, C.D. and Buttle, J.M., 2003. Impacts of clearcut harvesting on snow accumulation and melt in a northern hardwood forest. *Journal of Hydrology*, **271**: 197-212.

Nkemdirim, L.C., 1996. Canada's chinook belt. *International Journal of Climatology*, **16**: 441-462.

Nobis, M. and Hunziker, U., 2005. Automatic thresholding for hemispherical canopy-photographs based on edge detection. *Agricultural and Forest Meteorology*, **128**: 243-250.

O'Brien, H.W. and Munis, R.H., 1975. *Red and Near-Infrared Spectral Reflectance of Snow*. U.S. Army Corps of Engineers, C.R.R.a.E. Lab. Paper No. 24. Hanover, New Hampshire. pp. 16

Oke, T.R., 1987. *Boundary Layer Climates*, 2nd ed. London, England, Routledge, 435 pp.

Oldman Watershed Council, 2010. *Oldman River State of the Watershed Report 2010*, Oldman Watershed Council, Lethbridge Alberta, 284 pp.

Oliphant, A.J., Spronken-Smith, R.A., Sturman, A.J. and Owens, I.F., 2003. Spatial variability of surface radiation fluxes in mountainous terrain. *Journal of Applied Meteorology*, **42**: 113-128.

Parmesan, C., Root, T.L. and Willig, M.R., 2000. Impacts of extreme weather and climate on terrestrial biota. *Bulletin of the American Meteorological Society*, **81**: 443-450.

Peterson, N.R. and Brown, J., 1975. Accuracy of snow measurements, Proceedings of the 43rd Annual Meeting of the Western Snow Conference, Coronado, California, pp. 1-5.

Pfeffer, W.T. and Mrugala, R., 2002. Temperature gradient and initial snow density as controlling factors in the formation and structure of hard depth hoar. *Journal of Glaciology*, **48**: 485-494.

Pigeon, K.E. and Jiskoot, H., 2008. Meteorological controls on snowpack formation and dynamics in the southern Canadian Rocky Mountains. *Arctic, Antarctic, and Alpine Research*, **40**: 716-730.

Pomeroy, J.W. and Gray, D.M., 1995. *Snow Accumulation, Relocation and Management*. National Hydrology Research Institute. Science Report No. 7. Saskatoon Saskatchewan. pp. 144

Pomeroy, J.W., Gray, D.M., Hedstrom, N.R. and Janowicz, J.R., 2002. Prediction of seasonal snow accumulation in cold climate forests. *Hydrological Processes*, **16**: 3543-3558.

Pomeroy, J.W., Marks, D., Link, T., Ellis, C.R., Hardy, J.P., Rowlands, A. and Granger, R., 2009. The impact of coniferous forest temperature on incoming longwave radiation to melting snow. *Hydrological Processes*, **23**: 2513-2525.

Pomeroy, J.W., Parviainen, J., Hedstrom, N. and Gray, D.M., 1998. Coupled modelling of forest snow interception and sublimation. *Hydrological Processes*, **12**: 2317-2337.

Pomeroy, W. and Brun, E., 2001. Physical Properties of Snow. In: H.G. Jones, J. W. Pomeroy, D. A. Walker, and R. W. Hoham (Editor), Snow Ecology: An Interdisciplinary Examination of Snow Covered Ecosystems, pp. 45-126.

Prokop, A., 2008. Assessing the applicability of terrestrial laser scanning for spatial snow depth measurements. *Cold Regions Science and Technology*, **54**: 155-163.

Prokop, A., Schirmer, M., Rub, R., Lehning, M. and Stocker, M., 2008. A comparison of measurement methods: terrestrial laser scanning, tachymetry and snow probing for the determination of the spatial snow-depth distribution of slopes. *Annals of Glaciology*, **49**: 210-216.

Quinn, G.P. and Keough, M.J., 2002. *Experimental Design and Data Analysis for Biologists*, ed. Cambridge, U.K., Cambridge University Press, 537 pp.

Redding, T., Winkler, R.D., Teti, P., Spittlehouse, D.L., Boon, S., Rex, J., Dubé, S., Moore, R.D., Wei, A., Carver, M., Schnorbus, M., Reese-Hansen, L. and Chatwin, S., 2008. Mountain pine beetle and watershed hydrology. *In* Mountain Pine Beetle: From Lessons Learned to Community-based Solutions Conference

Proceedings, June 10-11, 2008. *B.C. Journal of Ecosystems and Management*, **9**: 33-50.

Rhea, J.O. and Grant, L.O., 1974. Topographic influences on snowfall patterns in mountainous terrain, Advanced Concepts and Techniques in the Study of Snow and Ice Resources, Monterey, California, pp. 182-192.

Riegl Laser Measurement Systems GmbH, 2005. *Long-Range Laser Profile Measuring System LPM-i800HA*, Horn, Austria, 4 pp.

Ritter, D.F., Kochel, R.C. and Miller, J.R., 2002. *Process Geomorphology*, 4th ed. ed. Toronto, McGraw-Hill, 560 pp.

Robinson, P.J. and Henderson-Sellers, A., 1999. *Contemporary Climatology*, 2nd ed. ed. Harlow, England, Pearson Education, 317 pp.

Rock, L. and Mayer, B., 2007. Isotope hydrology of the Oldman River basin, southern Alberta, Canada. *Hydrological Processes*, **21**: 3301-3315.

Rood, S.B., Pan, J., Gill, K.M., Franks, C.G., Samuelson, G.M. and Shepherd, A., 2008. Declining summer flows of Rocky Mountain rivers: Changing seasonal hydrology and probable impacts on floodplain forests. *Journal of Hydrology*, **349**: 397-410.

Russell, L.S. and Landes, R.W., 1940. *Geology of the Southern Alberta Plains, Geological Survey Memoir 221*. Department of Mines and Resources, B.o.G.a.T. Mines and Geology Branch. No. 2453. J.O. Patenaude, King's Printer for Canada, Ottawa. pp. 223

Schaerer, P.A., 1971. Relation between the mass of avalanches and charateristics of terrain at Rogers Pass, B.C., Canada, Snow and Ice Symposium. IAHS Publication 104. International Association of Hydrological Sciences, Wallingford U.K., pp. 378-380.

Schaerer, P.A., 1981. Avalanches. In: D.M. Gray and D.H. Male (Editors), Handbook of Snow: Principles, Processes, Management and Use. The Blackburn Press, Caldwell, New Jersey, pp. 475-518.

Schaffhauser, A., Adams, M., Fromm, R., Jörg, P., Luzi, G., Noferini, L. and Sailer, R., 2008. Remote sensing based retrieval of snow cover properties. *Cold Regions Science and Technology*, **54**: 164-175.

Schemenauer, R.S., Berry, M.O. and Maxwell, J.B., 1981. Snowfall Formation. In: D.M. Gray and D.H. Male (Editors), Handbook of Snow: Principles, Processes, Management and Use. The Blackburn Press, Caldwell, New Jersey, pp. 129-152.

Scherrer, S.C., Appenzeller, C. and Laternser, M., 2004. Trends in Swiss Alpine snow days: the role of local- and large-scale climate variability. *Geophysical Research Letters*, **31**. DOI: 10.1029/2004GL020255

Schmidt, R.A. and Gluns, D.R., 1991. Snowfall interception on branches of three conifer species. *Canadian Journal of Forest Research*, **21**: 1262-1269.

Schmidt, R.A., Jairell, R.L. and Pomeroy, J.W., 1988. Measuring snow interception and loss from an artificial conifer, Proceedings of the 56th Annual Meeting of the Western Snow Conference, Kalispell, Montana.

Seligman, G., 1980. *Snow Structure and Ski Fields*, 3rd ed. ed. Cambridge, England, International Glaciological Society, 555 pp.

Serreze, M.C., Clark, M.P., Armstrong, R.L., McGinnis, D.A. and Pulwarty, R.S., 1999. Characteristics of the western United States snowpack from snowpack telemetry (SNOTEL) data. *Water Resources Research*, **35**: 2145-2160.

Shapiro, S.S., Wilk, M.B. and Chen, H.J., 1968. A comparative study of various tests for normality. *Journal of the American Statistical Association*, **63**: 1343-1372.

Silins, U., Bladon, K., Stone, M., Emelko, M., Boon, S., Williams, C., Wagner, M. and Howery, J., 2009. *Southern Rockies Watershed Project: Impact of natural disturbance by wildfire on hydrology, water quality, and aquatic ecology of Rocky Mountain Watersheds Phase 1 (2004-2008)*, Southern Rockies Watershed Project, Edmonton, 89 pp.

Silins, U. and Wagner, M., 2007. *Southern Rockies Watershed Project. 2nd interim report*, 44 pp.

Slaymaker, O., 1993. Cold Mountains of Western Canada. In: H.M. French and O. Slaymaker (Editors), Canada's Cold Environments. McGill Queen's University Press, Montreal, pp. 171-197.

SnowHydro, 2004. SWE Coring Tube. Last Updated: 2004. Accessed: May 22, 2009. http://www.snowhydro.com/column3.htm

Soja, A.J., Tchebakova, N.M., French, N.H.F., Flannigan, M.D., Shugart, H.H., Stocks, B.J., Sukhinin, A.I., Parfenova, E.I., Chapin, F.S. and Stackhouse, P.W., 2007.

Climate-induced boreal forest change: Predictions versus current observations. *Global and Planetary Change*, **56**: 274-296.

Sommerfeld, R.A. and LaChapelle, E.R., 1970. The classification of snow metamorphism. *Journal of Glaciology*, **9**: 3-17.

Spittlehouse, D.L. and Winkler, R.D., 1996. Forest canopy effects on sample size requirements in snow accumulation and melt comparisons, Proceedings of the 64th Annual Meeting of the Western Snow Conference, Bend, Oregon, pp. 39-46.

Stahl, K., Moore, R.D. and McKendry, I.G., 2006. Climatology of winter cold spells in relation to mountain pine beetle mortality in British Columbia, Canada. *Climate Research*, **32**: 13-23.

Stähli, M., Papritz, A., Waldner, P. and Forster, F., 2001. Time-space linear regression analysis of the snow cover in a pre-Alpine semi-forested catchment. *Annals of Glaciology*, **32**: 125-129.

Stegman, S.V., 1996. Snowpack changes resulting from timber harvest: Interception, redistribution, and evaporation. *Water Resources Bulletin*, **32**: 1353-1360.

Steppuhn, H., 1981. Snow and Agriculture. In: D.M. Gray and D.H. Male (Editors), Handbook of Snow: Principles, Processes, Management and Use. The Blackburn Press, Caldwell, New Jersey, pp. 60-126.

Stern, N., 2007. *The Economics of Climate Change: The Stern Review*, ed. Cambridge, U.K., Cambridge University Press, 692 pp.

Stewart, I.T., Cayan, D.R. and Dettinger, M.D., 2005. Changes towards earlier streamflow timing across Western North America. *Journal of Climate*, **18**: 1136-1155.

Stokes, M.E., Davis, C.S. and Koch, G.G., 2006. *Categorical data analysis: using the SAS system, Second Edition*, ed. Cary, NC., SAS Publishing, 648 pp.

Storck, P., Kern, T. and Bolton, S., 1999. Measurement of differences in snow accumulation, melt, and micrometeorology due to forest harvesting. *Northwest Science*, **73**: 87-101.

Storck, P., Lettenmaier, D.P. and Bolton, S.M., 2002. Measurement of snow interception and canopy effects on snow accumulation and melt in a mountainous maritime climate, Oregon, United States. *Water Resources Research*, **38**: 1223-1238.

Sturm, M., Taras, B., Liston, G.E., Derksen, C., Jones, T. and Lea, J., 2010. Estimating snow water equivalent using snow depth data and climate classes. *Journal of Hydrometeorology*, **11**: 1380-1394.

Swanson, R.H., 1988. The effect of *in situ* evaporation on perceived snow distribution in partially clear-cut forests, Proceedings of the 56th Annual Meeting of the Western Snow Conference, Kalispell, Montana, pp. 87-92.

Toews, D.A.A. and Gluns, D.R., 1986. Snow accumulation and ablation on adjacent forested and clearcut sites in southeastern British Columbia, Proceedings of the 54th Annual Meeting of the Western Snow Conference, Phoenix, Arizona, pp. 101-111.

Trenberth, K.E., Jones, P.D., Ambenje, P., Bojariu, R., Easterling, D., Tank, A.K., Parker, D., Rahimzadeh, F., Renwick, J.A., Rusticucci, M., Soden, B. and Zhai, P., 2007. Observations: Surface and Atmospheric Climate Change. In: S. Soloman, D. Qin, M. Manning, Z. Chen, M. Marquis, K.B. Averyt, M. Tignor and H.L. Miller (Editors), Climate Change 2007: The Physical Science Basis. Contribution of Working Group I to the Fourth Assessment Report of the Intergovernmental Panel on Climate Change. Cambridge University Press, Cambridge, U.K., pp. 235-336.

Trimble Navigation Ltd., 2007a. *Trimble R7 GNSS System Datasheet*, Dayton, OH, 2 pp.

Trimble Navigation Ltd., 2007b. *Trimble S6 Total Station Datasheet*, Dayton, OH., 4 pp.

Troendle, C.A., Schmidt, R.A. and Martinez, M.H., 1988. Snow deposition in a forest stand with a clearing, Proceedings of the 56th Annual Meeting of the Western Snow Conference, Kalispell, Montana, pp. 78-86.

United States Army Corps of Engineers, 1956. *Snow Hydrology: Summary Report of the Snow Investigations*, North Pacific Division, Portland Oregon, 437 pp.

Urban, T.J., Schutz, B.E. and Neuenschwander, A.L., 2008. A survey of ICESat costal altimetry applications: Continental coast, open ocean island, and inland river. *Journal of Terrestrial, Atmospheric, and Oceanic Sciences*, **19**: 1-19.

Valt, M. and Cianfarra, P., 2010. Recent snow cover variability in the Italian Alps. *Cold Regions Science and Technology*, **64**: 146-157.

Varhola, A., Coops, N., Weiler, M. and Moore, D., 2010. Forest canopy effects on snow accumulation and ablation: an integrative review of empirical results. *Journal of Hydrology*, **392**: 219-233.

Vasicek, O., 1976. A test for normality based on sample entropy. *Journal of the Royal Statistical Society, Series B*, **38**: 54-59.

Warren, S.G., 1982. Optical properties of snow. *Reviews of Geophysics and Space Physics*, **20**: 67-89.

Wessa, P., 2008. Tukey lambda PPCC Plot (v1.0.2) in Free Statistics Software (v.1.1.23-r7), Office for Research Development and Education. Last Updated: 2008. Accessed: June 10, 2011. http://www.wessa.net/rwasp_tukeylambda.wasp/

Winkler, R.D., Spittlehouse, D.L. and Golding, D.L., 2005. Measured differences in snow accumulation and melt among clearcut, juvenile, and mature forests in southern British Columbia. *Hydrological Processes*, **19**: 51-62.

Winstral, A. and Marks, D., 2002. Simulating wind fields and snow redistribution using terrain-based parameters to model snow accumulation and melt over a semi-arid mountain catchment. *Hydrological Processes*, **16**: 3585-3603.

Winstral, A., Marks, D. and Gurney, R., 2009. An efficient method for distributing wind speeds over heterogeneous terrain. *Hydrological Processes*, **23**: 2526-2535.

Woo, M., 1997. *A Guide for Ground Based Measurement of the Arctic Snow Cover*. Meteorological Service of Canada, Climate Research Branch. Queen's Printer for Canada, Ottawa. pp. 30

Work, R.A., Stockwell, H.J., Freeman, T.G. and Beaumont, R.T., 1965. *Accuracy of field snow surveys, western United States, including Alaska*. U.S. Army Corps of Engineers, Cold Regions Reseach and Engineering Lab. Technical Report 163. Hanover, New Hampshire. pp. 43

Workum, R.H. and Hedinger, A.S., 1992. *Devonian Frasnian Stratigraphy, Rocky Mountain Front Ranges: Crowsnest Pass to Jasper, Alberta*. Natural Resourses Canada, Geological Survey of Canada. Open File 2509. Queen's Printer for Canada, Ottawa. pp. 182

Wulder, M.A., Bater, C., Coops, N., Hilker, T. and White, J., 2008. The role of LiDAR in sustainable forest management. *The Forestry Chronicle*, **84**: 807-826.

Zalikhanov, M.C., 1971. Hydrological role of avalanches in the Caucasus, Snow and Ice Symposium. IAHS Publication 104. International Association of Hydrologic Sciences Wallingford U.K., pp. 390-394.

Zhang, Y., Li, T. and Wang, B., 2004. Decadal change of the spring snow depth over the Tibetan Plateau: the associated circulation and influence on the east Asian summer monsoon. *Journal of Climate*, **17**: 2780-2793.